To the Graduate Council:

I am submitting herewith a dissertation written by Sehyun Nam entitled "Dynamics of Steady and Unsteady Melt Spinning." I have examined the final copy of this dissertation for form and content and recommend that it be accepted in partial fulfillment of the requirements for the degree of Doctor of Philosophy, with a major in Polymer Engineering.

Donald C. Bogue, Major Professor

We have read this dissertation
and recommend its acceptance:

Accepted for the Council:

Vice Chancellor
Graduate Studies and Research

DYNAMICS OF STEADY AND UNSTEADY MELT SPINNING

A Dissertation

Presented for the

Doctor of Philosophy

Degree

The University of Tennessee, Knoxville

Sehyun Nam

December 1982

3065049

ACKNOWLEDGMENTS

The author wishes to express appreciation to many persons who have assisted in various ways during the course of this research.

Sincere appreciation goes to Professor Donald C. Bogue, the author's advisor, for his helpful guidance and encouragement throughout his graduate study.

Appreciation is also extended to Professor James L. White for his helpful suggestions.

The author is indebted to the Polymer Engineering faculty members and student colleagues for many useful discussions and advice.

The author wishes to thank the polymer consortium for a research assistantship and the Department of Chemical, Metallurgical, and Polymer Engineering for a teaching assistantship.

The author also wishes to thank the members of the mechanical and electronic shop for their help throughout the process of this work.

Finally, the author is very grateful to his wife, Kuisook, and two sons, Taikwoo and Taiksoo.

ABSTRACT

The present work involves an overall study of isothermal melt spinning, including both steady state and unsteady state spinning ("draw resonance"). A systematic study of two commercial polypropylenes was carried out as a function of the variables which one normally associates with draw resonance and in addition the variables which have to do with the die flow. An integral viscoelastic analysis for steady spinning developed by Matsui and Bogue, which includes the shear rate in the die as a parameter, was solved numerically for comparing with data from steady spinning and also as a guide for correlating data in unsteady spinning.

The computer analysis gives predictions for the die swell and the velocity distribution along the spinline which are in good agreement with the experimental results and also with several differential analyses based on a convected Maxwell model. The computer solution is a more general solution than those based on the differential models, since the latter do not include the effect of the shear rate in the die. An important result from the steady analysis is that a maximum force occurs as the draw ratio is increased, provided that the rheological parameter which governs "thinning behavior" is sufficiently large.

The experimentally observed draw ratios for the onset of draw resonance and also the periods of the fluctuations are in the range of existing theoretical predictions. Despite this general agreement, however, there are clearly deviations which are related to the shear flow

in the die. In order to deal with this die flow effect, several correlating schemes were investigated. The most successful involved a ratio between the tensile force in the die and that in the spinline which somehow reflects the "mismatch" between the die flow and the spinline flow; the larger this ratio, the less stable is the spinline.

TABLE OF CONTENTS

CHAPTER		PAGE
I.	INTRODUCTION	1
II.	BACKGROUND	3
	A. Spinline Force and Mass Balance	3
	B. Steady State Spinning Analysis	6
	C. Unsteady Spinning Including Draw Resonance	11
	D. Die Swell	18
	E. Non-Isothermal Melt Spinning	24
III.	EXPERIMENTAL EQUIPMENT AND PROCEDURE	27
	A. Materials	27
	B. Equipment	27
	C. Experimental Procedure	31
IV.	PRESENTATION AND ANALYSIS OF RESULTS: STEADY SPINNING	36
	A. Theoretical Analysis	36
	B. Comparison with Experimental Results	57
V.	PRESENTATION AND CORRELATION OF RESULTS: UNSTEADY SPINNING	70
	A. Experimental Results	70
	B. Correlation of Results	79
VI.	SUMMARY OF IMPORTANT RESULTS AND CONCLUSIONS	102
	A. Steady Spinning	103
	B. Unsteady Spinning	105
LIST OF REFERENCES		108
APPENDIX.	SUMMARY OF NEWTONIAN AND INTEGRAL VISCOELASTIC ANALYSES FOR THE METL SPINNING PROBLEM AND COMPUTER PROGRAM	115
	A. Newtonian Analysis	115
	B. Integral Viscoelastic Analysis	116
	C. Computer Program for Isothermal Viscoelastic Integral Model	120
VITA		132

LIST OF TABLES

TABLE		PAGE
III-1.	Polypropylenes Used.	27
IV-1.	Summary of Rheological Parameters Used	51
IV-2.	Comparison of Measured and Calculated Forces	67
IV-3.	Predicted Spinline Force Under Various Die Flow Condition b = 0.6, τ_0 = 0.1 (Constant V_0 and Different Die Diameter)	68
IV-4.	Predicted Spinline Force Under Various Die Flow Condition b = 0.6, τ_0 = 0.1 (Same Die Diameter and Different V_0)	69
V-1.	Summary of Equations for the Period of Fluctuation and for the Spinline Residence Time.	82
V-2.	Calculated and Observed Periods of Fluctuation and Residence Times.	84
V-3.	Summary of Computer Results for Certain Dimensionless Correlating Groups (PP106-4 at Low Initial Velocity) . .	89
V-4.	Summary of Computer Results for Certain Dimensionless Correlating Groups (PP106-4 at High Initial Velocity). .	90
V-5.	Summary of Computer Results for Certain Dimensionless Correlating Groups (PP6823 at Low Initial Velocity). . .	91
V-6.	Summary of Computer Results for Certain Dimensionless Correlating Groups (PP6823 at High Initial Velocity) . .	92

LIST OF FIGURES

FIGURE		PAGE
II-1.	Schematic diagram of spinline in melt spinning.	4
II-2.	Critical draw ratio as a function of viscoelastic parameter and power law index (from Fisher and Denn). .	15
III-1.	Schematic diagram of equipment.	28
III-2.	Experimental set-up of apparatus.	29
	a. Overall view of the apparatus	29
	b. Close-up of take-up apparatus	29
	c. Reticon Scan camera, oscilloscope and digital readout	30
III-3.	Typical force and diameter fluctuation during draw resonance	33
III-4.	Typical double peak image of the fiber on the oscilloscope screen.	35
IV-1.	Predicted velocity distribution along the spinline. . .	39
IV-2.	Velocity distribution along the spinline for long spin length comparisons of computer results with various analytical results.	42
IV-3.	Velocity distribution along the spinline for short spin length comparisons of computer results with various analytical results.	43
IV-4.	Velocity distribution along the spinline (showing the "blow-up point")	44
IV-5.	Spinline force vs. draw ratio as a function of the parameter b	46
IV-6.	Theoretical velocity distribution along the spinline near the condition of the maximum force	48
IV-7.	Comparison of experimental data and theoretical fits of shear viscosity and first normal stress function . .	52
IV-8.	Reduced steady state elongational viscosity as a function of elongational rate	54

FIGURE		PAGE
IV-9.	Experimental diameter distribution along the spinline (PP106-4 at different shear rates)	58
IV-10.	Experimental diameter distribution along the spinline (PP6823 at different shear rates).	59
IV-11.	Experimental diameter distribution along the spinline (PP106-4 at different draw ratios with same shear rate)	60
IV-12.	Experimental diameter distribution along the spinline (PP106-4 and PP6823 at same draw ratio and same shear rate).	61
IV-13.	Comparison of experimental data with theoretical prediction using one element (PP106-4)	63
IV-14.	Comparison of experimental data with theoretical prediction using one element and three element model (PP106-4)	64
IV-15.	Comparison of experimental data with theoretical prediction using one element and three element model (PP6823).	65
V-1.	Typical force-time trace from chart recorder.	71
V-2.	Critical draw ratio as a function of initial velocity (PP106-4 with different spin length).	73
V-3.	Critical draw ratio as a function of initial velocity (PP6823 with different spin length).	74
V-4.	Critical draw ratio as a function of initial velocity (PP6823 with different die diameter)	75
V-5.	Critical draw ratio as a function of initial velocity (PP106-4 with different die diameter).	76
V-6.	Variation diameter fluctuation along the spinline . . .	77
V-7.	Critical draw ratio as a function of initial velocity (comparisons of isothermal case with non-isothermal)	78
V-8.	Critical draw ratio as a function of V_o/L	80

FIGURE PAGE

V-9. Predicted critical draw ratio as a function of the elasticity number using the maximum criterion 94

V-10. Correlation of critical draw ratio as a function of elasticity number and force ratio (PP106-4) 98

V-11. Correlation of critical draw ratio as a function of elasticity number and force ratio (PP6823). 99

CHAPTER I

INTRODUCTION

The melt spinning of fibers is an important industrial process, in which an extruded molten polymer is drawn and cooled in a continuous steady-state elongational flow. The fiber spinline sometimes experiences instabilities and exhibits periodic diameter fluctuations. These instabilities may be due to many causes including fluctuations in the delivery or take-up system. The important one known as "draw resonance" has to do with an inherent instability in the spinning process itself. While this problem and the problem of steady spinning have been treated extensively, there have been no attempts to connect them to the flow prior to the spinline, that is, the flow in the die. In the present work this connection will be considered.

The problem of the die flow involves an entry flow region, the straight tube flow and finally a post die (or die swell) region. These problems have been extensively studied. The flow patterns associated with various entry geometries have been studied in some detail, for example, by Ballenger and White (3), Han and Drexler (21), White and Kondo (84), and by other workers, as summarized in Han's book (33). It is a general observation that certain flow patterns often give rise to flow instabilities, part of the phenomenon known as "melt fracture."

As separate matters, the problems of die swell and spinline dynamics have been considered extensively and will be reviewed in detail in the next chapter. The spinline problem beginning at some point down-

stream of the die swell, has been assumed to be a purely elongational flow. It seems reasonable, however, that the nature of this elongational flow, particularly near the die, must be affected to some extent by the prior deformation history in the die. This connection has not developed, and therefore it is one of the purposes of the present work to study this connection.

Another major purpose deals with the question of unsteady spinning (i.e., the instability known as draw resonance). Certainly one would expect that the variables which affect the draw resonance include at least those which affect the steady spinning. As noted previously, one supposes that the steady spinning problem involves both the die swell region and the spinline region. Matsumoto and Bogue (51) noted that the die swell region seems to be very important in determining whether some materials (notably polypropylene) show instabilities or not. Also Han and Kim (34) have noted the pronounced effect of the die aspect ratio $(\frac{L}{D})$ on spinline instabilities, which are interpreted as probably related to the die swell region (i.e., the die length affects the die swell, which affects the stability). Therefore the effects on draw resonance of the flow in the die swell region as well as the flow in the spinline itself have been studied in the present work.

CHAPTER II

BACKGROUND

The problem of melt spinning in an overall sense requires consideration of the entire process whereby a solid polymer is melted and pushed by a screw extruder through a filtering system and die and into the spinline itself. The spinline flow involves both the near die (die swell) region and the far down-stream region, including the mechanics of the take-up device at the end of the line. The problem of die swell and spinline dynamics have been studied extensively and will be reviewed in detail later. The spinline problem, beginning at some point downstream of the die swell, has been assumed to be a purely elongation flow. Such analyses began with the work of Ziabicki in 1967 (94) and again in 1976 (95), and considerable further work has been done since that time. Melt spinning work as well as work on die swell will be reviewed.

A. Spinline Force and Mass Balance

Certain basic balances must be made as the starting point in the analysis of the spinning dynamics. A force balance was first reported by Ziabicki on the spinline in the melt spinning as shown in Figure I-1. The force acting on the spinline includes the applied tension (F_L) at the take-up, the tension or rheological force at some arbitrary position x_1 (F_{rheo}), gravity (F_{grav}), the force due to frictional air drag (F_{drag}), the force due to surface tension (F_s). The sum of these forces

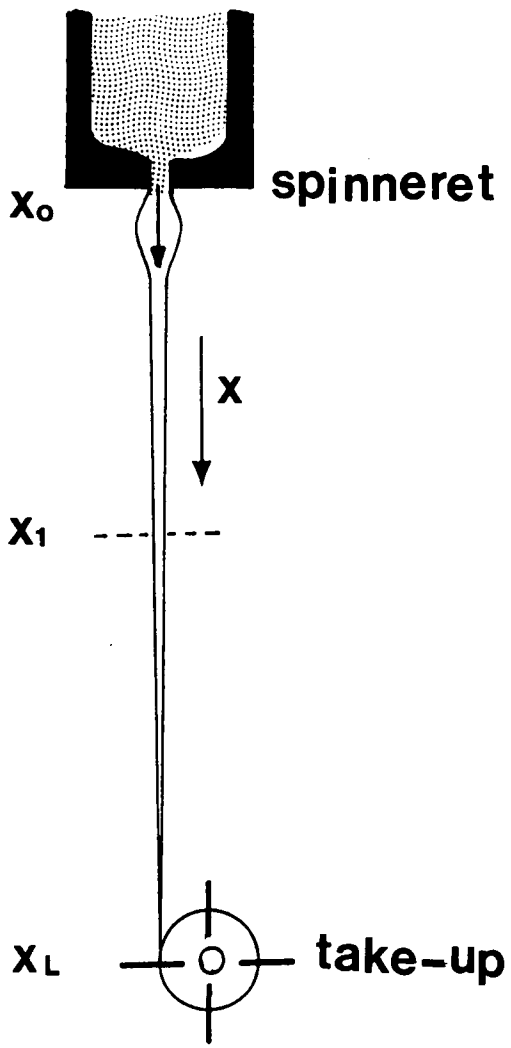


Figure II-1. Schematic diagram of spinline in melt spinning.

must equal the acceleration of the fiber element or equivalently, the carriage of momentum flux ($\rho Q(v_1 - v_2)$). Then the force balance is

$$F_L - F_{rheo} + F_{grav} - F_{drag} - F_s = \rho Q(v_L - v_1) \qquad \text{(II-1)}$$

These various force terms may be expressed as follows,

$$F_{grav} = \int_{x_1}^{x_L} \rho g A dx \qquad \text{(II-2)}$$

$$F_{drag} = \int_{x_1}^{x_L} C_D \frac{\rho v^2}{2} 2\pi R dx \qquad \text{(II-3)}$$

$$F_s = C\gamma \qquad \text{(II-4)}$$

$$F_{rheo} = \int_{o}^{A} \sigma_{11} da \qquad \text{(II-5)}$$

Where A is the cross-sectional area, C_D is the drag coefficient, σ_{11} is the tensile stress within the filament, ρ is the density and Q is volumetric flow rate, γ is the surface tension and C is a shape factor.

An important approximation to the applied forces on a spinline is to neglect all applied forces except for the applied tension at the take-up. This is valid for relatively low speed spinning. Finally the force balance becomes

$$F_{rheo} = F_L \qquad \text{(II-6)}$$

The second basic balance is the mass balance (or continuity equation) which can be stated as follows:

$$\frac{\partial a}{\partial t} + \frac{\partial (va)}{\partial x} = 0 \qquad \text{(II-7)}$$

where a is the cross-sectional area.

For steady state spinning this equation reduces

$$\frac{\partial (va)}{\partial x} = 0 \qquad \text{(II-8)}$$

or

$$Q = va = \text{const.} \qquad \text{(II-9)}$$

or

$$w = \rho va = \text{const.} \qquad \text{(II-10)}$$

For non-isothermal studies, one needs in addition an energy balance. This will be presented later in the section on non-isothermal spinning.

B. Steady State Spinning Analysis

To carry forward with the analysis of melt spinning, one must combine the force and mass balance with a constitutive equation, relating the force to the deformation history. This area has been reviewed in detail by White (88) in 1981 and the following sections summarize the important parts of that literature with some additional comments relative to the present work.

Matovich and Pearson (60) in 1969 have studied isothermal Newtonian fluids and also they extended their study to shear dependent inelastic liquids and to second-order viscoelastic fluids. Since this

original work a number of generalizations and modifications for various constitutive equations have been made, including those of Zeichner (92), Denn, Petrie, and Avenas (16), Fisher and Denn (23), White and Ide (84), Denn and Marrucci (17). Zeichner (92) in 1972 gave an analytical solution of the isothermal steady spinning for a convected Maxwell model, as a part of a larger study including spinline instabilities. His solution predicts a linear velocity profile along the spinline at high tensile stress under certain condition ($P_{11} >> P_{22}$). His results were summarized by Denn, Petrie, and Avenas (18) in 1975. They also reported a solution to the problem of steady spinning without a prior assumption about the normal stress inequality for a convected Maxwell model; they used a constant modulus and a single constant relaxation time. For their higher order differential equation two boundary conditions were required, not only v but also $\frac{dv}{dx}$ at x = 0 or, equivalently, the initial stress. But they claimed that the influence of the initial stress could be ignored except very close to die exit. Also they obtained a nearly linear velocity profile under conditions in which the imposed spinline stress was large compared to the shear modulus. Their results were in agreement with the experimental results of Kanal (46) and Spearot and Metzner (72). Fisher and Denn (23) in 1976 extended the prior analysis of Denn et al. (16) using a deformation relaxation time (based on the power law) and a constant shear modulus. They reported a steady state velocity profile and tension in agreement with experiment for a shear thinning polystyrene melt. Similary Ide and White (41) used the White-Metzner fluid model with a Bogue-White deformation rate dependent relaxation

time. Their work will be discussed later in detail. Denn and Marrucci (17) in 1977 applied a spectrum of relaxation times to determine the mechanics of isothermal melt spinning. They found that the relaxation time distribution leads to higher forces and more linear velocity profile than would be obtained for a Maxwellian material of the same mean properties in shear. As noted above, depending on the solution technique, certain assumptions about initial velocity or initial stress must be made. Petrie (63) has especially called attention to the initial value problem of the influence of the rheological force. Also White and Roman (82) considered the take-up force on the die swell.

In recent years there have been many studies of isothermal melt spinning type problem on different viscoelastic fluid models (11,63,64, 65). Gagon and Denn (26) in 1981 studied the computer simulation of steady polymer melt spinning including inertial and air drag effects and fluid viscoelasticity described by Phan-Thien and Tanner's constitutive equation (65) which can be reduced to the convected Maxwell model under certain conditions. Their results were compared with experiments on PET for high speed spinning.

In addition to the differential models just discussed the spinning problem has been also dealt with integral models. Integral models for viscoelastic polymer melts are more a complicated representation of rheological behavior than the differential models. The integral models have several advantages: they can deal easily with discontinuous deformation histories, such as the changes from shear to elongational flow at the exit of a die in melt spinning, and they can easily be generalized

to multiple time constants, as contrasted with having to solve simultaneous differential equations for differential type models. Early studies for integral model were done by Acierno, Dalton, Rodriguez and White (1) and Chen, Hagler, Abbott, Bogue and White (14). These studies mostly involved analysis of the spinline itself, and a comparison of this analysis with experiments, and did not include the effect of the die flow. Later the effect of die flow was explicitly included by Matsui and Bogue (53) who followed the kinematics from the die flow into the spinline. Their generalized integral stress equation (as given in Appendix B) was used in the present work.

An asymptote to the more complicated viscoelastic analysis is the simple isothermal Newtonian solution, in which one assumes that the viscosity of the fluid is independent of shear rate. The result is

$$v_x = v_o e^{kx}$$

where $k = \frac{F}{3\eta w}$, F is the rheological force, η is the viscosity and w is the mass rate. The details are shown in Appendix A.

The details are shown in Appendix A.

A differential viscoelastic analysis due to Zeichner (92) and later modified by White and Ide (84) is easily presented and instructive. They started with

$$\tau\left(v_1 \frac{\partial P}{\partial x_1} - 2P_{11} \frac{\partial v_1}{\partial x_1}\right) = 2G\tau \frac{\partial v_1}{\partial x_1} - P_{11} \qquad \text{(II-12)}$$

$$\tau\left(v_1 \frac{\partial P_{22}}{\partial x_1} + P_{22} \frac{\partial v_1}{\partial x_1}\right) = -G\tau \frac{\partial v_1}{\partial x_1} - P_{22} \qquad \text{(II-13)}$$

$$F = \sigma_{11}\pi R^2 = (P_{11} - P_{22})\pi R^2 = (P_{11} - P_{22})\frac{Q}{v} \qquad \text{(II-14)}$$

By rearranging the above three equations and assuming $P_{11} >> P_{22}$, they obtain

$$\tau\left(v_1 \frac{d}{dx_1} \frac{Fv_1}{Q} - 2 \frac{Fv_1}{Q} \frac{dv_1}{dx_1}\right) = 2G\tau \frac{dv_1}{dx_1} - \frac{Fv_1}{Q} \qquad \text{(II-15)}$$

After rearranging this becomes

$$\frac{F}{Q}\left(\frac{1}{\tau} - \frac{dv_1}{dx_1}\right) = 2G \frac{d \ln v_1}{dx_1} \qquad \text{(II-16)}$$

Ide-White modified above Zeichner's result using the Bogue-White constitutive assumption for the time constant

$$\tau = \frac{\tau_o}{1 + b\tau_o II_d^{1/2}} \qquad \text{(II-17)}$$

where b is an arbitrary parameter and II_d is the second invariant of the rate of deformation tensor. Finally Ide and White obtained

$$\frac{F}{Q}\{x_1 + (\sqrt{3b} - 1)\tau_o [v_1(x_1) - v_1(0)]\} = 2G\tau_o \ln \frac{v_1(x_1)}{v_1(0)} \qquad \text{(II-18)}$$

Another differential model which is easily understood was presented by Petrie (63) who used the Zaremba time derivative and obtained

$$P_{11} + \tau v_1 \frac{\partial P_{11}}{\partial x_1} = 2G \frac{\partial v_1}{\partial x_1} \qquad \text{(II-19)}$$

$$P_{22} + \tau v_1 \frac{\partial P_{22}}{\partial x_1} = -G\tau \frac{\partial v_1}{\partial x_1} \qquad \text{(II-20)}$$

which, combined with Equation II-14, gives

$$\frac{F}{Q}\left[v_1 + \tau V_1 \frac{\partial v_1}{\partial x_1}\right] = 3G\tau \frac{\partial v_1}{\partial x_1} \qquad \text{(II-21)}$$

or

$$\frac{F}{Q}\left(\frac{1}{\tau} + \frac{dv_1}{dx_1}\right) = 3G \frac{d \ln v_1}{dx_1} \qquad \text{(II-22)}$$

This result is very similar to Zeichner's result, Equation II-16, except for the sign before $\frac{dv_1}{dx_1}$. An interesting point made by Petrie is that viscoelastic fluid leads to a more rapid draw down than a Newtonian fluid. Other relationships between the various analyses will be discussed in the next chapter.

C. Unsteady Spinning Including Draw Resonance

Periodic diameter variations often occur in melt spinning operations, the source of which may or may not be identifiable with instabilities in the spinline. A special case of such variations known as "draw resonance" involves a certain type of stability analysis involving the dynamics of the spinning process. The theoretical and experimental aspects of this problem will be reviewed here. This effect was first observed in 1962 by Christensen (15), in a discussion of coating wire with polypropylene; a non-uniformity of gauge or coating weight was

observed. This phenomenon has since been investigated by many researchers, both experimentally and theoretically. Experimental results were reported by Bergonzoni and DiCresce in 1966 (5), Han et al. in 1972 (31), Donnelly and Weinberger in 1975 (20), Vassilatos in 1975 (78), Ishihara and Kase in 1976 (44), Blyler and Gieniewski in 1979 (9), Han and Apte in 1979 (35), Minoshima, White and Spruiell in 1979 (56), and Chang and Denn in 1979 (11) and 1980 (12). Theoretical analyses were reported by Kase et al. in 1966 (48), Pearson and Matovich in 1969 (61), Gelder in 1971 (27), Shah and Pearson in 1972 (62), Ishihara and Kase in 1975, 1976 (45,46), and Fisher and Denn in 1975, 1976 (23,24). A review by Petrie and Denn (62) gives a summary of the draw resonance literature up to 1976. Some of the important results cited there and also some more results will now be summarized.

The first theoretical analyses were carried out independently by Kase et al. (47) and by Pearson et al. (60) for isothermal spinning of a Newtonian fluid. They do not include inertial, gravitational and surface tension effects, all of which may usually be neglected for melt spinning. They use the following as their starting equations (60):

$$\frac{\partial(a^2)}{\partial t} + \frac{\partial(va^2)}{\partial x} = 0 \quad \text{(continuity)} \tag{II-23}$$

$$\frac{\partial\left(a^2 \frac{\partial v}{\partial x}\right)}{\partial x} = 0 \quad \text{(force)} \tag{II-24}$$

where $a(x,t)$ is the radius and $v(x,t)$ is the velocity as the fiber moves down the spinline in the direction x. A linear perturbation analysis is done by introducing perturbations on the form.

$$v(x,t) = \bar{v}(x)\ (1 + \beta(x,t)) \qquad \text{(II-25)}$$

and

$$a(x,t) = \bar{a}(x)\ (1 + \alpha(x,t)) \qquad \text{(II-26)}$$

A search for conditions where α grows yields a critical draw ratio of 20.21. Below the critical ratio, disturbances are damped out; above it, they grow in unbounded fashion. Recent non-linear theory by Ishihara and Kase (43) produces bounded periodic variations. A quite different approach based on the competition between a "throughput wave" velocity and the actual material velocity has been presented by Hyun (36), who predicts a critical draw ratio of 19.74, which is close to that obtained by the classical method of hydrodynamic stability theory. There has recently been a strong criticism of Hyun's theory by Denn (18), which was rebutted by Hyun (38). The connection (if any) between the appoaches is not currently resolved.

The first analysis was done for a Newtonian fluid but later extended to a viscoelastic liquid by Fisher and Denn (25), using a convected Maxwell model with a power law viscosity. The critical draw ratio depends on the power law parameters n and a viscoelastic parameter (a kind of Weissenberg number) defined by

$$\alpha = \frac{3^{\frac{n-1}{2}} K}{G} \left(\frac{V_o}{L}\right)^n \qquad \text{(II-27)}$$

where K is a constant defined in power law viscosity function, G is an elastic shear modulus, V_o is the velocity at the maximum die swell and

L is the length of the melt zone. The result is shown in Figure II-2, for D_R and $\alpha^{\overline{n}} \sim 0.1$ where D_{Rcr} is the critical draw ratio begins to increase, indicating a stabilizing* effect of elasticity and shortly thereafter the stability envelope turns back on itself, indicating a region of stability at high draw ratio under isothermal spinning conditions.

The stability of the non-isothermal spinning of inelastic liquids was studied by Shah and Pearson in 1972 (69) and by Kase in 1974 (48). In their analyses of the non-isothermal case, the model involves one relaxation time with an Arrhenius type temperature dependence; such formulations do not allow one to consider solidification at a transition temperature.

Important recent papers which describe experimental results are those of Blyler and Gieniewski (8,9). In this work draw resonance was generated in an experimental fiber spinline under a variety of imposed conditions. It was found that a necessary condition for draw resonance was a tensile viscosity which failed to increase strongly along the spinline. In this situation a dynamic instability is initiated, characterized by a localized thinning of the filament at the position of maximum axial velocity gradient. A periodic fluctuation of filament diameter

---

*Throughout the dissertation, the phrases "more stable" or "stabilizing" will be used to mean a delayed onset of draw resonance (i.e., draw resonance starting at a high draw ratio) and "less stable" or "destabilizing" for the reverse case. Severity of draw resonance (i.e., the amplitude of the fluctuation) will be denoted by that term.

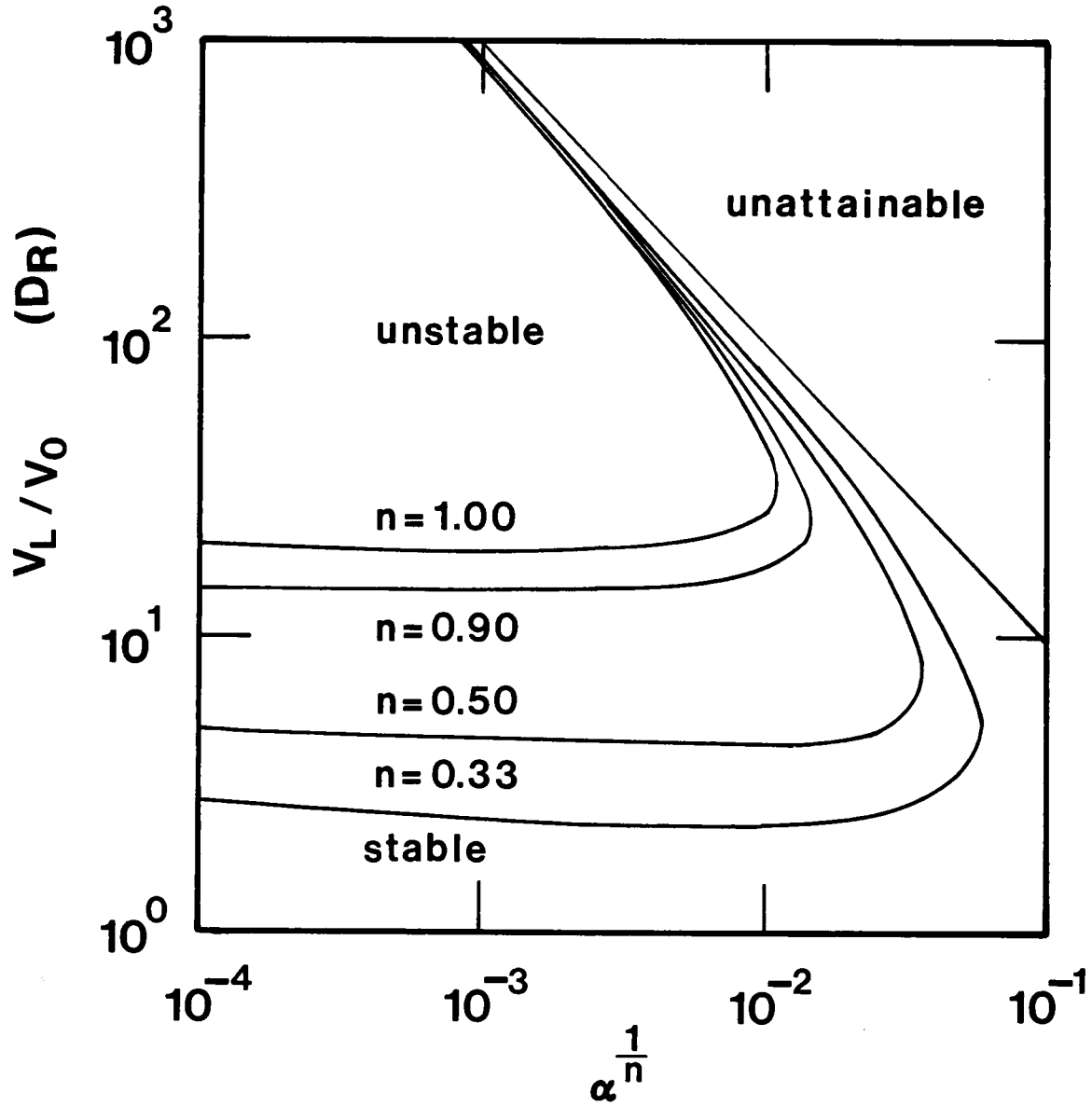


Figure II-2. Critical draw ratio as a function of viscoelastic parameter and power law index (from Fisher and Denn).

was set up, providing the fluid mass accumulating upstream reaches the point of maximum filament thinning prior to rupture. The dependence of period and amplitude on various operating parameters was described. Also ways of eliminating the instabilities were discussed by changing melt temperature and the ambient axial temperature profile along the spinline.

Han and Apte (35) investigated the effects of molecular structure and cooling conditions of the severity of draw resonance using viscoelastic materials (high density polyethylene, polypropylene, and polystyrene), and almost Newtonian behavior materials (nylon-6 and polyethylene terephthalate). They found that the severity of draw resonance depended on the molecular structure and the way the molten threadline was cooled. For viscoelastic materials, cooling "destabilized" the molten threadline outside the isothermal chamber (meaning that cooling gave to rise to more severe diameter fluctuations above the critical draw-down ratio). It should be noted that theoretical predictions deal with stability, that is, with the breakdown of a steady flow, while severity is a measure of the magnitude of fluctuations after the instability starts.

Minoshima, White and Spruiell (55) reported that they observed two types of diameter fluctuations during spinning of polypropylene. One of these was random in character and seems to occur to varying extents under all spinning conditions in which the threadline was drawn down. And second type of diameter fluctuation had a well-defined wavelength or period and a much larger amplitude. They also reported that narrowing the molecular weight distribution stabilized the spinline relative to both random disturbances and draw resonance.

Chang and Denn (11) carried out an experimental study of continuous isothermal drawing (spinning) of a Newtonian and a viscoelastic liquid. They reported that a draw resonance instability occurred in accordance with predictions from stability theory for the Newtonian liquid and for the viscoelastic liquid at slow throughputs, but a delay in the onset of draw resonance at high throughputs of the viscoelastic liquid cannot be explained in the context of existing theory. Recently Chang and Denn (12) studied the sensitivity of the stability of isothermal melt spinning using Phan-Thien's two parameter constitutive equation. Due to a shear thinning structure they did not obtain a second stable region which is the result of Fisher and Denn (23) at high draw ratios. Also Chang, Denn and Geyling in 1981 (13) studied the stability of continuous isothermal drawing of a Newtonian fluid, taking inertial, surface tension, and gravitational effects into account. Their results agreed qualitatively with experiment, that is, gravity stabilizes the spinline while surface tension destabilizes it.

Petrie and Denn (62) in their review paper concluded that the broad outlines of the draw resonance problem are now understood in the sense that many experimental observations can be explained qualitatively with existing theory. There is no dispute, theoretical or experimental, that cooling should suppress the severity of draw resonance in the case of Newtonian fluids, but there is some dispute in the case of viscoelastic fluids. The theory says that cooling is usually stabilizing (except in certain limits); however, several groups, in particular Han and coworkers (31), have shown that spinning into an isothermal chamber

and that the length of the die has an effect on the severity of draw resonance (34). Also Matsumoto and Bogue (51) have shown that certain observations cannot be explained with the existing theoretical framework, specifically the destabilizing effect of certain cooling histories in the case of polystyrene and the destabilizing effect of short dies (presumably a die swell effect) in case of polypropylene. And also Chang and Denn (11) could not explain a delay in the onset of draw resonance at high throughputs in the context of existing theory. Matsumoto and Bogue suggested that there is a complicated rheological interplay between cooling and deformation rate, especially near the glass transition temperature T_g. Also they suggested that the competitive relaxation and cooling processes in the die swell region and the thin region just below it were the ingredients of a new kind of draw resonance theory.

D. Die Swell

When viscoelastic liquids (as well as Newtonian fluids in creeping flow) emerge from a die, they expand, an effect usually known as "die swell" (also known as the "Barus effect" or "extrudate swell") (81). Die swell is described in terms of the swelling ratio.

$$B = \frac{d}{D} \qquad \text{(II-28)}$$

where d is the extrudate diameter and D is the capillary diameter. There have been many attempts to develop theoretical equations for die swell or to correlate it with other rheological properties. The many

theoretical and experimental references concerning this phenomenon will now be reviewed.

Die swell theories can be broadly divided into several categories. The first is a high momentum flux type theory as first presented by Metzner, Houghton, Sailor and White (14). Their derivation is valid for dilute polymer solution at high Reynolds numbers but is not applicable to polymer melts since the momentum flux is negligibly small compared with the rheological forces.

The second is an elastic type analysis. Spencer and Dillon (73) calculated die swell from the solid-like recovery of shear stress. Nakajima and Shida (58) assumed that die swell originated not in shear stress, but in normal stress differences in the capillary; later Bagley and Duffey (2) proposed a similar result. Graessley et a. (30) calculated the flow through a capillary. Later Vlachopoulos et al. (80) obtained a result similar to that of Graessley et al. (30) based on the recoverable shear strain on the wall.

The third kind of analysis starts with a viscoelastic formulation, although many become finally an elastic analysis because only instantaneous swell (and not delayed swell) effects are included. Such an analysis is the original one due to Tanner (74), who considers a recovery at the die exit to balance the viscoelastic stresses developed in the shear flow in the die; because the latter flow is nonhomogeneous, an arbitrary averaging across the radius must be introduced. He obtained the instantaneous die swell.

$$B = \left[1 + \frac{1}{2}\left(\frac{N_1}{2\sigma_{12,w}}\right)^2\right]^{1/6} \qquad \text{(II-29)}$$

where $N_1 = \sigma_{11} - \sigma_{22}$ and $\sigma_{12,w}$ is the shear stress at the wall. Tanner (75) and Tanner et al. (59) used a finite element method to compute the swell of a Newtonian jet at very low Reynolds numbers and they found a good agreement between the computed swelling of about 13% and earlier experimental values. Therefore Tanner suggested a modification to equation II-28 by a simple addition of a correction term 0.1,

$$B = \left[1 + \frac{1}{2} \left(\frac{N_1}{2\sigma_{12,w}} \right)^2 \right]^{1/6} + 0.1 \qquad \text{(II-30)}$$

This seems to give reasonable agreement between predicted die swell and experimental results for polystyrene (80). Tanner's theory for die swell is based on the following assumptions: 1) the liquid is incompressible, 2) the polymer is extruded under isothermal conditions, 3) the die is very long so that die entrance effects can be neglected (in other words the residence time of the melt within the capillary exceeds its memory or characteristic time), 4) inertial, gravity, drag, and surface tension forces can be ignored, 5) recovery far from the die exit can be neglected (that is, the recovery is instantaneous or elastic). White (82) reproduced Tanner's result using a Finger fluid ($\varepsilon = 0$) with a single element Maxwellian relaxation time and assuming a homogeneous flow field. White and Roman (83) expanded it to include a non-zero take-up force,

$$B^6 = [B(0)]^6 - \frac{4\lambda_{eff} F}{\pi D^2 \eta} B^2 \qquad \text{(II-31)}$$

where $B(0)$ is the extrudate swell in the absence of applied force, λ_{eff}

is the effective relaxation time, η is viscosity (both evaluated at the capillary wall), and D is the spinneret diameter.

Another viscoelastic type of analysis using multiple time constants was done by Matsui (52) and Wust (90). Some of the basic ideas are embedded in an analysis done by Lodge (50) who showed that multiple time constants give rise to both an instantaneous and delayed recoil, whereas a single time constant gives only instantaneous recoil. And therefore one would expect that die swell involves both an instantaneous and a delayed portion. Such a result for die swell has in fact been found as a part of a more general analysis first done by Matsui (52). Matsui derived a constitutive equation for the rheological tensile stress σ_{11}, assuming that the velocity distribution in the die is a well developed parabolic or other form and that this flow changes instantaneously to a uniform elongational flow at the die exit (see Matsui and Bogue (52)). If the value of the axial stress is known or if it is taken to be zero (free die swell), Wust (90) was able to show that Matsui's equation predicted die swell. He further developed Matsui's equation and finally obtained the following result

$$B^6 = \frac{(1 + FK_n)\, B^2}{\frac{\bar{\sigma}_{11}}{\sum_n G_n} + B^2}$$

$$= 1 + FK_n - \left(\frac{\bar{\sigma}_{11}}{\sum_n G_n}\right) B^4 \qquad \text{(II-32)}$$

where $FK_n = \dfrac{4\zeta^3\, d\zeta}{(K_n^{-1} + b\zeta)^2}$

$$K = \frac{r\,\bar{V}_n}{R}\,\text{die} \equiv \dot{\gamma}\tau_n\,\text{die}$$

$$\zeta = \left(\frac{r}{R}\right)\,\text{die}$$

The subscript "die" denotes that the variable is to be evaluated in the die, $\bar{\sigma}_{11}$ is the radius-averaged tensile stress, V is the mean velocity in the die, r is the radial distance, R is the die radius. This is similar but not identical to the results of White (82), White and Roman (83) (for zero take-up force) and to Tanner (14). For zero force (i.e., $\bar{\sigma}_{11}$ = 0) and for a Lodge fluid (b = 0), equation (6) reduces to

$$B^6_{(o)} = 1 + FK \qquad \text{(II-33)}$$

$$B^6_{(o)} = 1 + (\dot{\gamma}\tau)^2 \qquad \text{(II-34)}$$

However there is a 1/2 which appears in the previous result (Tanner's theory equation II-28)) but not in Wust's result. The 1/2 appears because of the addition of a lateral shear recovery term in the stress balance. This is not done in Wust's analysis which came from an analysis of melt spinning.

There have been continuing efforts to obtain a rigorous solution of the die swell problem by using a numerical finite element method. Tanner et al. (59) found good agreement between computed die swell for Newtonian fluid and experimental value. The same method was applied to a simple inelastic power law fluid by Tanner et al. (76). Later Reddy and Tanner (67) used this method to predict the die swell for a second-order viscoelastic fluid.

There has been extensive work on the effect of molecular weight and molecular weight distribution (MWD) on the die swell in capillary flow by Graessley et al. (30), Han (33), Mendelson et al. (54), Vinogradov and coworkers (79), and Minoshima, White and Spruiell (56). They concluded that die swell properties were strongly dependent on the MWD. Here at The University of Tennessee Racin and Bogue (66) showed that die swell is very strongly dependent on the molecular weight distribution of polystyrene. By varying shear rate and from the spinneret under isothermal conditions, they attempted to improve the fit with experiment by modifying Tanner's expression. Recently Minoshima, White and Spruiell (56) have reported an experimental die swell study of the influence of molecular distribution of a series of polypropylenes by varying molecular weight and distribution. They reported that narrowing the molecular distribution increased the slope of the elongational viscosity-elongation rate curve and decreases both instantaneous and delayed die swell. A similar MWD effect on the die swell for polystyrene was shown by Racin and Bogue (66).

Most of these die swell studies have involved flow through capillary dies but recently Huang and White (36) reported a comparative experimental study of die swell from long slit and capillary die for rheologically characterized polystrene and polypropylene melts. And also they investigated the die swell of polymer melts from small (length)/(cross section) ratio slit and capillary dies. The experimental results were compared with theories of die swell based on equations similar to equation (II-28) or its analogy for slit dies.

E. Non-Isothermal Melt Spinning

Heat transfer from the fiber to the surrounding medium involves radiation and forced convection mechanisms. Kase and Matsuo (47) derived a heat balance equation as follows:

$$C_p \rho \pi R^2 \left(\frac{\partial T}{\partial t} + V\frac{\partial T}{\partial x}\right) - 2\pi[h(T - T^*) + \sigma\varepsilon(T^4 - T^{*4})] = 0 \qquad \text{(II-35)}$$

where R is the local radius of the filament, h is the coefficient of heat transfer at the fiber surface, T is the local temperature of the fiber, T^* is the environmental air temperature, t is the time, σ is the Stefan-Boltzmann constant, ε is the emissivity, ρ is the density of the fiber and C_p is the isobaric specific heat.

The radiant heat loss is usually very small compared to the convective heat loss; therefore, Equation II-35 becomes

$$V\frac{\partial T}{\partial x} + \frac{\partial T}{\partial t} = \frac{2\sqrt{\pi}h}{C_p A \rho}(T - T^*) \qquad \text{(II-36)}$$

where A is the cross-sectional area. In steady state the time derivative team can be dropped and combined with the mass balance equation

$$Q = \rho VA = \text{constant} \qquad \text{(II-37)}$$

to give

$$\frac{dT}{dx} = \frac{2h\sqrt{\pi A}}{C_p Q}(T - T^*) \qquad \text{(II-38)}$$

There is a problem in obtaining the heat transfer coefficient h at the fiber surface. Kase and Matuso (47) computed the temperature profile

numerically in melt spinning and correlated it by means of the Nusselt number as follows:

$$Nu = \frac{hd}{K} = \frac{2h}{K}\sqrt{\frac{A}{\pi}} \qquad \text{(II-39)}$$

$$Nu = 0.42\ Re^{0.334} \qquad \text{(II-40)}$$

where Re is Reynolds number $(\frac{dV\rho}{\eta})$, K is the thermal conductivity of air, ρ is the density of air, and η is the viscosity of air. From the above Equations II-39 and II-40, the heat transfer coefficient was obtained as follows:

$$h = 0.3875\ (K \cdot \eta^{-0.334})A^{-0.334} \cdot V^{0.334} \qquad \text{(II-41)}$$

Combined with physical properties of air ($K\eta$ - 1.22×10^{-4}) finally the heat transfer coefficient becomes

$$h = 0.473 \times 10^{-4} \cdot A^{-0.334} \cdot V^{0.334} \qquad \text{(II-42)}$$

The heat transfer coefficient was also correlated similarly by Sano and Orii (68) as follows:

$$h \alpha d^{0.67}\ V^{0.33} \qquad \text{(II-43)}$$

Other studies for the heat transfer coefficient were reviewed by White (88).

Later Shah and Pearson (69) formulated another dimensionless group, the Stanton number, which represents the ratio of heat transport from the fiber to the convective heat transfer. They defined the Stanton number as follows:

$$N_{st} = \frac{2\Gamma V_o^{1/6} L\pi^{1/2}}{\rho C_p Q^{1/2}} \qquad \text{(II-44)}$$

where Γ is an empirical constant. Another parameter in non-isothermal spinning is the viscosity dependence upon temperature defined as follows:

$$\chi = \chi(T_o)e^{-KT} \qquad \text{(II-45)}$$

Finally they obtained a single plot of critical draw ratio versus S (where $S = KN_{st}e^{-N_{st}}$), which showed that very large values of the maximum stable draw down ratio were obtained when $S > 1.0$. The value of Stanton number in industrial spinning operations varies between 0.1 and 1.0. Under these conditions increasing the Stanton number increases the spinline stability.

Fisher and Denn (24) in 1977 extended their previous analysis of the mechanics and stability of melt spinning to include the effect of heat transfer between the filament and the surroundings as well as the effect of melt elasticity. Their analysis was restricted to a Maxwell model of fluid viscoelasticity which had a single relaxation time and deformation rate independent viscosity and modulus. They found that cooling inhibited the onset of draw resonance and that the interaction of cooling and viscoelasticity resulted in a stabilization at high Stanton numbers.

Recently George (28) in 1982 developed a model of non-isothermal melt spinning for speeds above which the effects of gravity, inertia and aerodynamic drag became significant. Temperature and velocity profiles were calculated and agreed with experimental data.

CHAPTER III

EXPERIMENTAL EQUIPMENT AND PROCEDURE

A. Materials

The materials investigated were two commercial polypropylene with different molecular weights and different molecular weight distributions, as described in Table III-1.

Table III-1. Polypropylenes Used

	Company	Melt Index	$M_w \times 10^{-5}$	M_w/M_n
PP 6823	Hercules	0.33	4.6	9
PP 106-4	Arco	11.6	2.32	4.7

B. Equipment

A schematic diagram of the present apparatus is shown in Figure III-1 and the experimental set up is shown in Figure III-2. Polymer melt was driven from an Instron Cappillary Rheometer through a die (diameter of 0.058", 0.041", 0.027", 0.019" and die aspect ratios ($\frac{L}{D}$ of 5, 30)), into a long heated chamber (1.0" inside diameter of 1.5 cm, 3 cm, and 6 cm long), which was equipped with wide glass window. Finally the fiber went into an ice-water quench bath as shown in Figure III-1. Two sets of heaters were used to heat the 6 cm long chamber, each of which was controlled by a thermocouple and controller feed back system. The thermocouples were located 1 cm and 4 cm from the die exit for 6 cm long

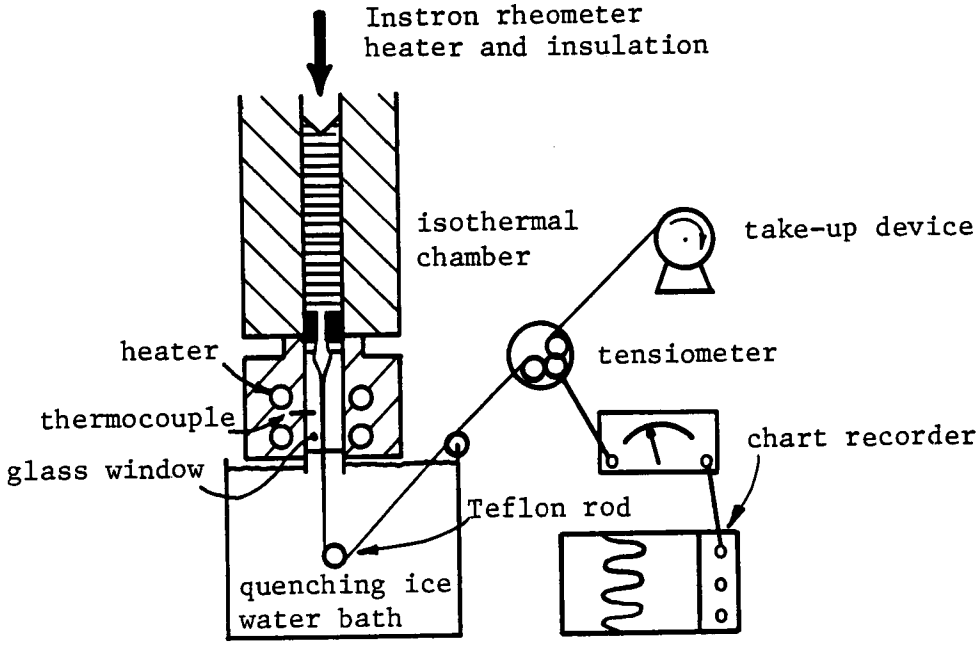
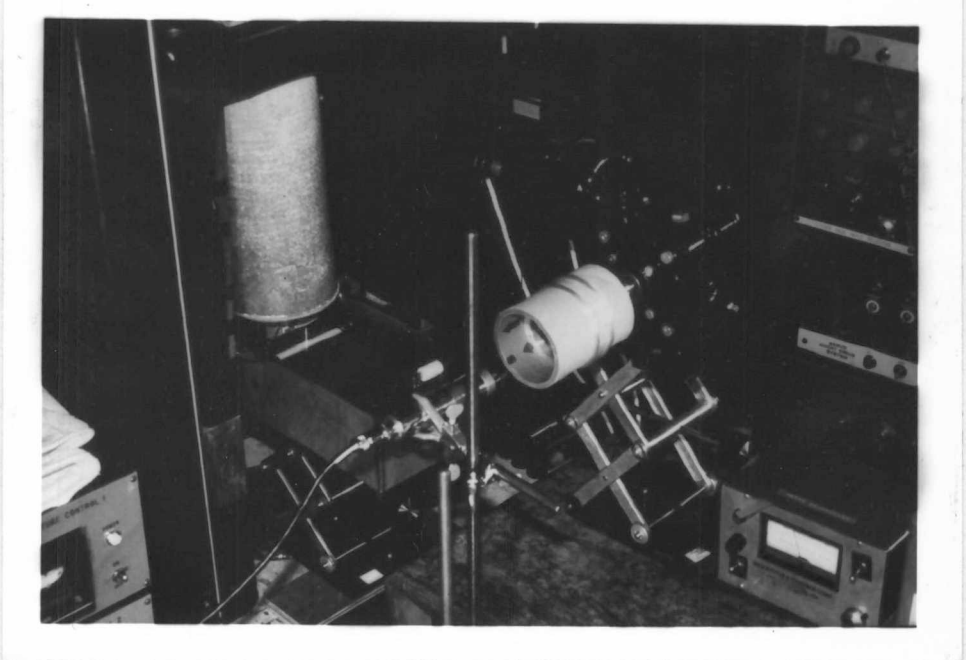


Figure III-1. Schematic diagram of equipment.

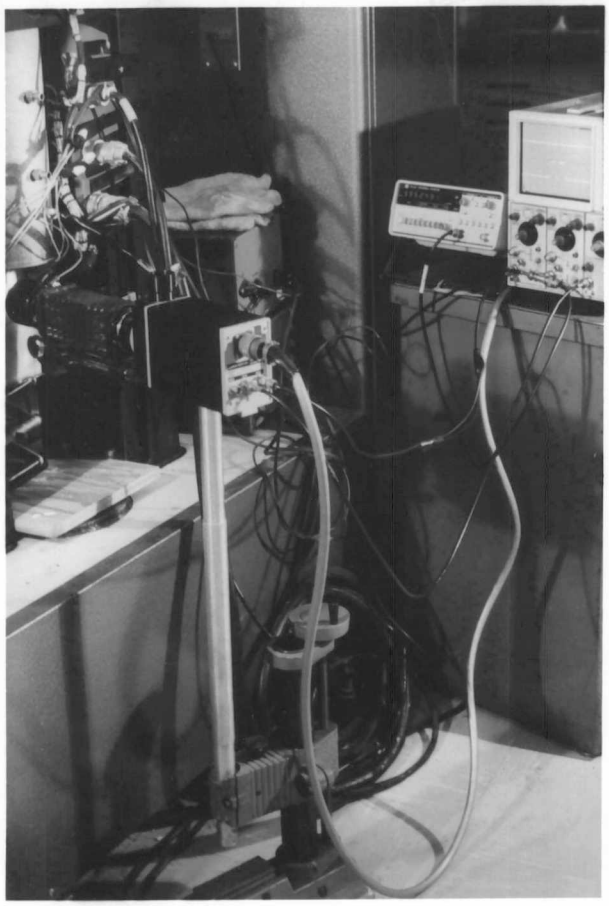


a. Overall view of the apparatus.



b. Close-up of take-up apparatus.

Figure III-2. Experimental set-up of apparatus.



c. Reticon Scan camera, oscilloscope and digital readout.

Figure III-2 (continued)

chamber, one thermocouple at 1.5 cm from the die exit for 3 cm long chamber and one thermocouple at 0.75 cm for 1.5 cm long chamber were used to maintain the temperature 180 ± about 2°C for PP106-4 and 200 ± 2°C for PP6823. One heater set was used for 1.5 cm and 3 cm long chamber.

Not shown in Figure III-1 was a Reticon Line Scan camera (EG&G Reticon, Sunnyvale, Calif., Model LC 100V1024-1 Line Scan camera with lens viewer), which was later added to the equipment to measure the diameter of the spun fiber. This was done by looking through the glass windows, using a strong light source (light from a 35 mm Kodak slide projector) as back lighting. Details of the using of this camera will be discussed in the next section. Other equipment were a Rothschild tensiometer, Strip chart recorder (Model EV-205-11, Heath Co.), a Potentiometric amplifier (Model chart EV-200-01, Heath Co.), and a take-up device with three different speed motors (one 1/15 HP, 1.6 RPM max., the second one 1/15 HP, 12 RPM max., the third one 1/8 HP, 345 RPM max., all B and B motors with tachometers).

C. Experimental Procedure

In studying the kinematics of melt spinning many process variables were changed in the experimental program. These were 1) throughput rate (by changing the Instron plunger speed), 2) take-up speed, 3) spin length, 4) die diameter, 5) die length, 6) the extension temperature, 7) environmental temperature (isothermal chamber or air temperature). Except for a few qualitative studies on nonisothermal spinning, almost all of the data presented are isothermal spinning, wherein the extrusion temperature is the same as the environment temperature. Polymer melt was forced

through the die and then passed through the isothermal chamber and finally quenched into an ice-water bath. The force was monitored with the tensiometer (100 mV full scale, using 4 g and 40 g measuring head device, depending on spun fiber thickness) for the purpose of monitoring instabilities "on-line." Diameter variations in the finished fiber were also measured with a thickness gauge and it was found that the on-line tensiometer readings gave a reasonable approximation to the magnitude of the diameter fluctuations and almost the same periodicity, as shown in Figure III-3. Note the different scales at the top and bottom.

The use of the tensiometer was to provide an on-line quantitative measure of diameter fluctuations. It was also desired to obtain an absolute measurement of the force, for comparison with theory. Such a measurement is complicated by the presence of frictional forces in the take-up system. To obtain the actual tension, a calibration procedure was carried out by the method done by Mimoshima (56). A weight (0.2, 0.5, and 1 g) was hung on the spun fiber and tension was measured at the same experimental condition. The frictional forces between thread and Teflon rods were measured.

A Reticon Scan camera was connected to two read-out devices, an oscilloscope screen and a digital monitor for detecting the spun fiber diameter. This measurement was made at intervals of 0.7 - 2 mm distance by moving the camera up and down with an elevating device shown in Figure III-2, C. An 18.5 cm long Bellows was extended from a Reticon Scan camera to get a magnification of about 30 with a Tokina variable zoom lens (70 mm, 2.7 ft. focal length, and No. 11 lens opening). The image

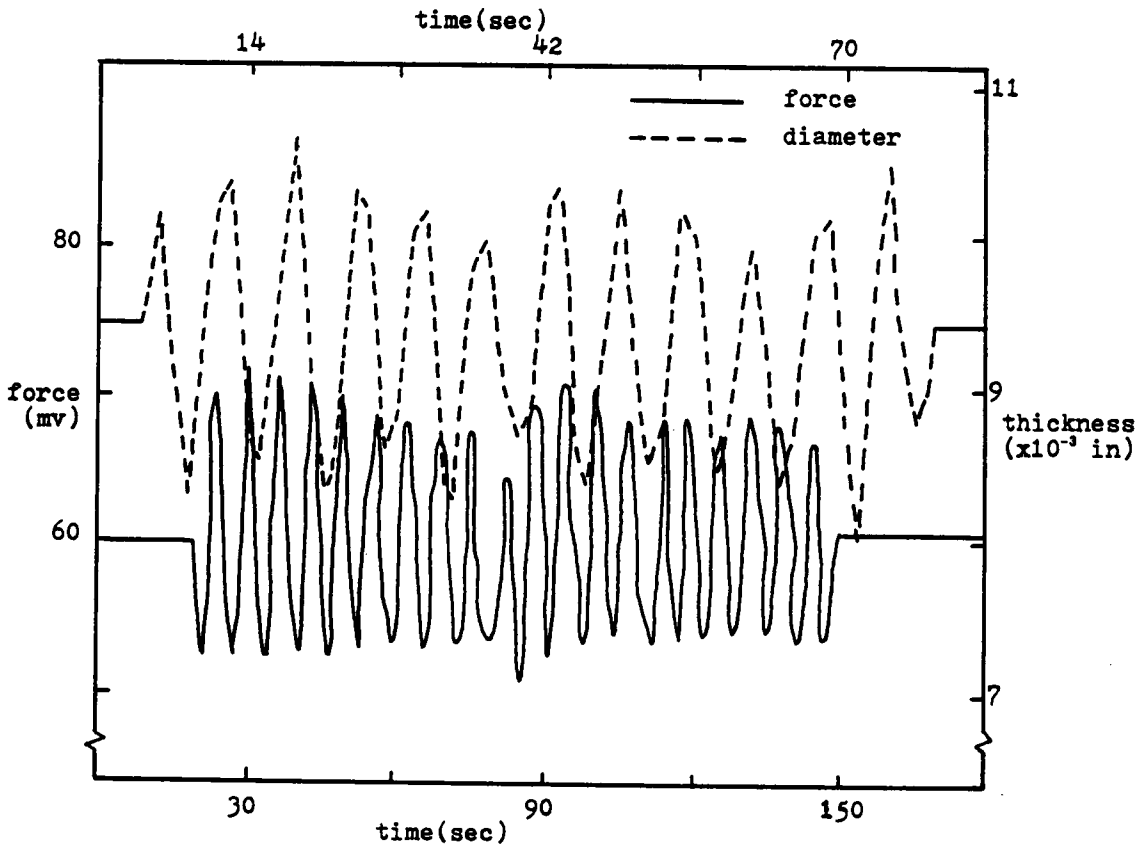


Figure III-3. Typical force and diameter fluctuation during draw resonance.

from the oscilloscope screen was measured with a caliper and compared with the image of known fiber diameter to get the true fiber diameter. There was a problem in using the digital read-out because there was a symmetrical double peak image on the oscilloscope screen due to the transparent fiber in the center. However, it was found by calibration with stationary solid fibers of known diameter that the width across the double peaks (as shown in Figure III-4) is the actual total width of the fiber. The reading speed from a digital read out was controlled by gain control. Two different pigments with concentration of 0.2% (ultramarine blue and black) from Hercules were used to get an image, but this effort was not successful because the dyed polymer melt was not homogeneous. The irregular spun fiber caused more friction on the Teflon guide roll and affected the reproducibility of the onset of draw resonance. But dyeing the polymer melt was very helpful in measuring the die swell.

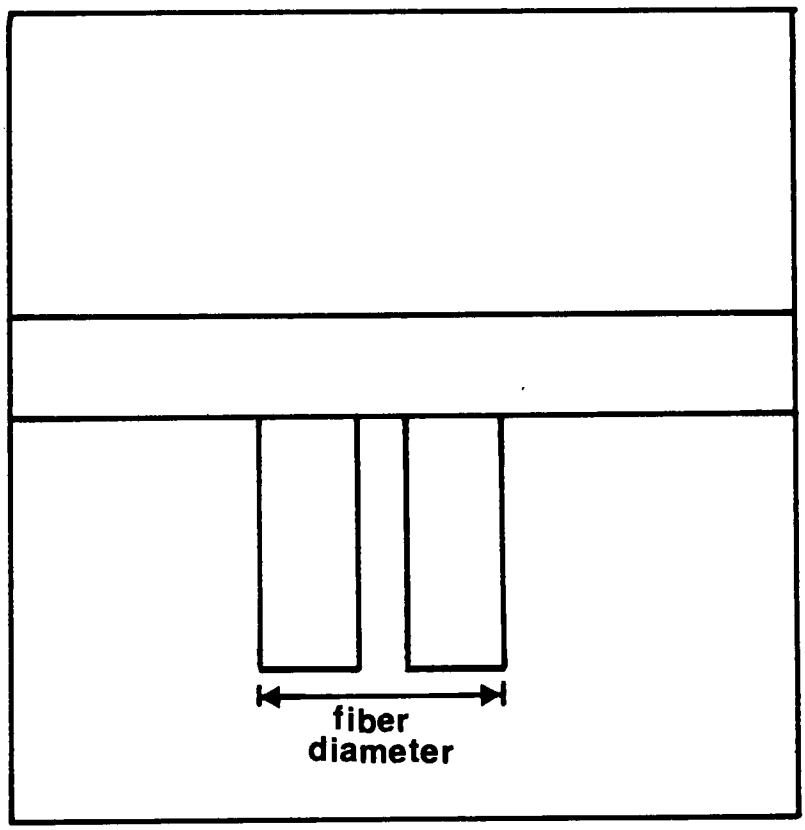


Figure III-4. Typical double peak image of the fiber on the oscilloscope screen.

CHAPTER IV

PRESENTATION AND ANALYSIS OF RESULTS: STEADY SPINNING

A. Theoretical Analysis

The general analysis presented in Appendix B includes both the velocity development along the spinline and also the velocity change exactly at the die exit (that is, the die swell problem). Because the literature on the spinline is separate from the literature on die swell (although the results of the present work indicate that they should be connected), these two different problems will be discussed separately.

Die Swell

Wust (90) reduced Matsui's general equation and obtained a result for the die swell, as shown in Equations II-31 and II-32. In dimensionless variables ϕ and γ^* ($\phi = \frac{F}{\pi R_0^2 G}$, $\gamma^* = \tau\dot{\gamma}$) this equation becomes:

$$B^6 = 1 + \gamma^{*2} - \phi B^2 \qquad \text{(IV-1)}$$

where B is the swelling ratio with tension. When there is no tension ($\phi = 0$), this equation becomes

$$B(o)^6 = 1 + \gamma^{*2} \qquad \text{(IV-2)}$$

where B(o) is the swelling ratio without tension. Therefore forming the ratio B over B(o) from above Equations IV-1 and IV-2, one obtains

$$\left[\frac{B}{B(o)}\right]^6 = \frac{1 + \gamma^{*2} - \phi B^2}{1 + \gamma^{*2}} \qquad \text{(IV-3)}$$

then

$$\left[\frac{B}{B(o)}\right]^6 = 1 - \frac{\phi B^2}{B(o)^6} \qquad \text{(IV-4)}$$

This is identically the result given by White and Roman (82,, Equation II-36) if one makes a change of symbols as follows:

$$\left[\frac{B}{B(o)}\right]^6 = 1 - \frac{\tau F}{\pi R^2 \eta} \frac{B^2}{B(o)^6} \qquad \text{(IV-5)}$$

Using $\eta = G\tau$, one obtains

$$\left[\frac{B}{B(o)}\right]^6 = 1 - \frac{\phi B^2}{B(o)^6} \qquad \text{(IV-6)}$$

Equations IV-4 and IV-6 are, of course, identical, although the starting points are not. Tanner (74) did a more complete analysis of die swell than that of Matsui and Wust, but the results are similar, differing only by a factor of 2 (see Equation II-8). White and Roman (83) followed Tanner's analysis and obtained the ratio $\frac{B}{B(o)}$. Although the various analyses gave different results for B and B(o) the differences disappeared when the ratio $\frac{B}{B(o)}$ was formed.

Wust's analytical results (89) and the various analyses leading to $\frac{B}{B(o)}$ should agree identically to the computer solutions of the integral equation in Appendix B. This was checked by taking a very small

value of X^* ($X^* = 0.01$), which approximates the situation at the die exit. For various choices of ϕ and V^*, the predictions for B(o) and B were in agreement with the analytical results to three significant figures. This provides a check not only on the mathematical steps but on the computer program.

Velocity Distribution Along the Spinline

Various analytical analyses of steady spinning have been done, as summarized in Chapter II. The more general analyses, such as the Fisher-Denn analysis based on a convected Maxwell model, are not presented in analytical form and therefore cannot be conveniently compared with the computer results. Those that are available in analytical form will be summarized below in terms of the dimensionless groups V^* and ϕ ($V^* = \frac{V_X}{V_o}$, $\phi = \frac{F}{\pi R_o^2 G}$).

Zeichner's Equation II-15 becomes

$$\frac{\phi}{2}[X^* - (V^* - 1)] = \ln V^* \qquad \text{(IV-7)}$$

or

$$V^* = 1 + X^* - \frac{2 \ln V^*}{\phi} \qquad \text{(IV-8)}$$

Figure IV-1 shows his result in general; for $\phi >> 2 \ln V^*$, this equation reduces to

$$V^* = 1 + X^* \qquad \text{(IV-9)}$$

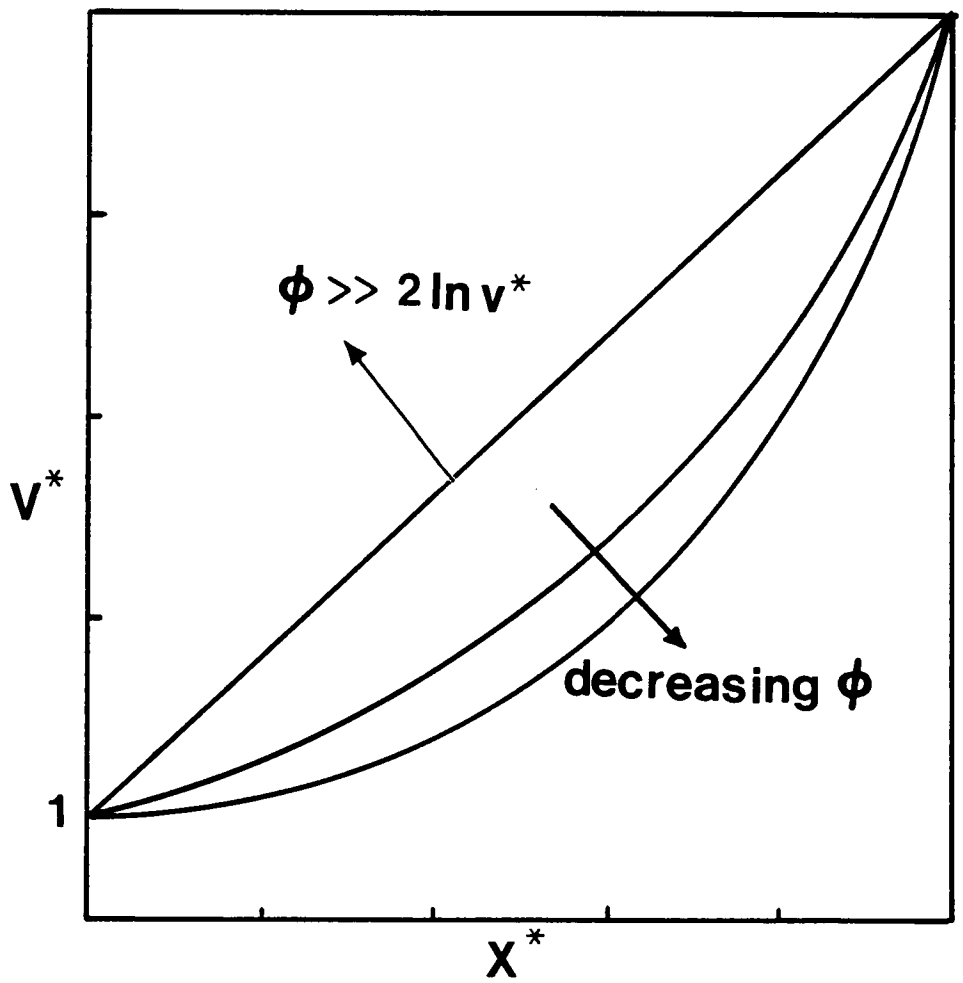


Figure IV-1. Predicted velocity distribution along the spinline.

White-Ide (84) modified Zeichner's equation by introducing the Bogue-White parameter b and obtained the following:

$$\frac{\phi}{2}\left[X^* + (\sqrt{3}b - 1)(V^* - 1)\right] = \ln V^* \qquad \text{(IV-10)}$$

For b = 0 it reduces to Zeichner's equation. Because the Ide-White equation does not reduce to the Newtonian asymptote, the present author arbitrarily modified the Ide-White result by introducing the factor 3 instead of the factor 2 in the first term:

$$\frac{\phi}{3}\left[X^* + (\sqrt{3}b - 1)(V^* - 1)\right] = \ln V^* \qquad \text{(IV-11)}$$

This equation will be referred to as modified White-Ide equation. Petrie's equation (63), based on a Zaremba derivative, is

$$\frac{\phi}{3}\left[X^* - (1 - V^*)\right] = \ln V^* \qquad \text{(IV-12)}$$

One can pass Equations IV-11 and IV-12 to the Newtonian asymptote by imposing the condition $X^* >> |V^* - 1|$:

$$\frac{\phi}{3} \cdot X^* = \ln V^* \qquad \text{(IV-13)}$$

In the present work Equation 9 in Appendix B was solved on the computer by choosing the force (ϕ), the Bogue-White parameter (b), the dimensionless shear rate (γ^*) and the step size (ΔX^*). For example, the step size ΔX^* was 0.2 when the final X^* was 10, and ΔX^* was 5 when the final X^* was 300. The dimensionless radius R^* and the dimensionless velocity V^* are equal to unity at the exit of the die ($X^* = 0$). Then

one guesses at the next R^* and V^* and calculates the dimensionless force (ϕ). If this calculated force is different from the given force, different R^* and V^* are assumed for the next step down until the calculated force equals to the given force. By this repeated process, one can step down the spinline to obtain the velocity distribution V^* or the radius distribution R^* along the spinline.

Some of the results are summarized in Figures IV-2 and IV-3. In Figure IV-2 the computer results are compared with the Zeichner/White-Ide result, the modified White-Ide result, the Petrie result, and finally the Newtonian asymptote. The results pass to the Newtonian asymptote when X^* is large and ϕ is small. Also one sees a shear rate effect at the exit of die (die swell) in Figure IV-2. The results for small X^* are shown in Figure IV-3. These results are compared with the linear asymptote (Equation IV-4), which comes from the analysis of Fisher-Denn (23) and Ide-White (41), and also compared with the Newtonian case. Several points are of interest. By the introduction of various conditions of die shear flow and force, one can reproduce the linear asymptote, although it does not come about (because of the die swell effect) in all possible cases. By these various comparisons confidence was thus gained in the computer solution techniques.

Another interesting result that came from the computer studies was that no solution could be obtained at certain values of X^* under certain conditions. In Figure IV-4, no solution was obtained beyond the points marked with an X. The value of this critical point depends on the Bogue-White parameter b and the dimensionless force ϕ. This

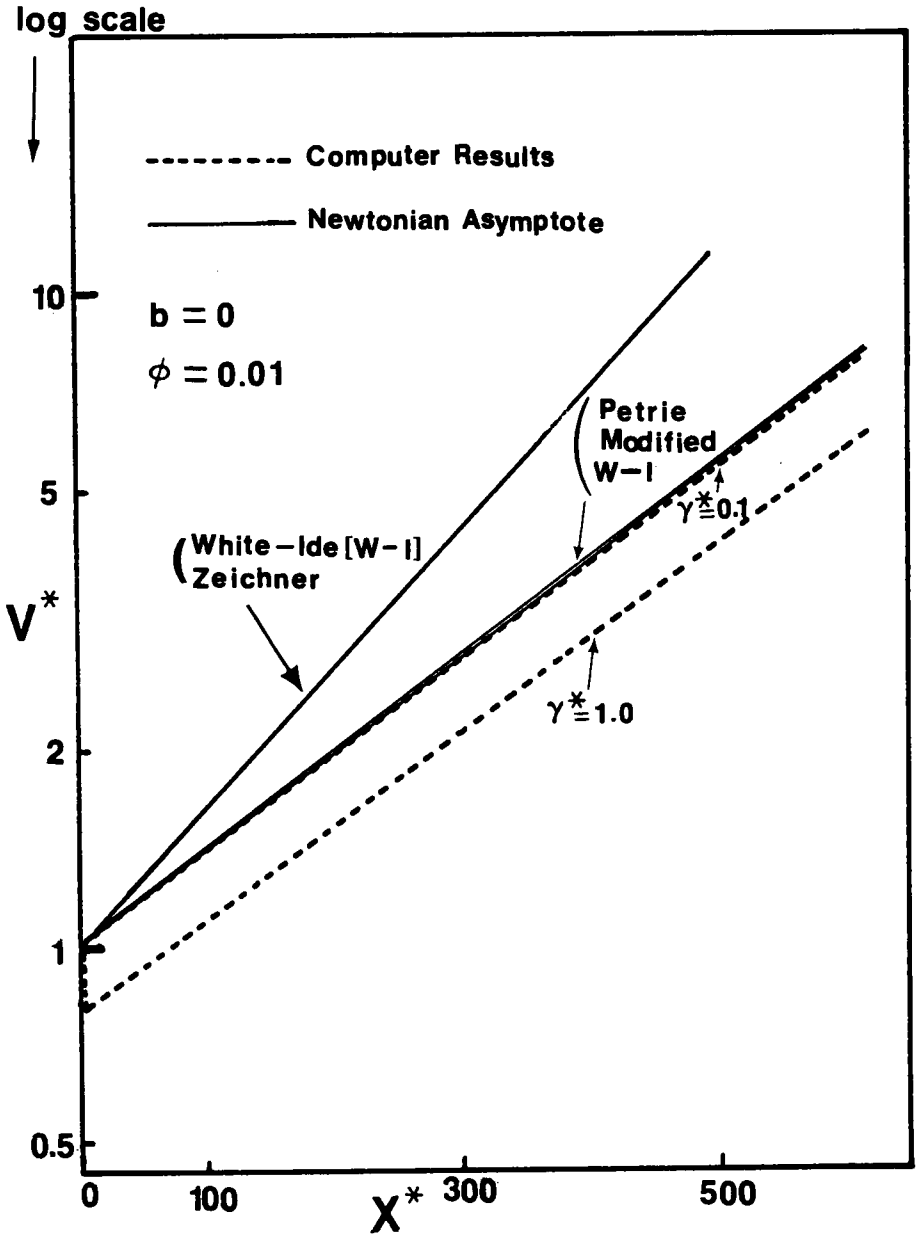


Figure IV-2. Velocity distribution along the spinline for long spin length comparisons of computer results with various analytical results.

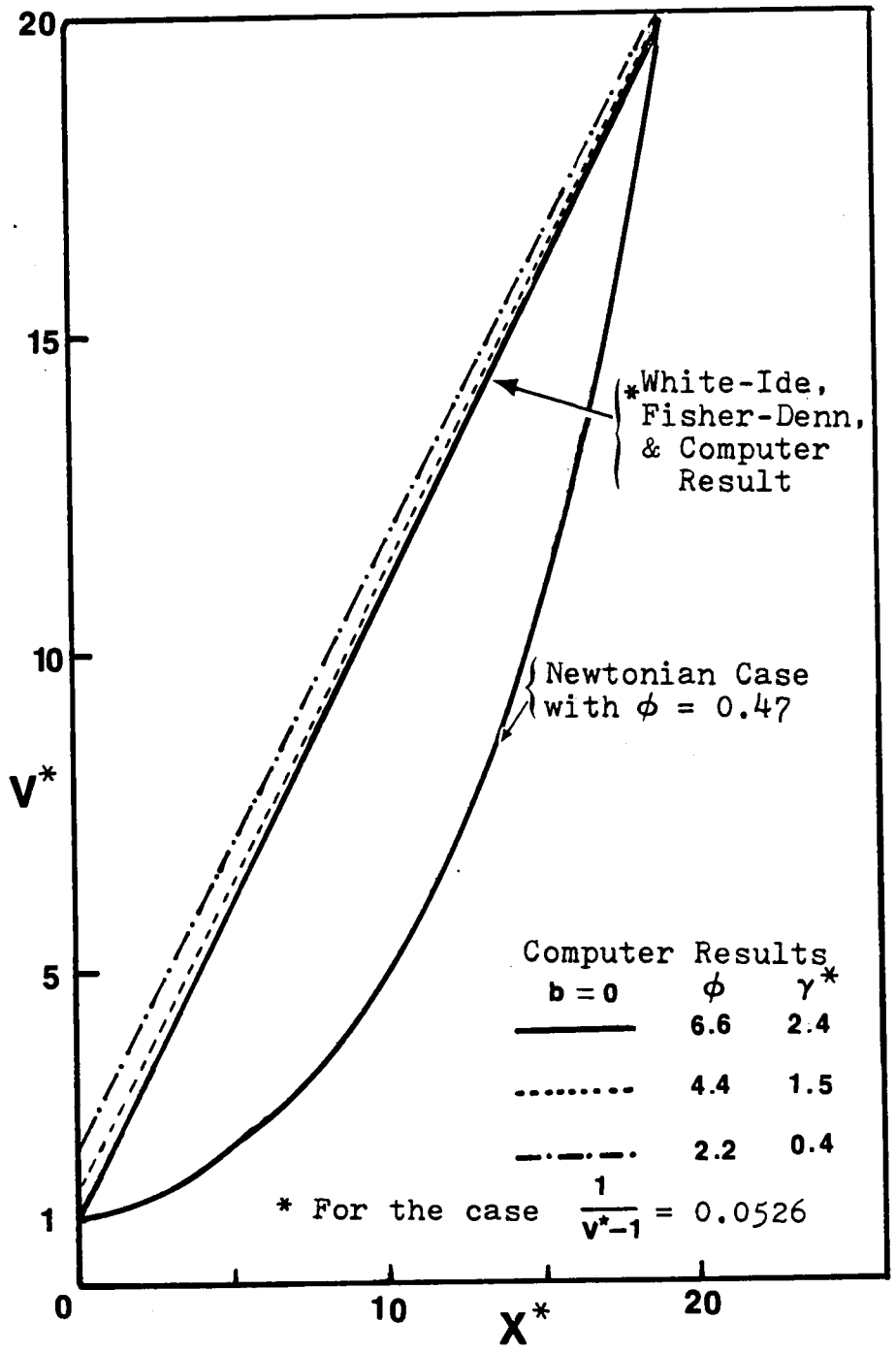


Figure IV-3. Velocity distribution along the spinline for short spin length comparisons of computer results with various analytical results.

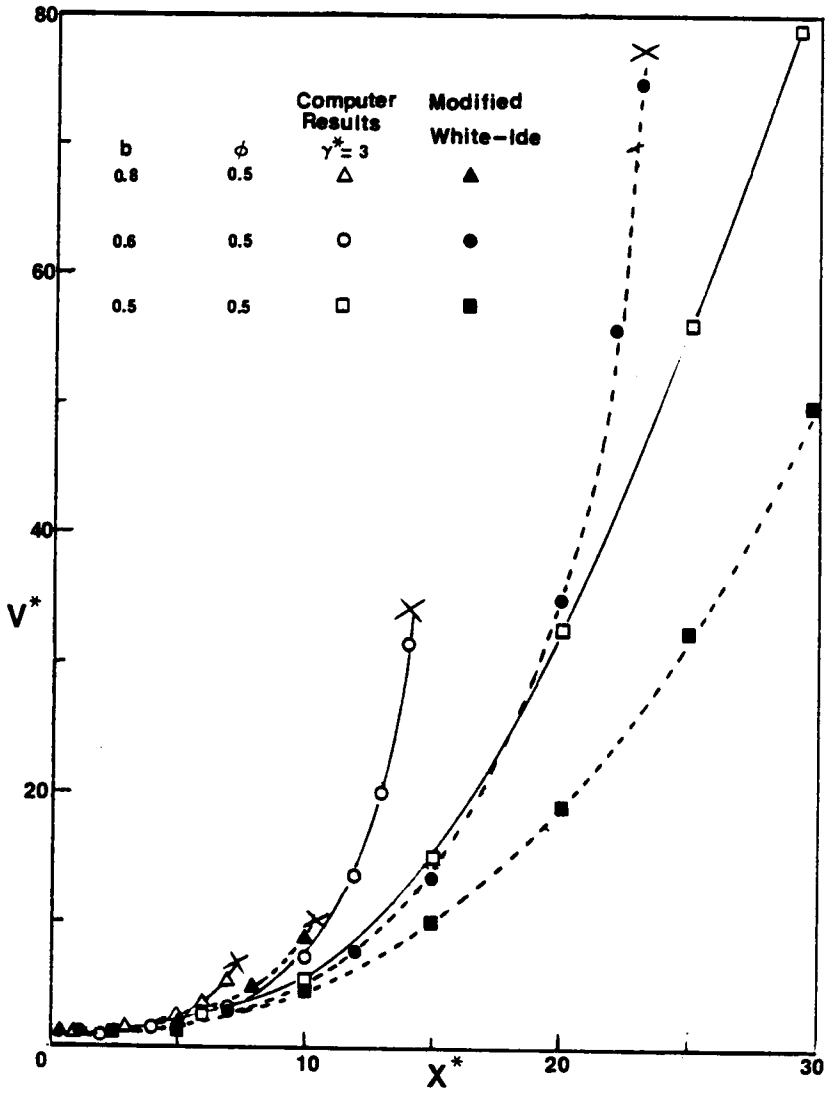


Figure IV-4. Velocity distribution along the spinline (showing the "blow-up point").

result motivated us to look for similar behavior in the Ide-White Equation II-14. Rearranging Equation IV-12, one obtains

$$\phi = \frac{3 \ln V^*}{X^* + (\sqrt{3}b - 1)(V^* - 1)} \qquad \text{(IV-14)}$$

Various force-velocity curves (ϕ vs. V^*) were obtained, depending on the Bogue-White parameter b as shown in Figure IV-5. The appearance of a maximum in this plot leads us to differentiate the force with respect to V^*. Setting the derivative equal to zero ($\frac{d\phi}{dV^*} = 0$), one obtains the maximum force

$$\phi_{max} = \frac{3}{(\sqrt{3}b - 1)V^*} \qquad \text{(IV-15)}$$

The X^* corresponding to ϕ_{max} is

$$X^*_{max} = [V^*(\ln V^* - 1) + 1](\sqrt{3}b - 1) \qquad \text{(IV-16)}$$

Because there is no computer solution of velocity at X^*_{max}, we termed this point the "blow-up point." Thus when the Bogue-White parameter b is less than $\frac{1}{\sqrt{3}}$, the fluid will be spinnable under any conditions as shown in Figure IV-5, although in actual practice, the stress became so high at large V^* that the material would break by a cohesive mechanism. However, when $b > \frac{1}{\sqrt{3}}$, there is a maximum force, which gives several interesting results. The curves in Figure IV-5 were calculated from Equation IV-14.

Another interesting point to be made from Figure IV-4 is that the effect of the die flow has a significant effect well down the spinline.

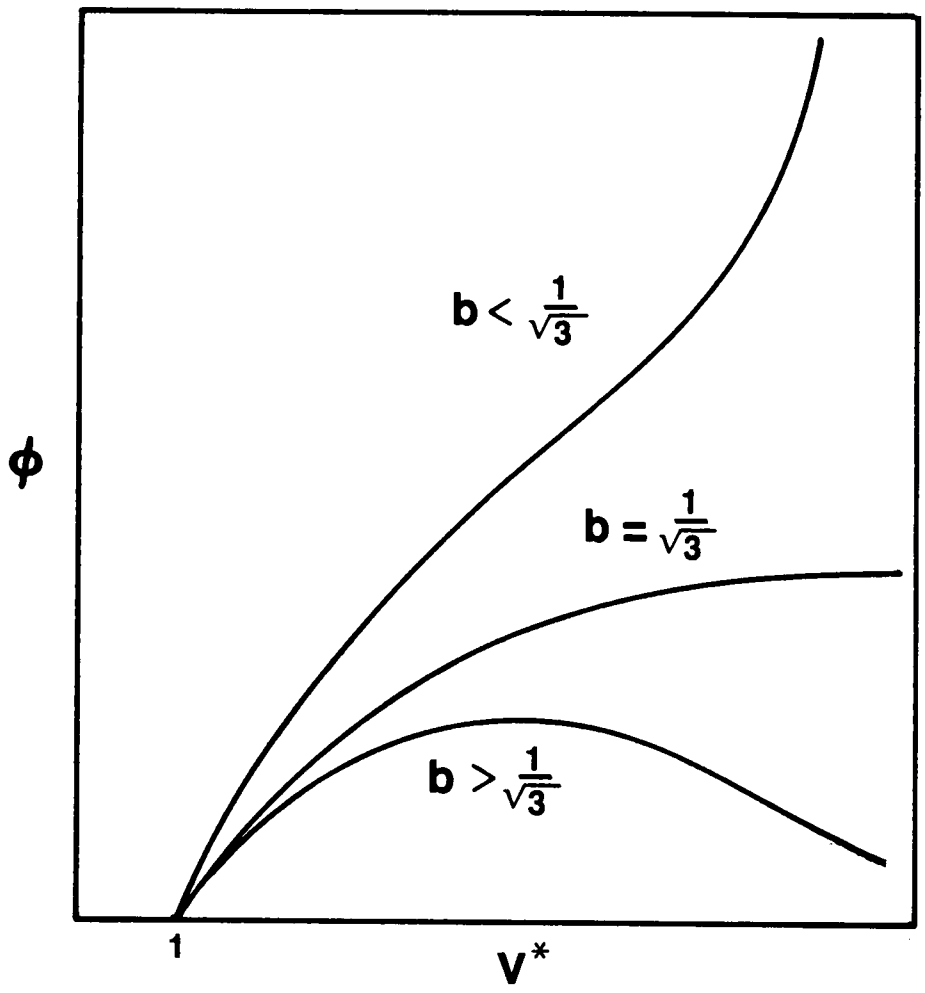


Figure IV-5. Spinline force vs. draw ratio as a function of the parameter b.

That is, if one compares the modified White-Ide results (which contains no die flow effect) with those obtained from the computer (which do contain a die flow effect) one sees noticeable differences far removed from the die exit. This is in contrast with Figure IV-2, where, except for an initial effect due to the die swell, the character of the velocity distribution along the spinline is essentially the same. Thus the die swell (or die flow) problem is related to the entire spinline dynamics for spinning conditions near the "blow-up point."

When the nonlinear parameter b is larger than $\frac{1}{\sqrt{3}}$, double-valued draw ratios V^* are obtained as shown in Figure IV-5. The double-valued behavior can be illustrated in another way by plotting V^* vs. X^* at various values of ϕ as shown in Figure IV-6. As can be seen in the curve marked with squares ($\phi = 0.537$), $\frac{dV^*}{dX^*}$ approaches infinity at the critical X^*. This can be demonstrated analytically by first rearranging the Equation IV-14 to obtain

$$X^* = \frac{3}{\phi} \ln V^* - (\sqrt{3}b - 1)(V^* - 1) \qquad \text{(IV-17)}$$

let $\sqrt{3}b - 1 = K > 0$ since $b > \frac{1}{\sqrt{3}}$. Now differentiating Equation IV-17 with respect to X^* one obtains

$$\frac{dV^*}{dX^*} = \frac{1}{(\frac{3}{\phi}\frac{1}{V^*} - K)} \qquad \text{(IV-18)}$$

The force ϕ in the spinline is constant along the spinline (i.e., ϕ is independent of X^*).

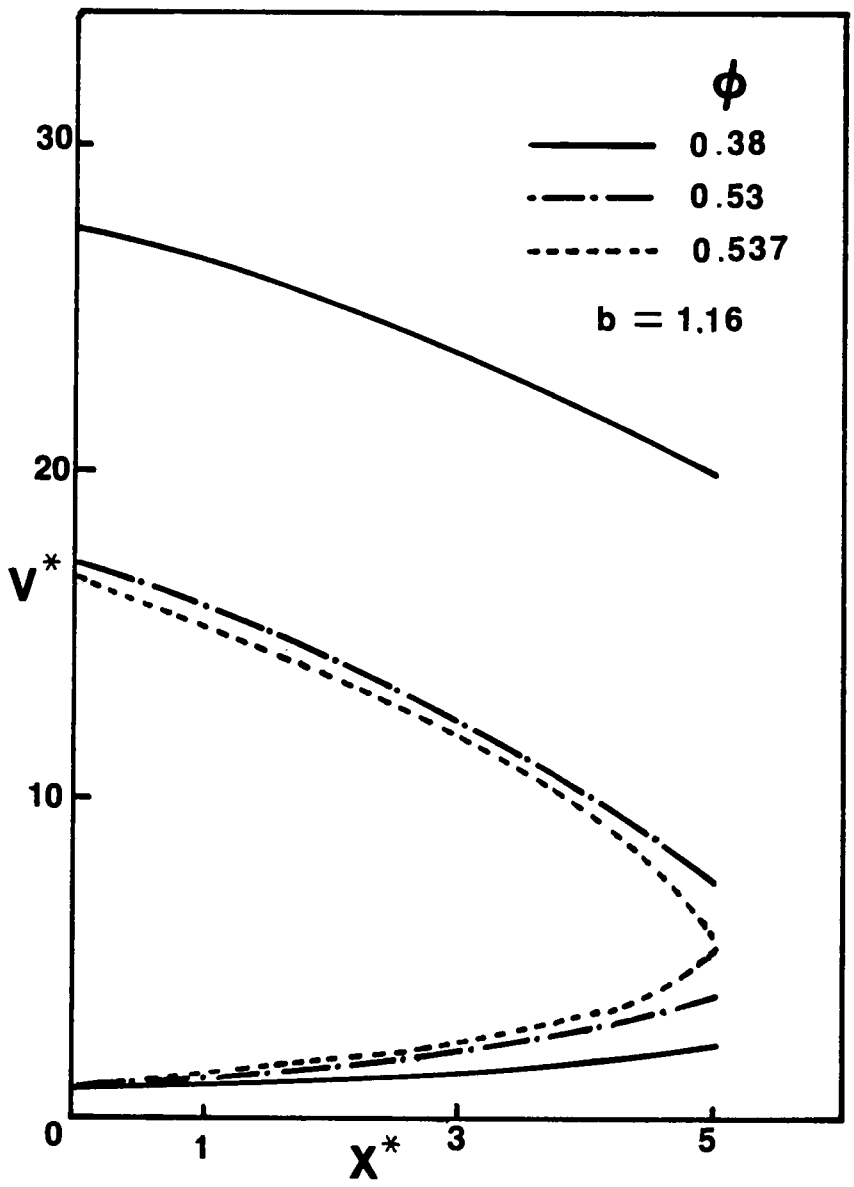


Figure IV-6. Theoretical velocity distribution along the spinline near the condition of the maximum force.

Then the velocity gradient $\frac{dV^*}{dX^*}$ at the maximum force becomes

$$\left.\frac{dV^*}{dX^*}\right|_{V^*=\frac{3}{K\phi^2}} = \frac{1}{K(\frac{\phi}{\phi} - 1)} = \infty \qquad \text{(IV-19)}$$

The denominator is zero, therefore the gradient is infinite at the maximum point ("the blow-up point"); this is associated with incipient ductile failure. This argument will be used in Chapter V for correlating the onset of draw resonance. Also the fact that the upper parts of the curves in Figure IV-6 are not physically realizable will be discussed later.

Evaluation of Material Parameters

The evaluation of the rheological parameters (such as the modulus G, the relaxation times τ, and the nonlinear parameter b) involve fitting the predictions for certain basic response functions to the experimental data. The response functions for which data are available are those for steady shear flow and for dynamic (sinusoidal shear) flows. The theoretical results for these functions are as follows:

For steady shear flow

$$\sigma_{12} = \sum_n G_n \frac{\dot{\gamma}\tau_n}{1 + b\dot{\gamma}\tau_n} \qquad \text{(IV-20)}$$

or

$$\eta = \frac{o}{1 + b\dot{\gamma}\tau_o} \qquad \text{(IV-21)}$$

$$\sigma_{11} - \sigma_{22} = N_1 = 2\sum_n G_n(\frac{\dot{\gamma}\tau_n}{1 + b\dot{\gamma}\tau_n})^2 \qquad \text{(IV-22)}$$

where σ_{12} is the shear stress and N_1 is the first normal stress difference. For dynamic shear flow

$$G' = \sum_n \frac{G_n \omega^2 \tau_n^2}{1 + \omega^2 \tau_n^2} \qquad \text{(IV-23)}$$

and

$$G'' \quad \sum_n \frac{G_n \omega \tau_n}{1 + \omega^2 \tau_n^2} \qquad \text{(IV-24)}$$

where G' is the dynamic elastic modules and G'' is the dynamic loss modulus and ω is the frequency.

In the work of Yamane (91) for PP6823 and of Minoshima (55) for PP106-4, shear stress and normal stress data were presented, from which values for certain parameters were determined. From the zero shear viscosity data and from a certain range of shear rates of interest in the present work (10-1000 sec^{-1} for PP106-4, 1-100 sec^{-1} for PP6823), the parameters b and τ_o were obtained by using Equation IV-21. The first G value was set to about 6×10^5 ($dyne/cm^2$) and then τ_o values were obtained for both polypropylenes (1.25 sec for PP6823 and 0.1 sec for PP 106-4). Roughly speaking τ_o sets the magnitude of the viscosity whereas b sets the shape of it. The results are in Table IV-1.

From the generalized correlations for G' and G'' as presented by Patel (93), three Gs and three τs were obtained for the polymers of this work by using Equations IV-23 and IV-24. These data were fit in the frequency range 10 to 1000 sec for PP106-4 and in the range 1 to 100 sec for PP6823 to an accuracy of about 25%. When the zero shear viscosity

TABLE IV-1. SUMMARY OF RHEOLOGICAL PARAMETERS USED

Polymer	T (°C)	η_o (poise)	b	One element		Three element		A	C
				τ (sec)	G(dyne/cm^2)	τs (sec)	Gs (dyne/cm^2)		
PP6823	200	8.9×10^5	0.9	1.25	7.1×10^5	0.05	6×10^5	1.81×10^{-4}	1.76
						0.5	2.5×10^5		
						5	1.35×10^5		
PP106-4	180	4.8×10^4	0.6	0.1	4.8×10^5	0.01	5×10^5	6.1×10^{-3}	1.48
						0.1	1×10^5		
						1	2.5×10^4		

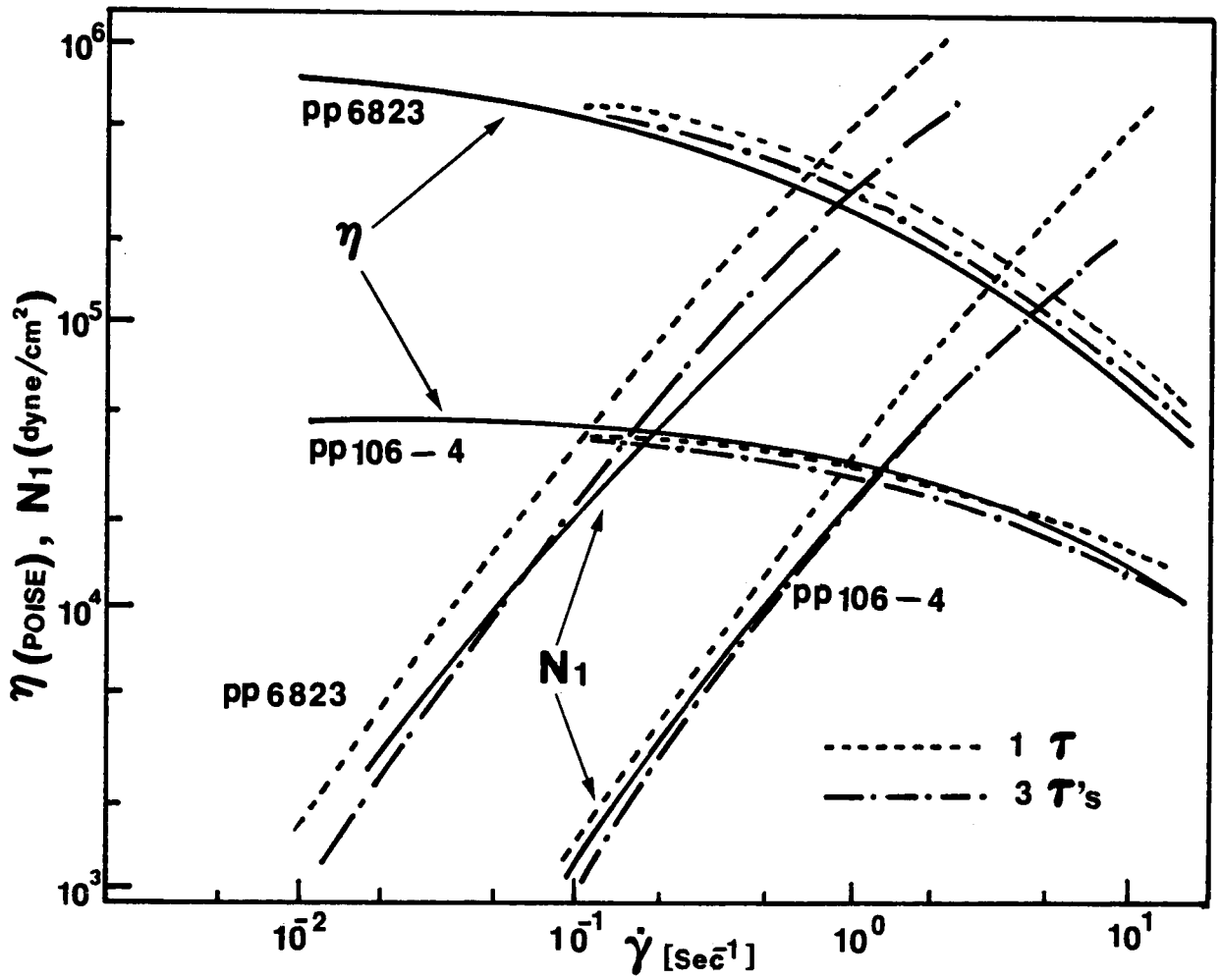


Figure IV-7. Comparison of experimental data and theoretical fits of shear viscosity and first normal stress function.

was calculated with the resulting three Gs and three τs, the accuracy was about 20%. Normal stress data were also considered. Using the Gs and τs and the b of Table IV-1 (either the one element or the three element case), the normal stress data could be fit in the shear rate range 0.1 to 1 to an accuracy of about 25%. The results are shown in Figure IV-7.

There are elongational viscosity measurements for PP6823 by Ide (42) and for PP106-4 by Minoshima (55). The elongational behavior of these two polymers are different as shown in Figure IV-8. For PP6823 of broad molecular weight distribution at low elongational rates, the transient elonational viscosity increases to much more than $3\eta_0$ and then it decreases at higher elongational rates. For PP106-4 of narrow molecular weight distribution, at low elongational rates, the elongational viscosity (χ) increases more gently from $3\eta_0$ to a large value. According to previous workers (42,56,91), the transient elongational viscosity of narrow molecular weight distribution materials measured at low elongational rates achieves a steady state for long periods of time. However, broad molecular weight distribution polypropylenes measured at all elongational rates do not achieve steady state. Some use of the qualitative ideas embodied in Figure IV-8 will be made later. For the purpose of fitting rheological parameters no direct use was made of Figure IV-8 because the Bogue-White model often does not work quantitatively for such data. For example, to obtain an elongational viscosity (χ) that decreases with elongational rate ($\dot{E}$), it is necessary that $b > 1.16$. However, using such a large b value for PP6823 does not give reasonable results for the shear viscosity. Therefore a smaller value ($b = 0.9$) for PP6823 was

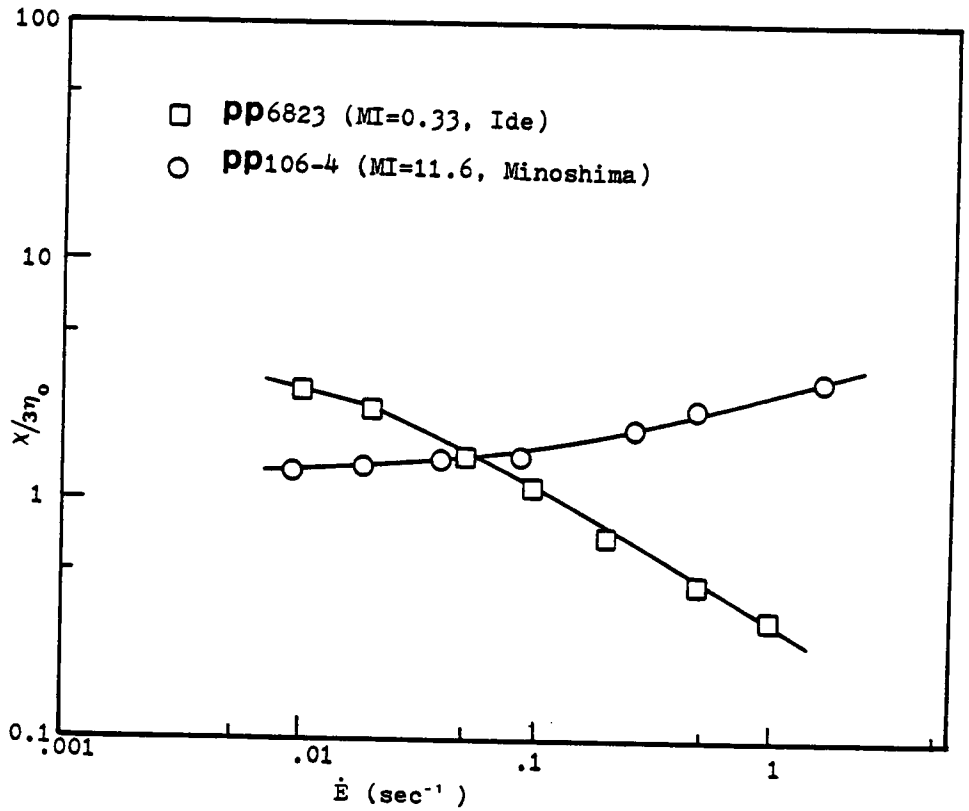


Figure IV-8. Reduced steady state elongational viscosity as a function of elongational rate.

taken for that material. Qualitatively, however, the different elongational behavior of the polymers is reflected in the fact b (0.9) for PP6823 is larger than that (0.6) for PP106-4.

For later use it was found that the dependence of the first normal stress difference N_1 as a function of the shear stress could be fit by the empirical equation as follows:

$$N_{1w} = A\sigma_{12w}^{C} \tag{IV-25}$$

then

$$\frac{d \log N_1}{d \log \sigma_{12w}} = C \tag{IV-26}$$

From the normal stress data, the parameters A and C were obtained as shown in Table IV-1. Then at high shear stress region the normal stress was obtained by extrapolating Equation IV-25.

Later, in connecting with correlating the onset of draw resonance, it was desired to evaluate the total normal stress in the direction of flow in the die σ_{11}, in addition to the difference of normal stress in the die N_1. Rigorously one should use some average of these values across the radius but for simplicity the wall value was selected as being characteristic of the magnitudes of these parameters. One starts with the definition of the total normal stress at the wall (as indicated by subscript "w").

$$\sigma_{11w} = -P_w + \tau_{11w} \tag{IV-27}$$

where σ_{11w} is the total stress, τ_{11} is the extra stress and P is the isotropic stress. From the exit pressure at the wall ($\sigma_{22w} = -P_{Ew}$):

$$-P_{Ew} = -P_w + \tau_{22w} \tag{IV-28}$$

combined with Equation IV-27 and IV-28 gives

$$\sigma_{11w} = -P_{Ew} + N_{1w} \tag{IV-29}$$

From the relationship of ext pressure drop with the first and second normal stress differences as given by White and Kondo (86), one obtains

$$-P_{Ew} = N_{1w} + N_{2w} \tag{IV-30}$$

This equation combined with Equation IV-29 gives

$$\sigma_{11w} = 2N_{1w} + N_{2w} \tag{IV-31}$$

The second normal stress difference N_{2w} is found to be negative and between 0 and -0.5 of the value of N_{1w} (32) and then it can be written,

$$N_{2w} = -\varepsilon\, N_{1w} \tag{IV-32}$$

Combined with Equations IV-31 and IV-32 gives

$$\sigma_{11w} = (2 - \varepsilon)N_{1w} < 2N_{1w} \tag{IV-33}$$

Combined with Equations IV-25 and IV-33, one obtains

$$\sigma_{11w} = (2 - \varepsilon)A\, \sigma_{12w}^{C} \tag{IV-34}$$

Finally a dimensionless σ^*_{11w} was defined

$$\sigma^*_{11w} = \frac{\sigma_{11w}}{G} \qquad \text{(IV-35)}$$

This value will be used in Chapter V and the typical value ε used in the present work is 0.1.

B. Comparison with Experimental Results

Steady spinning data (diameter as a function of position) were measured for both polypropylenes in order to study the near die (die swell) behavior, the tension in the spinline and finally the velocity development along the spinline. The diameter measurements were made with the Reticon Scan video camera, as described in detail in Chapter III. The experiments were carried out using a spin length of 3 cm. The die swell measurements started at less than 0.5 mm from the exit of die and were made in intervals of 1 or 2 mm thereafter. The data so obtained are shown in Figures IV-9, IV-10, IV-11, and IV-12 as the closed symbols.

As expected the die swell for the runs with an applied force (the open symbols) are less than the die swells with no applied force (the closed symbols). In order to fit the die swell data with no applied force, as shown in Figures IV-9, IV-10, IV-11, and IV-12, two different approaches were taken. The first, following Tanner (76), is simply to add 0.12 for PP106-4 and 0.17 for PP6823 in addition to the die swell obtained from the die shear rate calculation. These initial adjustment values varied with molecular weight distribution and this difference of B(o) was observed experimentally. The other approach is to adjust the

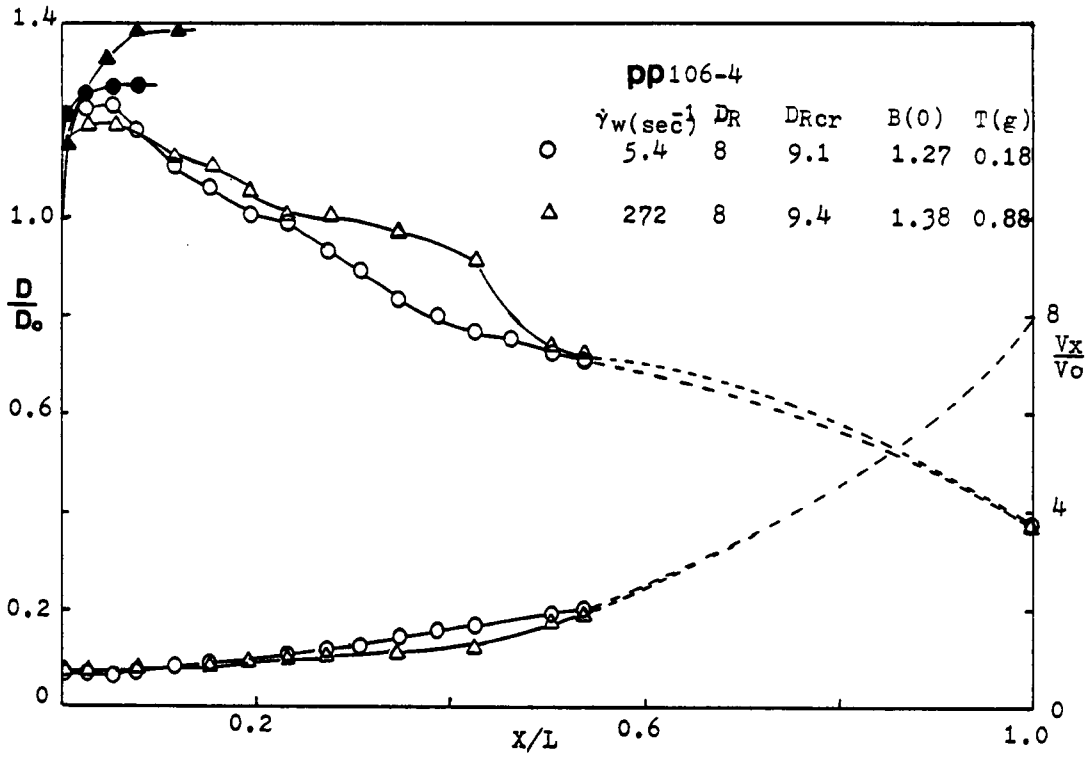


Figure IV-9. Experimental diameter distribution along the spinline (PP106-4 at different shear rates).

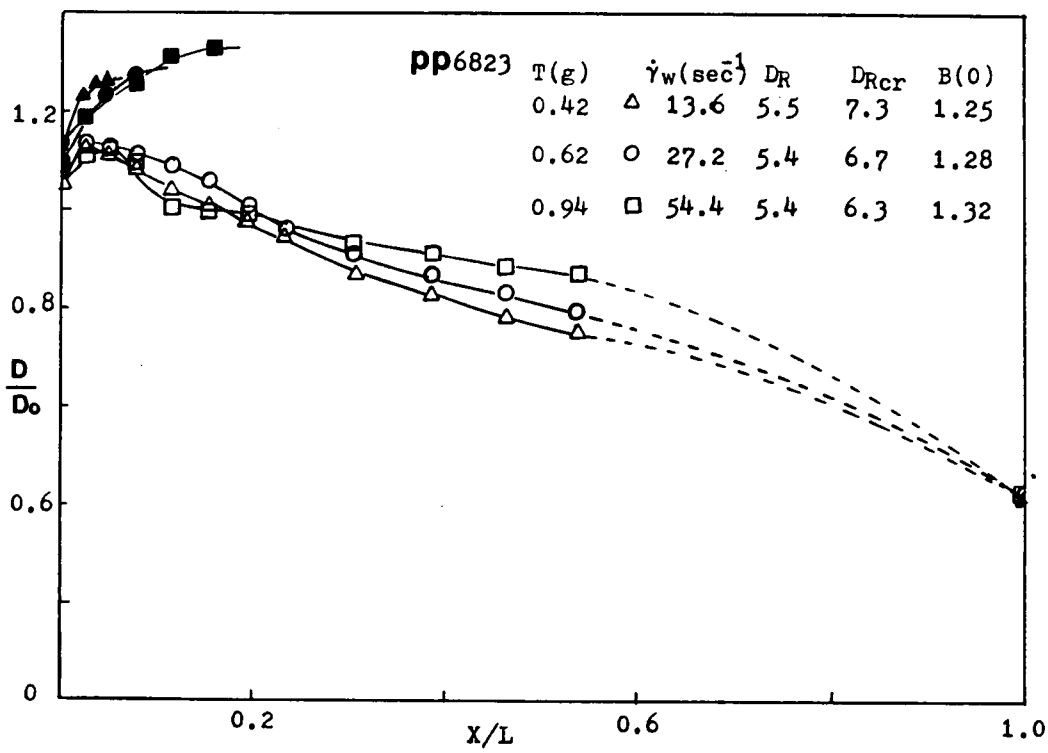


Figure IV-10. Experimental diameter distribution along the spinline (PP6823 at different shear rates).

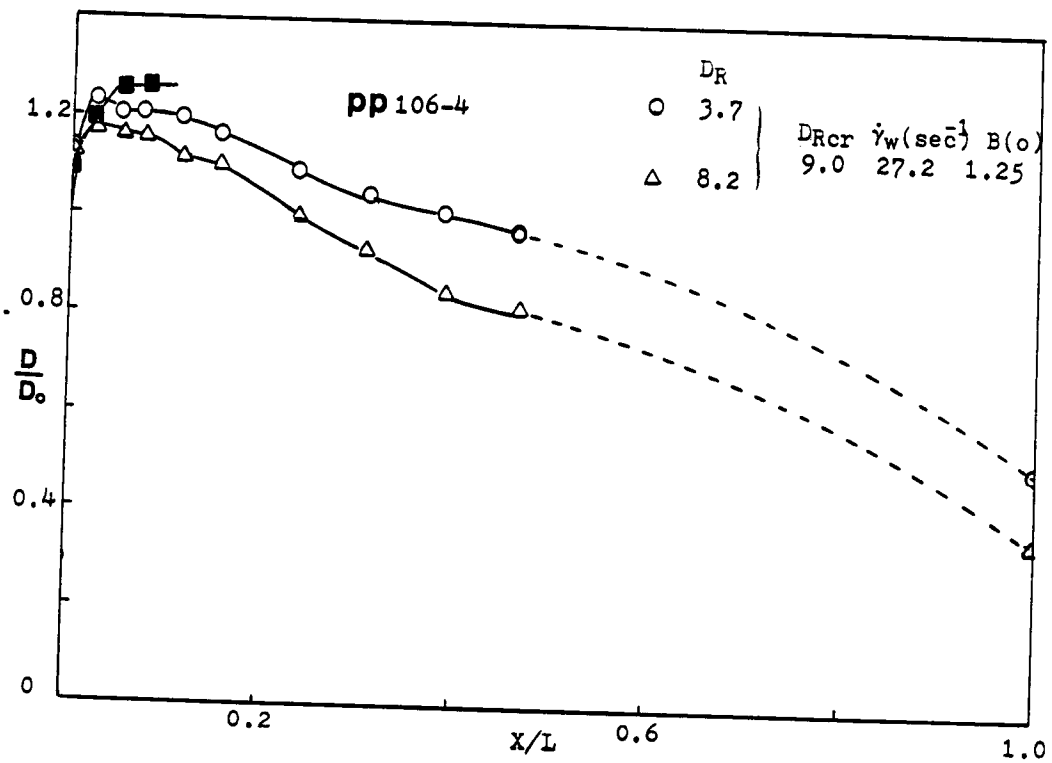


Figure IV-11. Experimental diameter distribution along the spinline (PP106-5 at different draw ratios with same shear rate).

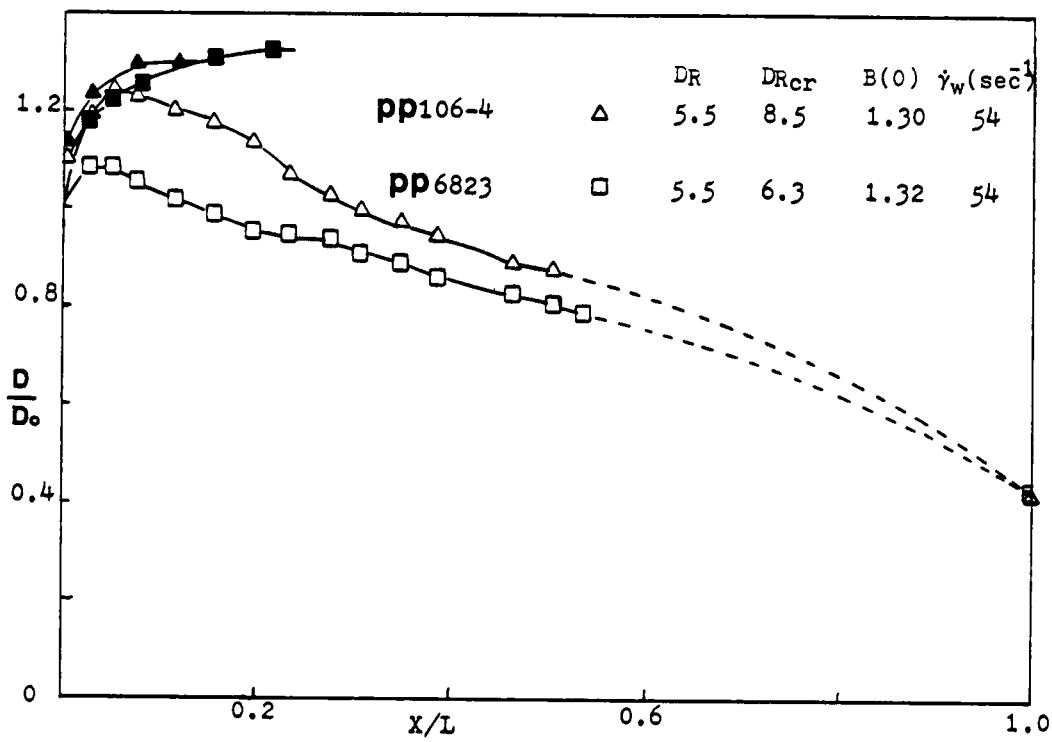


Figure IV-12. Experimental diameter distribution along the spinline (PP106-4 and PP6823 at same draw ratio and same shear rate).

wall shear rate to obtain the same die swell B(o) observed from the experiment. These adjusted values and other parameters were not changed in the subsequent runs for application of a take-up force.

In addition to the measurement of die swell were measurements of the spinline tension and the radius distribution along the spinline. The tension of the spinline at constant draw ratio was measured for both polymers as shown in Figures IV-9 and IV-10. This experimental procedure for measuring tension was described in Chapter III and follows that of Minoshima (56). There were experimental difficulties because of the friction between the fiber and the Teflon rods. Therefore, the measured tension has only relative meaning in comparing various runs rather than providing a measure of the exact force in the spinline. The comparison with calculated results will be discussed later. There are noticeable differences in tension, at the same draw ratio, which are related to the die shear rates, the tension being higher if the shear rate is higher.

Velocity distribution along the spinline were obtained by carrying out a computer solution of Equation 9 in Appendix B, as shown in Figures IV-13, IV-14, and IV-15. Typical sets of spinning data for the two polymers were chosen and compared with the radius and velocity distributions calculated from the computer, considering both the cases of one τ and three τs. Delayed die swell without take-up force was obtained with three τs but not with one τ; the fit in the former case was quite satisfactory. And also the delay die swell with take-up force using three τs was obtained at small force. Fairly good agreement is shown in Figure IV-15.

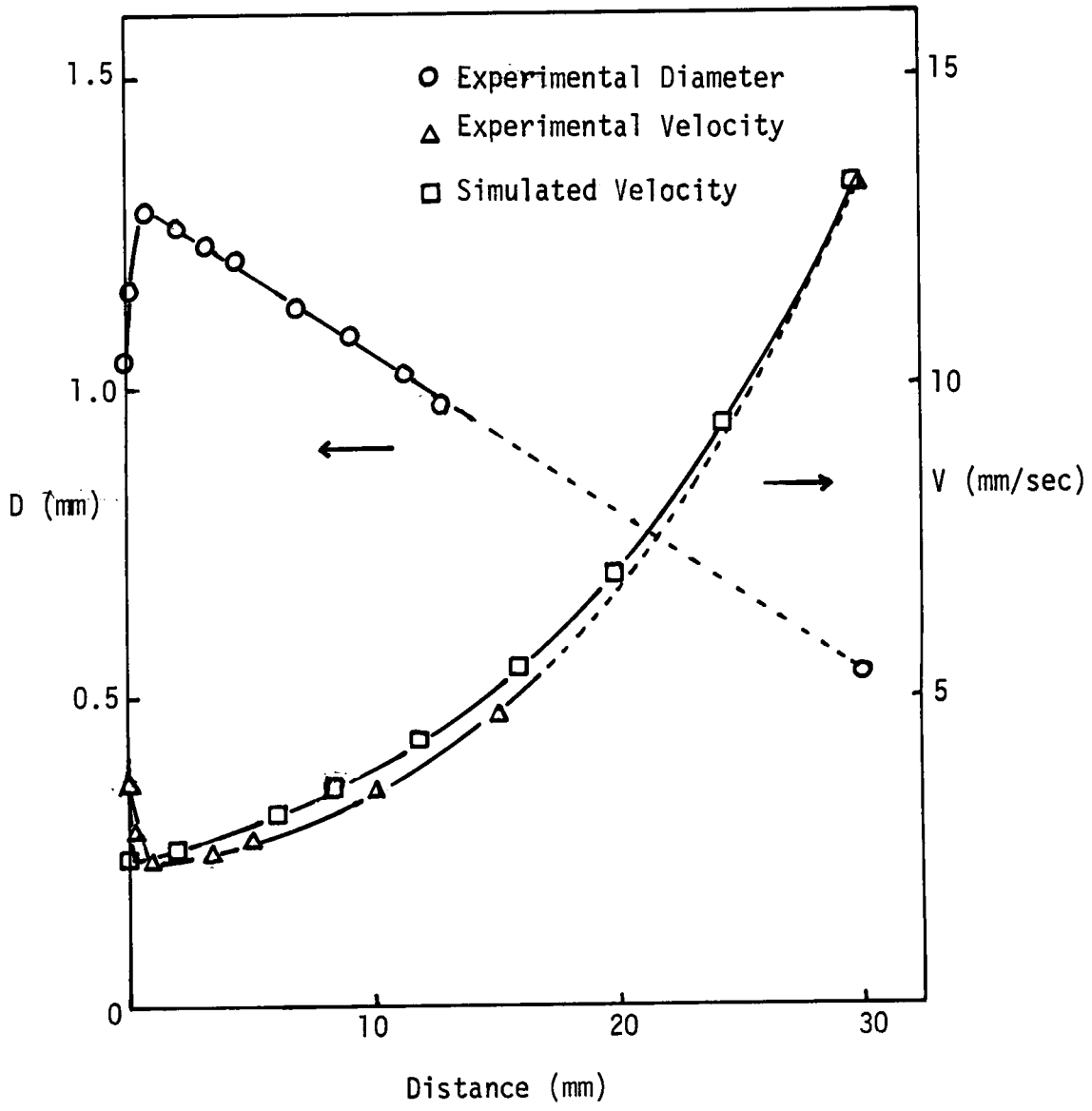


Figure IV-13. Comparison of experimental data with theoretical prediction using one element (PP106-4).

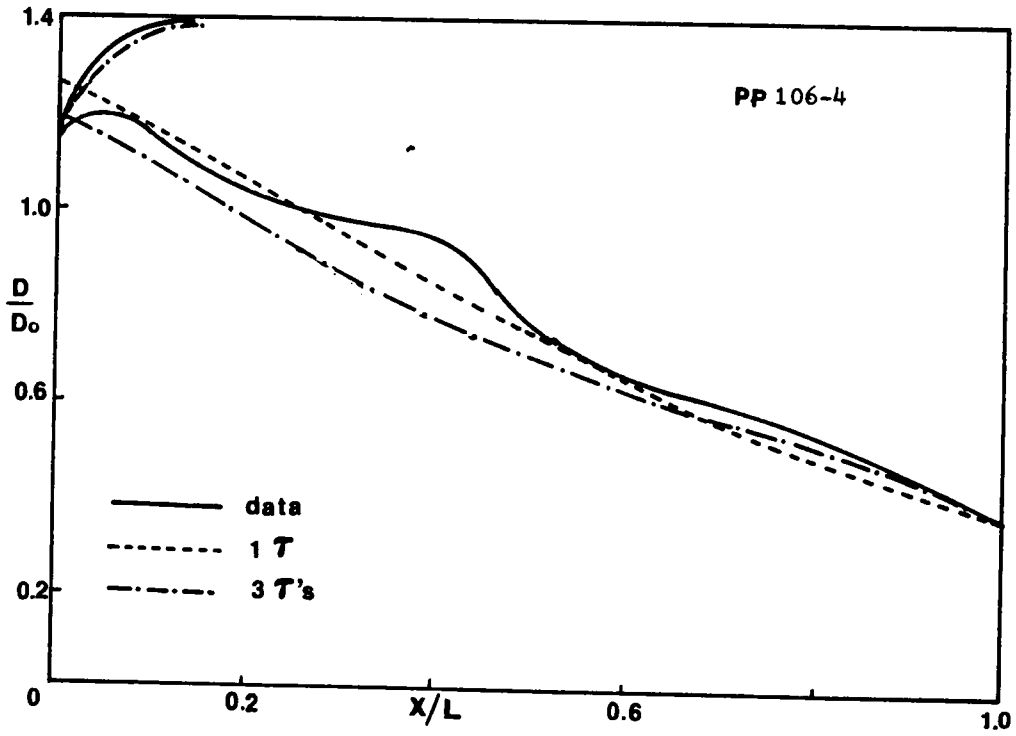


Figure IV-14. Comparison of experimental data with theoretical prediction using one element and three element model (PP106-4).

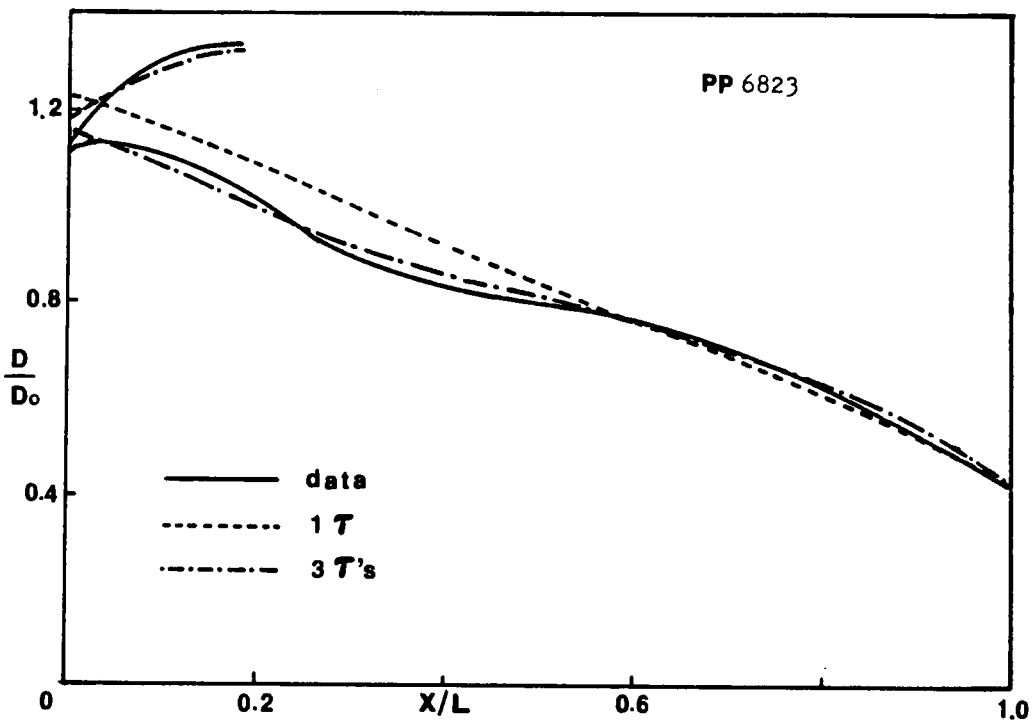


Figure IV-15. Comparison of experimental data with theoretical prediction using one element and three element model (PP6823).

The die swells with and without applied force were measured as 1.38 and 1.19 at a wall shear rate $\dot{\gamma}_w = 272\ sec^{-1}$ as shown in Figure IV-14. These die swells from the computer solutions were 1.33 and 1.28 at a dimensionless force $\phi = 0.32$ with one element model whereas 1.34 and 1.17 at the dimensionless force $\phi = 2.32$ with three elements model. The results of both cases were in agreement with the results of White-Roman (Equation IV-6) within 10%. There was a plateau radius distribution, observed along the spinline at the higher shear rates. It was observed experimentally that a large throughput moved the plateau region downstream as shown in Figure IV-15. But this kind of behavior was not obtained in the computer solutions.

The diameter of the spun fiber (D = 0.0135") was measured with a thickness gauge and compared with the calculated value (D = 0.0144") to an accuracy of about 7% with 0.041" die diameter at a draw ratio 8 (D_R = 8). This result says that overall experimental measurements for the fiber diameter (including plunger speed of Rheometer, calibration of the take-up motor, and the diameter of die) are very good.

Having carried out a solution to Equation 9 of Appendix B, it is now possible to return to the matter of comparing the calculated and measured values of the spinline tension as shown in Table IV-2.

The ratios between $(F_1/F_2)_{expt.}$ and $(\phi_1/\phi_2)_{comp.}$ for the two polymers are fairly close. Actual dimensionless ϕ's were obtained from the measured force by the definition ($\phi = \frac{F}{G\pi R_o^2}$) with one G.

Using three τ's lead to higher forces than using one τ and also the former case smoothes the radius distribution along the spinline. This observation agrees with Denn and Marrucci (17).

TABLE IV-2. COMPARISON OF MEASURED AND CALCULATED FORCES

Polymer	Draw Ratio D_R	Case	Wall shear rate $\dot{\gamma}_w$ (sec^{-1})	Measured Force F(g)	Calculated ϕ from meas. F	Computer ϕ		$\left(\frac{F_1}{F_2}\right)$ expt	$(\phi_1/\phi_2)_{comp.}$	
						one τ	three τs		one τ	three τs
PP106-4	8	1	5.4	0.18	0.044	0.093	0.325	4.9	7.6	7.1
		2	272	0.88	0.21	0.71	2.30			
PP6823	5.4	1	27.2	0.60	0.14	0.56	1.98	1.57	1.64	1.71
		2	54.4	0.94	0.23	0.92	3.39			

Purely computer solutions were obtained for two different cases as shown in Table IV-3 and IV-4.

TABLE IV-3. PREDICTED SPINLINE FORCE UNDER VARIOUS DIE FLOW CONDITION $b = 0.6$, $\tau_o = 0.1$ (CONSTANT V_o AND DIFFERENT DIE DIAMETER)

	I	II	III	IV
X^*_L	1.27	1.27	1.27	1.27
V^*_L	14.2	14.5	14.2	14.2
$\dot{\gamma}_w$	50	100	200	400
B(o)	1.223	1.279	1.317	1.340
B	0.970	1.039	1.087	1.114
ϕ_{cr}	1.07	1.9	3.04	4.7
$\frac{B}{B(o)}$	0.793	0.812	0.825	0.831
$\left.\frac{dV^*}{dX^*}\right\|_o$	1.0	0.84	0.76	0.70

TABLE IV-4. PREDICTED SPINLINE FORCE UNDER VARIOUS DIE FLOW CONDITION b = 0.6, τ_o = 0.1 (SAME DIE DIAMETER AND DIFFERENT V_o)

	I	II	III	IV
X^*_L	5.08	2.54	1.27	0.64
V^*_L	14.3	14.4	14.2	13.8
$\dot{\gamma}_w$	50	100	200	400
B(o)	1.223	1.279	1.317	1.340
B	1.125	1.122	1.086	1.066
ϕ_{cr}	1.07	1.9	3.04	4.7
$\frac{B}{B(o)}$	0.920	0.877	0.825	0.796
$\left.\frac{dV^*}{dX^*}\right\|_o$	0.23	0.42	0.76	1.33

From the value of ϕ from computer solution and experimental data it is found that the higher throughput need more force at the same draw ratios. Other information was added for later use.

CHAPTER V

PRESENTATION AND CORRELATION OF RESULTS: UNSTEADY SPINNING

A. Experimental Results

The first question in dealing with the matter of draw resonance is to decide which fluctuations are merely "noise" or due to some unknown mechanism and which are "true" draw resonance, in the sense of being related to the theoretical analyses. Some experimenters, for example, have observed small disturbances of only a few percent (31), while others (56) have noted the tendency of polypropylene to show small, irregular fluctuations over a wide range of spinning conditions. These latter disturbances were termed "forced oscillations" as distinct from draw resonance. In the present work rather distinct and periodic fluctuations were observed. Typical data for PP6823 are shown in Figure V-1. The left-hand portion (D_R = 5.4) is considered stable spinning; the middle portion (D_R = 6.1) is considered to show draw resonance. In this case the critical draw ratio value (D_R=5.9) is taken to be that when the fluctuation is about 5%. If the draw ratio is increased only somewhat above the critical value (for example, D_R=6.8), the fluctuation increased rapidly to several hundred percent and finally spinline broke. If the draw ratio is subsequently reduced, the spinning again becomes steady below the critical draw ratio. The behavior of PP106-4 is somewhat different from that of PP6823. The magnitude of fluctuation above the critical draw ratio is increasing slowly to 20-30%. The spinline of PP106-4 broke when

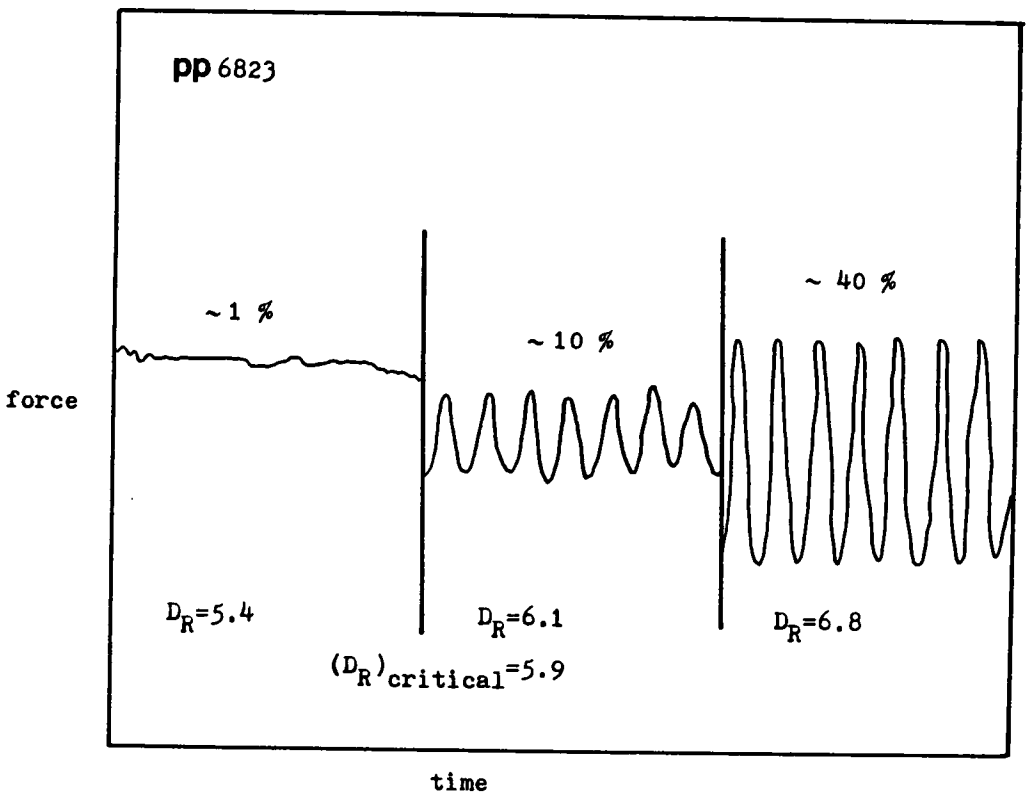


Figure V-1. Typical force-time trace from chart recorder.

the draw ratio is more than 25% of the critical draw ratio while the spinline of PP6823 broke at 10% above the critical draw ratio.

Having established that the fluctuations which were observed are large and periodic ones ("draw resonance"), the condition under which the draw resonance starts were investigated. The critical draw ratio as a function of the die velocity at three different spin lengths and two die L/D ratios are plotted in Figures V-2 and V-3. There is the clear effect of die L/D, with the shorter die being less stable than the longer die, in agreement with Matsumoto (51) and Han's observations (31). Also one notes a distinct minimum (with V_o as the independent variable) in the case of PP106-4 and a much less distinct minimum (or none at all) in the case of PP6823. There are other plots to show the different die diameters as shown in Figures V-4 and V-5. In order to avoid the melt fracture one must maintain the die velocity V_o below some critical value. Critical draw ratio data plotted against V_o do not correlate well, therefore other dimensionless groups, which include V_o will be discussed later.

Also the development of the magnitude of the fluctuations along the spinline was measured for PP106-4, at D_R = 8.4, with 3 cm spin length Typical data measured at intervals of 2.3 mm is shown in Figure V-6. The period of fluctuation did not change along the spinline, but the magnitude ratio of the fluctuation increased from 1.2 near the die exit to about 4 at the take-up position when the draw ratio (9.0) was somewhat above the critical ratio (8.4).

Non-isothermal spinning was more stable than isothermal spinning, as shown in Figure V-7, but no quantitative analysis was made of it. The experimental results are discussed in Chapter II.

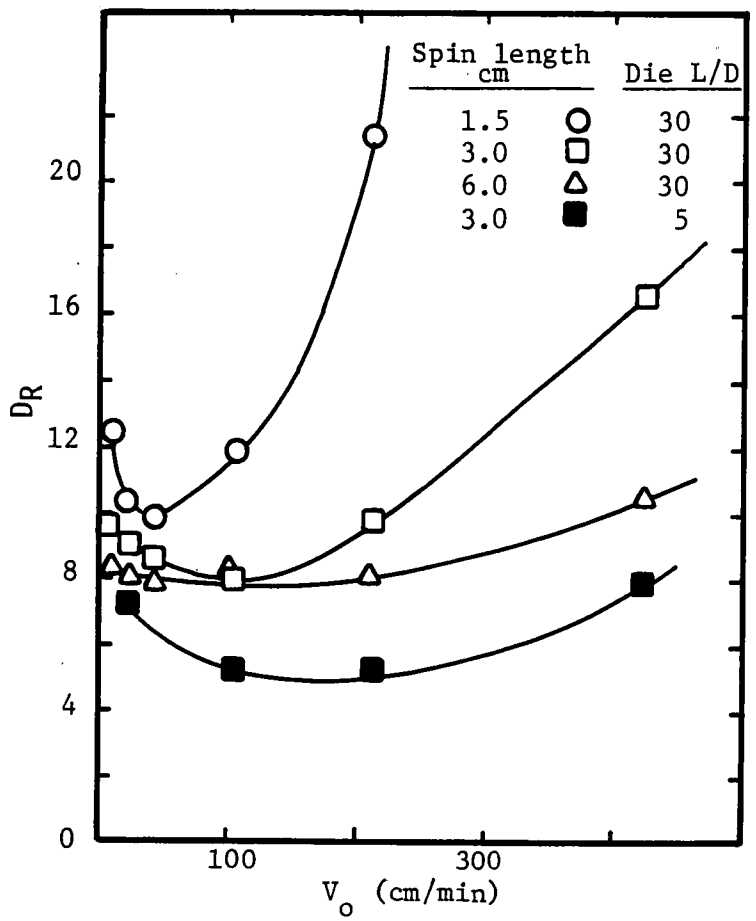


Figure V-2. Critical draw ratio as a function of initial velocity (PP106-4 with different spin length).

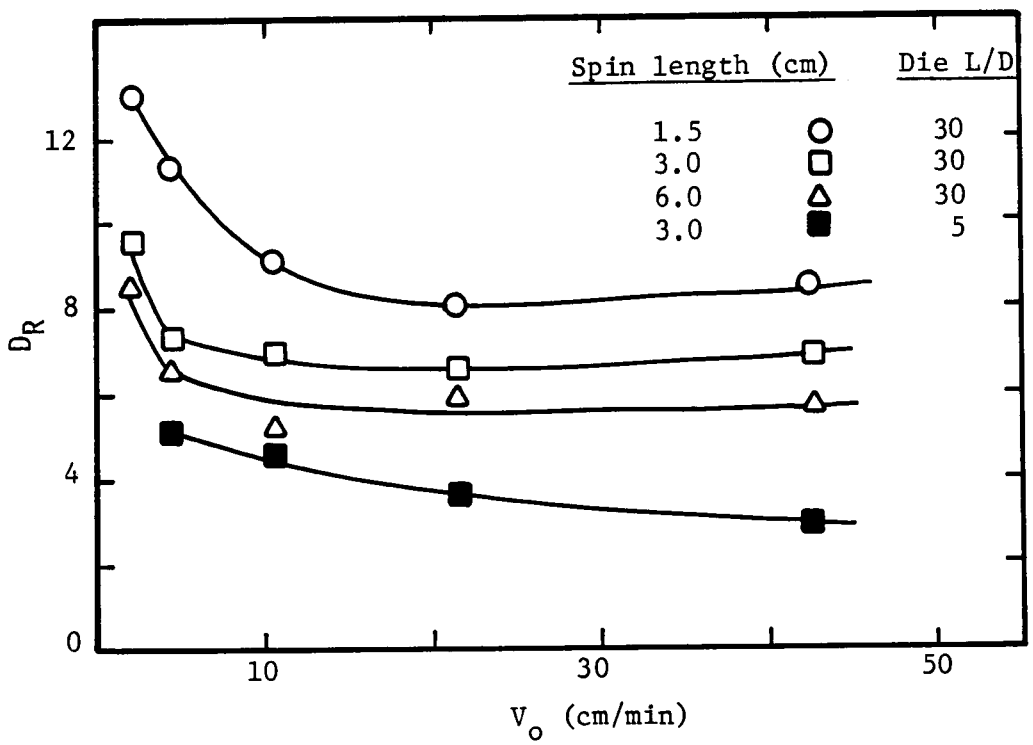


Figure V-3. Critical draw ratio as a function of initial velocity (PP6823 with different spin length).

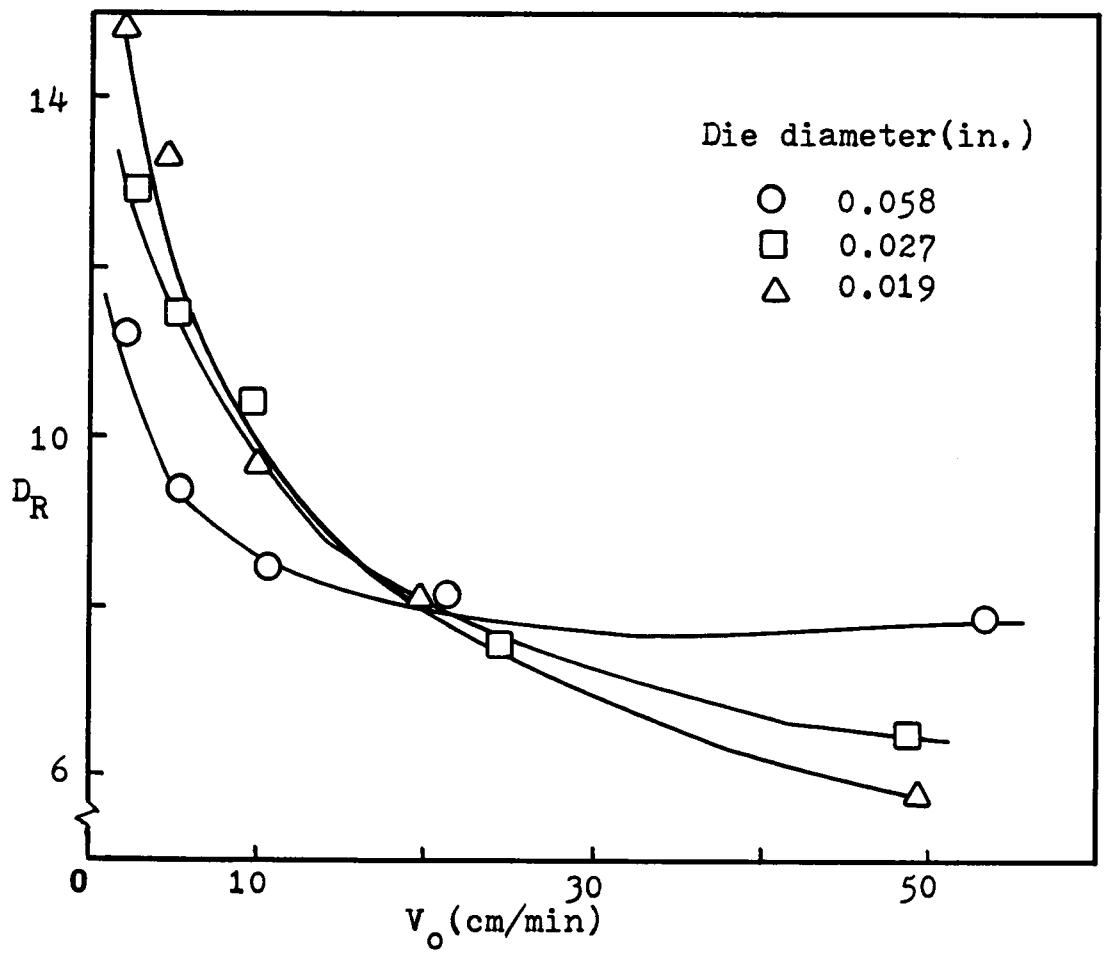


Figure V-4. Critical draw ratio as a function of initial velocity (PP6823 with different die diameter).

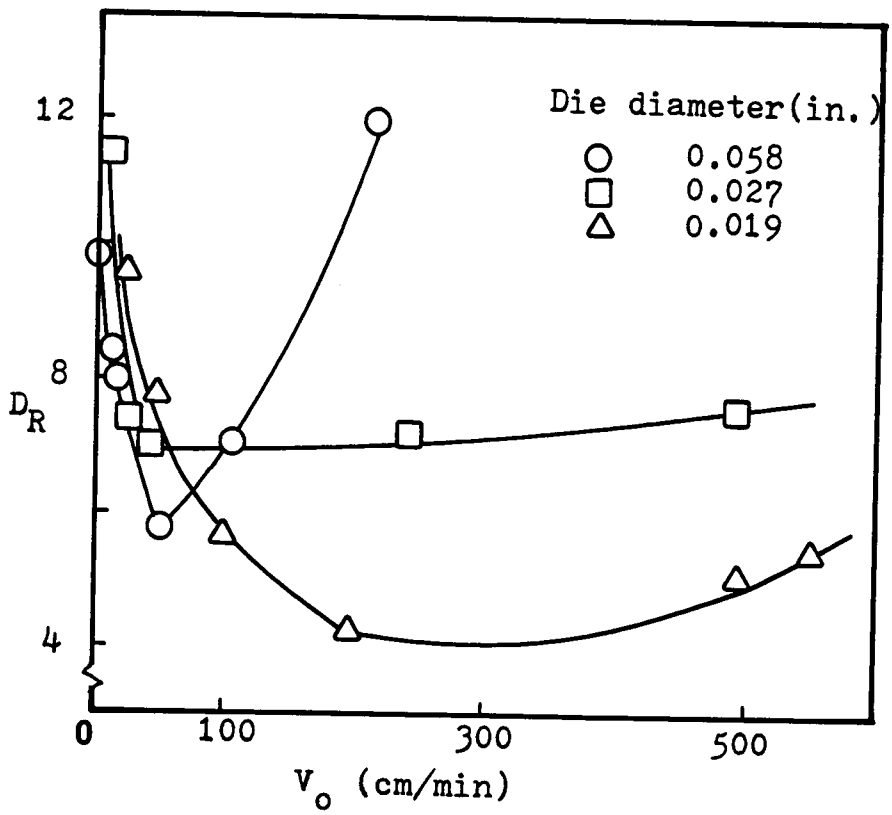


Figure V-5. Critical draw ratio as a function of initial velocity (PP106-4 with different die diameter).

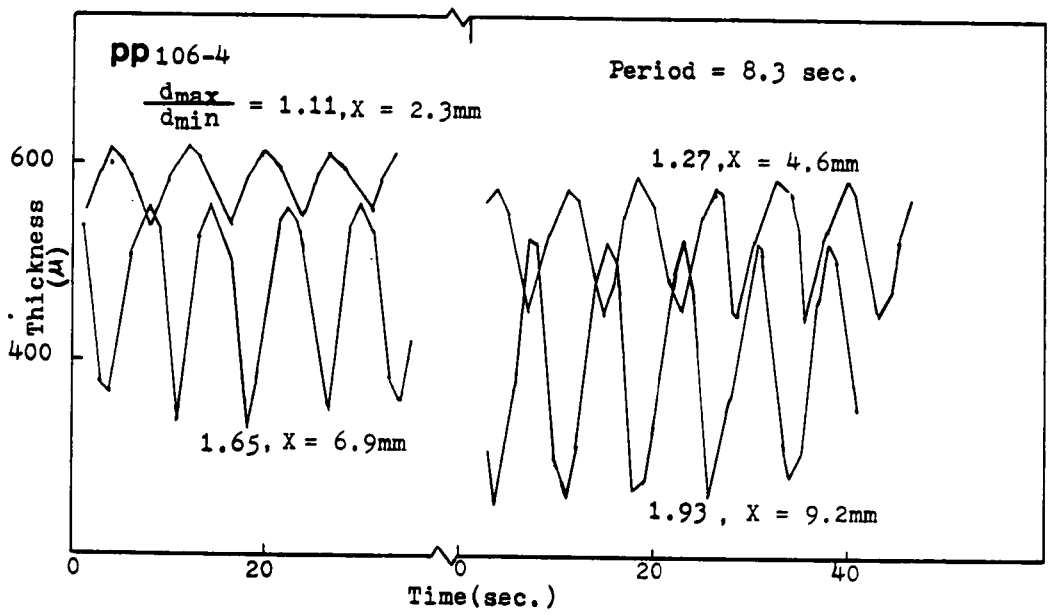


Figure V-6. Variation diameter fluctuation along the spinline.

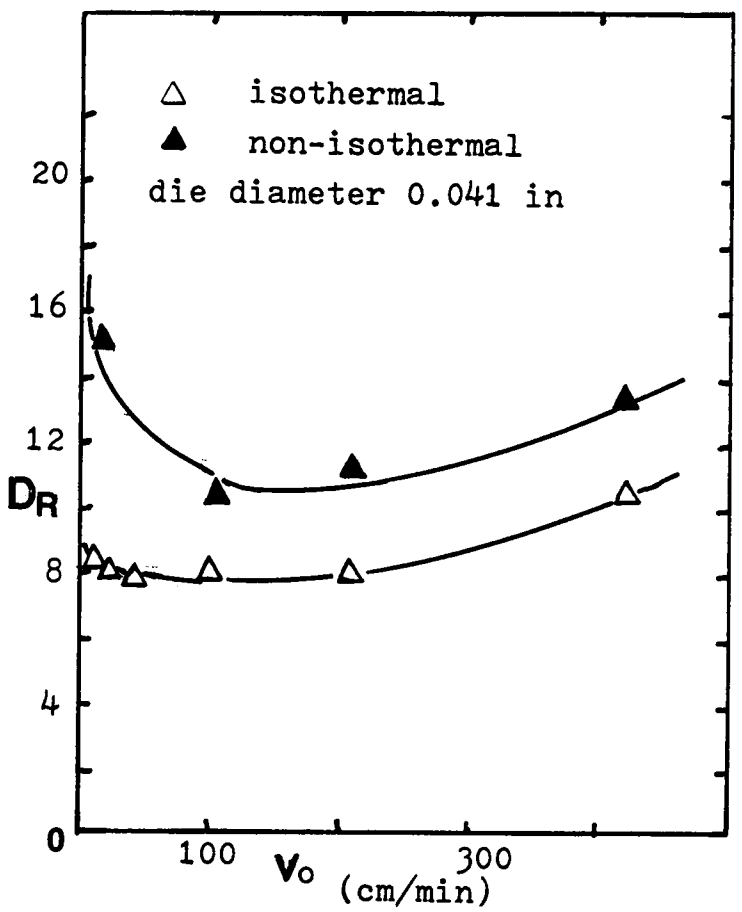


Figure V-7. Critical draw ratio as a function of initial velocity (comparisons of isothermal case with non-isothermal).

A plot to show the shear rate effect and elongational rate effect on the onset of draw resonance is presented in Figure V-8. This plot did not give an evident effect of these variables on draw resonance; therefore, other correlating variables are needed and will be discussed in the next section.

B. Correlation of Results

Characterization of Draw Resonance

The question of deciding on the criteria for the onset of draw resonance was discussed in some detail in Section A of this chapter. Rather distinct changes in the magnitude of the fluctuations (from essentially no fluctuation to almost a 5% variation of the diameter) were observed over a narrow range of draw ratio (less than a 10% change of draw ratio). This was the operational definition of the "critical draw ratio" as observed experimentally. Also it was noted that there was a distinct periodicity in the fluctuation. Because there are some theoretical predictions for the period of the disturbance, the matter of the periodicity will now be considered in more detail.

A general prediction for the period of the fluctuation involves identifying the magnitude of the imaginary part of the critical eigenvalue. Chang and Denn (12) give this result in the form

$$t_p = \frac{2\pi L}{\lambda_I V_o} \qquad \text{(V-1)}$$

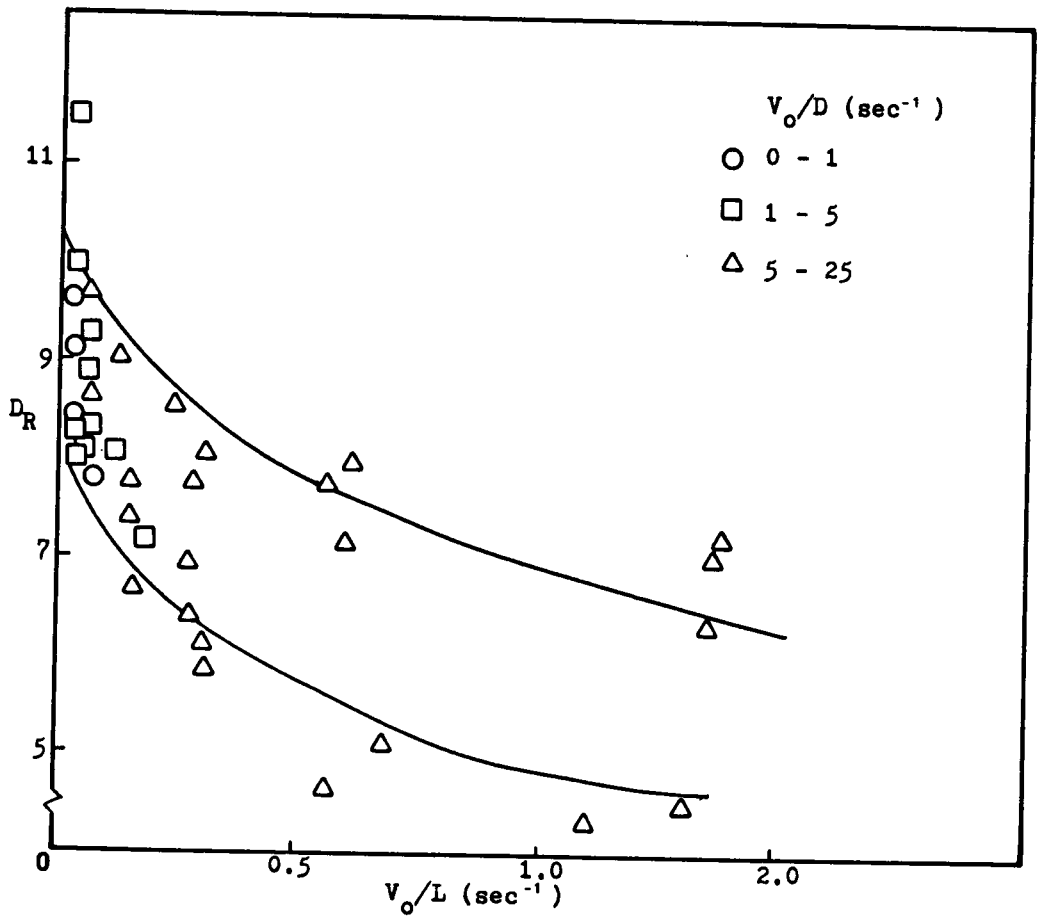


Figure V-8. Critical draw ratio as a function of V_o/L.

where L is the spin length, V_o is the initial velocity and λ_I is the magnitude of the imaginary part of the eigenvalue.

Unfortunately numerical values for the eigenvalue λ_I are not given in most of the analyses, although a value is available for the isothermal Newtonian case (that is, $\lambda_I \equiv 14.01$). Therefore the predicted period is

$$t_p(N) = 0.448 \frac{L}{V_o} \qquad \text{(V-2)}$$

A different but equivalent result has been given by Pearson (60), Kase (43) and Weinberger (20) as follows

$$t_p(N) = \frac{1.35}{\ln \frac{V_L}{V_o}} \cdot \frac{L}{V_o} \qquad \text{(V-3)}$$

Inserting the critical draw ratio 20.2, one obtains again exactly Equation V-2.

While the analog of Equation V-3 is not in the literature for the power law case, probably the form is the same as that of Equation V-3. For the power law fluid with $n < 1$, one typically sees critical draw ratios in the range 5 to 15 from Denn's plot shown in Figure II-2, p. 15; therefore the constant in Equation V-3 is probably larger than 0.448 for the power law case.

As noted by Fisher and Denn (23), there is a rather direct connection between the period of the draw resonance and the residence time of the fluid in the spinline. They studied analytically the onset and growth of the spinning instability for an isothermal Newtonian liquid by examining the nonlinear dynamics and found that all disturbances

approach a stable finite-amplitude oscillation with a period that equals twice the residence time at higher draw ratios.

The residence time depends, of course, on the detailed kinematics of the spinline, but it can be calculated for certain spinning conditions. The general equation is

$$t_{res} = \int_0^L \frac{dx}{V(x)} \tag{V-4}$$

For the Newtonian case and power law case, the results are as shown in Table V-1. The result for the integral model of the present work cannot be put in analytical form but can be obtained from the computer solution as follows:

$$t_{res}\ (I) = \int_0^L \frac{dV}{dx}$$

$$= \tau_o \int_0^{x^*} \frac{dx^*}{V^*} \tag{V-5}$$

TABLE V-1. SUMMARY OF EQUATIONS FOR THE PERIOD OF FLUCTUATION AND FOR THE SPINLINE RESIDENCE TIME

t_p (gen)	t_p (N)	t_{res} (gen)	t_{res} (N)	t_{res} (PL)
$\frac{2\pi L}{\lambda_I V_o}$	$\frac{1.35}{\ln \frac{V_L}{V_o}} \frac{L}{V_o}$	$\int_0^L \frac{dX}{V(X)}$	$\frac{1 - V_o/V_L}{\ln V_L/V_o} \frac{L}{V_o}$	$\frac{(n-1)(1 - D_R^{-1/n})}{(D_R^{n-1/n} - 1)}$

The theory of Hyun (37), which in dispute in a physical sense (see Chapter II), does nonetheless give a prediction for the onset of draw resonance in terms of the residence time. Hyun introduces another kind of residence time, called the "throughput wave residence time" t_{res} (TH) which is the same in both power law case and Newtonian case, given by

$$t_{res}\ (TH) = \int_0^L \frac{dx}{V(x)}$$

$$= L\int_0^L \frac{d(\frac{X}{L})}{V_0 + \frac{X}{L}(V_L - V_0)}$$

$$= \frac{L}{V_0} \frac{\ln \frac{V_L}{V_0}}{\frac{V_L}{V_0} - 1} \qquad (V\text{-}6)$$

Hyun's criterion for the draw resonance is

$$2t_{res}\ (TH) = t_{res} \qquad (V\text{-}7)$$

Although Hyun does not specifically deal with the matter of the period, the argument seems to imply that it is equal to the residence time, that is

$$t_p = t_{res} \qquad (V\text{-}8)$$

The various predictions for the period and for the residence time, as well as experimental values for the former, are summarized in Table V-2.

TABLE V-2. *CALCULATED AND OBSERVED PERIODS OF FLUCTUATION AND RESIDENCE TIMES

Wall shear rate $\dot{\gamma}_w$ (sec^{-1})	Initial velocity V_o (cm/sec)	Critical draw rates $D_{Rcr.}$	Period		Residence time				
			t_p (obs) (sec)	t_p (N) (sec)	t_{res} (N) (sec)	t_{res} (PL)(sec)		t_{res} (I)(sec)	
						n = 0.5	n = 0.7	one τ	three τ's
544	7.08	16.5	0.42	0.204	0.141	0.247	0.178	0.279	0.209
272	3.55	9.8	0.94	0.50	0.332	0.466	0.391	0.576	0.446
136	1.77	8.1	1.72	1.09	0.771	0.952	0.816	1.117	0.805
27.2	0.355	9.0	7.4	5.19	3.42	4.694	3.97	4.43	3.41

*PP106-4, 3 cm spinlength, 0.041" die, 180°C.

In general there seems to be considerable agreement between the periods and the residence times. There are, finally, three predictions for the ratio of the period to the residence time, as follows:

$$t_p(N)/t_{res}(N) = 1.42 \quad \text{(linear)} \tag{V-10}$$

$$t_p(N)/t_{res}(N) = 2.0 \quad \text{(limit, large amplitude)} \tag{V-11}$$

$$t_p/t_{res} = 1.0 \quad \text{(presumed from Hyun)} \tag{V-12}$$

The observed ratio depends on how one calculates the residence time. Fortunately the calculation for residence time does not depend strongly on the model used as long as thinning-type behavior is introduced (see the last four columns in Table V-2). Using the residence time t_{res} (I) for the one element model as typical, one can calculate a ratio t_p (obs)/ t_{res} (I) in the range 1.9 to 2.3. Thus the observed ratios are in very good agreement with the large amplitude limit predicted by Fisher and Denn (Equation V-11). It seems clear, then, the mechanism of the instability being observed experimentally is connected with the mechanism of the draw resonance theory.

Correlation of the Onset of Draw Resonance

From Matsumoto's work it was felt that the die swell region is important in understanding the onset of draw resonance. This was deduced from the strong effect of the die aspect ratio (L/D) and the qualitative observation from Matsumato's motion pictures that the material was in a "melt draw" just below the die swell region as draw resonance

occurred. These observations motivated many of the experiments of the present work, which involved making systematic changes of the variables which affect the die swell, i.e., the shear rate in the die, which in turn can be varied by changing the mass throughput or the die diameter. In addition to these variables, those that are normally thought to affect the draw resonance (take-up speed, spinline length, extrusion temperature and chamber temperature) were included. With so many variables to be considered, it is necessary to look at the combinations of variables which occur in the theory to help decide how to proceed with the analysis of the data.

Existing theory for the draw resonance of viscoelastic materials (for example, that of Fisher and Denn (25)) suggests that the correlating groups for the critical draw ratio are an elasticity number ($\alpha = \frac{3\,\frac{n-1}{2}\,K}{G}\left(\frac{V_o}{L}\right)^n \propto \frac{\tau V_o}{L}$) and material parameters such as n. Die flow effects would, therefore, only appear in the ratio V_o/L for a given material. The observations of Matsumoto (51) and those of the present work show that the effect of the die flow is much more complicated than that.

An important question is, then, whether the theories are simply not general enough to deal with the observed die flow effect or whether there is a basic contradiction between theory and experiment. The experimental critical draw ratios ($DR_{cr.}$) are mostly in the range 5 to 20 (see Figures V-2 and V-3), whereas the prediction of Fisher and Denn gives critical draw ratios in the range 5-15, depending on the power law index n (i.e., $DR_{cr.} = 15$ when $n = 0.9$, and $DR_{cr.} = 5$ when $n = 0.5$). And also the observed period in the present work is about twice the

residence time, as the finite disturbance theory predicts. Thus there is agreement in a general sense between theory and experiment and the theory is probably capable of explaining the mechanism of the instability being observed. However, there are systematic trends in the experimental data (somehow related to the shear rate) which cannot be explained by the theory. It is clear therefore that some kind of correlating scheme, beyond existing theory, will be needed.

The existing theoretical analyses of draw resonance presume an arbitrary initial tensile stress and it is stated that the magnitude of this initial value does not affect the results (16). However, perhaps this is not true over a wide range of initial stress values or for different constitutive equations. One possible analytical procedure would be, therefore, to reformulate the existing analyses using different initial stress values, or possibly different constitutive equations. It was our intuitive feeling, however, that the die swell region is a most important one in determining the onset of draw resonance. The differential equations which have been used for the stability analyses do not allow treatment of the die swell problem, whereas the integral equation used in the present work does allow such treatment (see Appendix B). A stability analysis based on these more complicated equations might be possible, but it will not be easy, particularly given the nature of the kinematics near the die exit. Therefore it was decided to analyze the steady spinning solutions in a systematic way to gain qualitative understanding of, and possible correlating parameters for, the unsteady spinning (draw resonance) problem.

Since several experimental observations involve an emphasis on the die swell region, one reasonable correlating group might be the ratio B/B(o), where B is the die swell with take-up force and B(o) is the "potential die swell," i.e., that without force. It was thought that the smaller the ratio B/B(o), the more stable the spinning would become, since an applied force would reduce the sudden (and perhaps destabilizing) release of the shear-induced stresses. The ratio B/B(o) was obtained from various computer runs as shown in Tables V-3, V-4, V-5, V-6. The group B/B(o) was satisfactory at high initial velocity (for PP106-4) as shown in Table V-4. But it was not satisfactory at low initial velocity as shown in Table V-3. Moreover, generalized plots of all of the data ($D_{R_{cr}}$ vs. B/B(o)) scattered inconsistently and so no useful conclusion could be drawn. One of the difficulties is that the ratio B/B(o) does not vary significantly (see Tables V-3 and V-5) and therefore this ratio cannot be used conveniently as a plotted correlating variable.

The second correlating group which was considered is the derivative of the velocity gradient after the instantaneous die swell at the exit of the die. A large gradient might be thought to produce "more thinning," which would cause the spinline to eventually be more unstable. In fact, however, the larger gradient $\left.\frac{dV^*}{dX^*}\right|_o$ stabilized the spinline, as shown in Table V-4. Also the gradient argument was not in agreement with the die swell argument (ratio B/B(o)), as shown in Table V-4. Because of these inconsistencies, the group $\left.\frac{dV^*}{dX^*}\right|_o$ was not felt to be a useful one as an overall correlating parameter.

TABLE V-3. SUMMARY OF COMPUTER RESULTS FOR CERTAIN DIMENSIONLESS CORRELATING GROUPS (PP106-4 AT LOW INITIAL VELOCITY)

Results \ Die diameter (inches)	0.058	0.027	0.019
Experimental results:			
$\dot{\gamma}_w$ (sec^{-1})	36	78	111
$D_{R_{cr}}$	6.5	7.5	8.5
X^*_{cr}	45	45	45
Computer results:			
B(o)	1.191	1.261	1.286
B	1.179	1.249	1.274
ϕ_{cr}	0.134	0.150	0.159
ϕ_m	0.22	0.23	0.235
B/B(o)	0.9899	0.9905	0.9910
$dV^*/dX^*\|o$	0.026	0.025	0.025
X^*_{cr}/X^*_m	0.52	0.58	0.62
ϕ_{cr}/ϕ_m	0.61	0.65	0.68

Experimental data for PP106-4 at V_o = 40 cm/min, spinlength 3 cm computer solution with τ_o = 0.1, b = 0.6.

TABLE V-4. SUMMARY OF COMPUTER RESULTS FOR CERTAIN DIMENSIONLESS CORRELATING GROUPS (PP106-4 AT HIGH INITIAL VELOCITY)

Results \ Die diameter (inches)	0.058	0.027	0.019
Experimental Results:			
$\dot{\gamma}_w$ (sec^{-1})	181	389	555
$D_{R_{cr}}$	10.5	7.5	4.5
X^*_{cr}	9	9	9
Computer results:			
B(o)	1.312	1.339	1.347
B	1.261	1.294	1.309
ϕ_{cr}	0.687	0.65	0.56
ϕ_m	0.784	0.81	0.815
B/B(o)	0.961	0.966	0.972
$dV^*/dX^*\|o$	0.0995	0.085	0.070
X^*_{cr}/X^*_m	0.82	0.74	0.61
ϕ_{cr}/ϕ_m	0.88	0.80	0.69

Experimental data for PP106-4 at V_o = 200 cm/min, spinlength 3 cm computer solution with τ_o = 0.1, b = 0.6.

TABLE V-5. SUMMARY OF COMPUTER RESULTS FOR CERTAIN DIMENSIONLESS CORRELATING GROUPS (PP6823 AT LOW INITIAL VELOCITY)

Results \ Die diameter (inches)	0.058	0.027	0.019
Experimental results:			
$\dot{\gamma}_w$ (sec^{-1})	4.5	9.7	13.9
$D_{R_{cr}}$	9.6	11.8	12.5
X^*_{cr}	14.4	14.4	14.4
Computer results:			
B(o)	1.231	1.259	1.279
B	1.213	1.242	1.263
ϕ_{cr}	0.205	0.212	0.217
ϕ_m	0.210	0.214	0.217
B/B(o)	0.9854	0.9865	0.9875
$dV^*/dX^*\|o$	0.0368	0.0346	0.0332
X^*_{cr}/X^*_m	0.96	0.98	1.00
ϕ_{cr}/ϕ_m	0.98	0.99	1.00

Experimental data for PP6823 at V_o = 5 cm/min, spinlength 1.5 cm computer solution with τ_o = 1.25, b = 0.9.

TABLE V-6. SUMMARY OF COMPUTER RESULTS FOR CERTAIN DIMENSIONLESS CORRELATING GROUPS (PP6823 AT HIGH INITIAL VELOCITY)

Results \ Die diameter (inches)	0.041	0.027	0.019
Experimental results:			
$\dot{\gamma}_w$ (sec^{-1})	32	49	69
$D_{R_{cr}}$	6.0	5.0	3.5
X^*_{cr}	11.6	11.6	11.6
Computer results:			
B(o)	1.324	1.355	1.372
B	1.296	1.328	1.348
ϕ_{cr}	0.40	0.402	0.38
ϕ_m	0.405	0.41	0.42
B/B(o)	0.9789	0.9801	0.9826
$dV^*/dX^*\|o$	0.053	0.049	0.044
X^*_{cr}/X^*_m	0.97	0.94	0.84
ϕ_{cr}/ϕ_m	0.99	0.98	0.90

Experimental data for PP106-4 at V_o = 25 cm/min, spinlength 6 cm computer solution with τ_o = 1.25 sec, b = 0.6.

The third correlating group which was considered had to do with the maximum force (or "blow-up point") argument. This maximum force was first observed in the computer solutions, as shown in Figure IV-4, p. 44. And using the maximum force criterion, critical draw ratio was plotted as a function of the elasticity number ($1/X^*$) as shown in Figure V-9. Increasing the shear rate decreased the critical draw ratio.

Experimentally it was observed that there was a thinning region in the spinline followed by a fluctuation (draw resonance) and finally breakage, as draw ratio was increased. In the case of PP6823 the spinline broke at a draw ratio about 5-15% above the onset of draw resonance while in the case of PP106-4 it broke about 10-30% above the onset of draw resonance.

It is not immediately obvious that there is any connection between the maximum force criterion (which has to do with the occurrence of a maximum in a plot of spinline force vs. draw ratio) and the onset of draw resonance or the point of breakage. This connection involves a physical picture of how the spinline would behave near this critical point. Figure IV-6, p. 48, shows a plot of the velocity distribution along the spinline as calculated from the modified Ide-White equation (Equation IV-12) for several values of the spinline force ϕ. The result is double-valued in V^*. The computer solution of the present work, however, produces only the bottom set of curves for each value of ϕ. The upper set of curves (which involves an increase of diameter with distance) is not physically realizable because the very large diameter shrinkage (or velocity increase) at $X^* = 0$ cannot be realized if finite shear rates in the

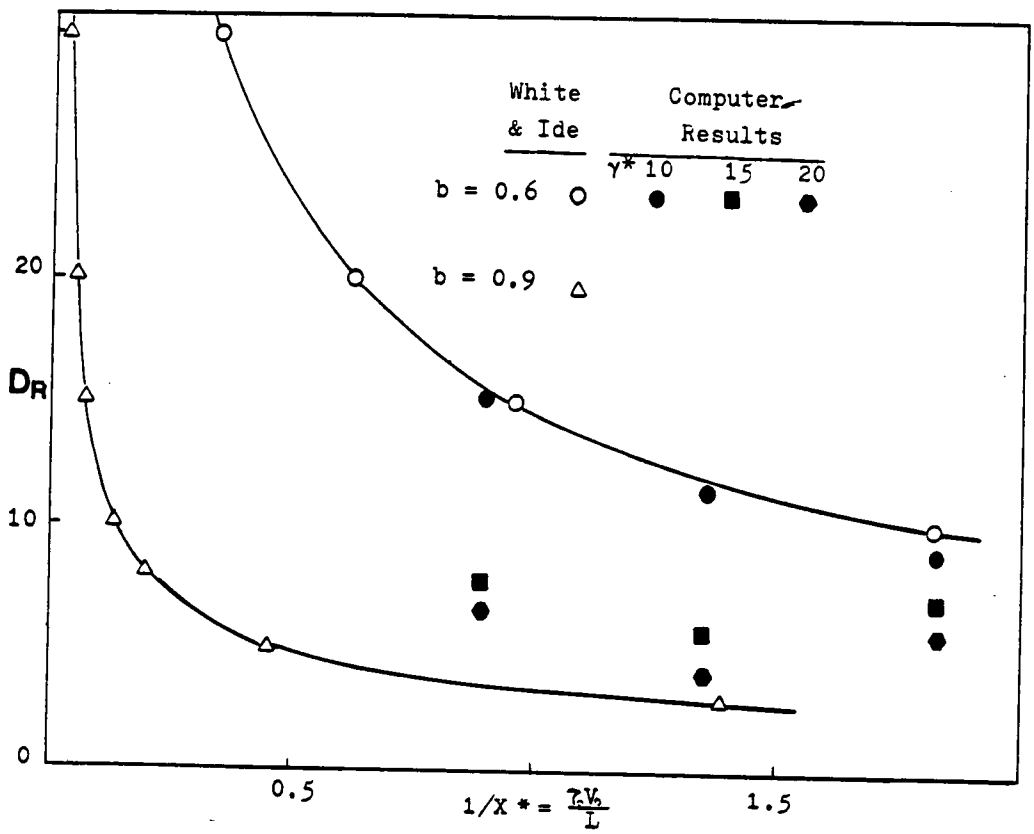


Figure V-9. Predicted critical draw ratio as a function of the elasticity number using the maximum force criterion.

die upstream of this point are used (even for zero shear rate in the die and ϕ = 0.54, the diameter shrinkage is only about 10%, not 80% as shown in Figure IV-6, p. 48). At the maximum force point ("blow-up point"), the velocity gradient dV^*/dX^* approaches infinity at the take-up position. This infinite gradient of dV^*/dX^* was obtained in the computer solution and later this infinite value was also calculated analytically from the modified White-Ide equation as shown in Equation IV-19, p. 47. If the take-up speed is increased beyond the critical value, one must imagine an infinite velocity gradient over a finite distance (i.e., a ductile failure). Therefore it is reasonable to associate the maximum force criterion (or "blow-up point") as a point of incipient ductile failure. Given the observed (and physically reasonable) connection between the onset of draw resonance and breakage, one can now reasonably associate the onset of draw resonance with the maximum force point ("blow-up point").

The comparison of the experimental onset of draw resonance with the computer solution for the maximum force point can be done in several ways. Those involve correlating the ratios X^*_{cr}/X^*_m and ϕ_{cr}/ϕ_m, where the numerators are the experimentally known values of X^*_{cr} at the take-up point and the force ϕ_{cr} calculated by the computer at the onset of draw resonance (as indicated by subscript "cr"). The denominators X^*_m and ϕ_m are computer-calculated values of X^* and ϕ at the "blow-up point" (i.e., the point where the velocity gradient becomes infinite), in the first case holding ϕ constant at ϕ_{cr} and in the second case holding X^* constant at X^*_{cr}. That is both numerator and denominator in the ratio ϕ_{cr}/ϕ_m are calculated at the same value of X^*_{cr} and those in the ratio X^*_{cr}/X^*_m are calculated at the same value of ϕ_{cr}.

The two ratios which characterize the idea of the maximum force criterion are, then, ϕ_a/ϕ_m and X^*_{cr}/X^*_m. The results are summarized in Tables V-3, V-4, V-5 and V-6. In Table V-5 the ratios are almost unity and therefore could be used as criteria for the onset of draw resonance. For the more thinning polymer (PP6823, b = 0.9) the ratios are of the order 0.8-1.0 whereas for the less thinning polymer (PP106-4, b = 0.6) the ratios are of the order 0.5-0.9. Thus in an overall sense there is certainly some connection between the onset of draw resonance and the maximum force criterion (the so called "blow-up point"). However the lower ratio seem clearly to be associated with low shear rates in the die whereas the high ratios are associated with high shear rates. Thus some further argument, involving shear rate as a parameter, seems to be needed.

Somewhat similar experimental results were reported by Chang and Denn (11), who observed filament break-up after the onset of draw resonance. They used corn syrup containing 0.5 wt. % Separan AP-30 (a polyacrylamide) which they treated as a viscoelastic fluid. Just before the breakage of the filament, the measured force goes through a maximum and the fluctuation of the filament (draw resonance) starts. They recorded the draw ratio at the onset of draw resonance ($D_{R_{cr}}$) and the maximum draw ratio at the breakage of filament (D_{R_m}). The ratio $D_{R_{cr}}/D_{R_m}$ varied from two to three depending on the spinning conditions (i.e., the initial velocity and spin length). And they also reported the force at the onset of draw resonance and the force at the point of the breakage. The

force ratios were of the order 0.5-1.0. Thus their experimental observations seem to be related to the present correlating parameter ϕ_{cr}/ϕ_m, although they did not make an argument based on a mathematical analysis.

The fourth correlating group which was considered did involve the shear rate, which seems to be the missing parameter in the previous correlation scheme. This fourth group was the ratio σ^*_{11w}/ϕ_{cr}, where σ^*_{11w} the dimensionless tensile stress in the die was defined in Equation IV-35, p. 56, using the shear and normal stresses measured experimentally and where ϕ_{cr} was calculated by computer at the onset of draw resonance.

The onset of the instability might be imagined to be related to the sudden release of the stresses caused by the die flow. If these stresses are released suddenly near the die exit, then the spinline might be unstable; on the other hand, if the stress can be maintained or released slowly, the spinline might be stable. Or, in other words, the instability might be related to the "mismatch" between the tensile stress generated in the die shear flow and the stress generated by elongational flow in the spinline. This leads to considering the dimensionless group $\sigma_{11w}{}^*/\phi_{cr}$, which is directly related to the group N_1^*/ϕ_{cr} (see Equation IV-33, p. 56). The ratios $\sigma_{11w}{}^*/\phi_{cr}$ were computed for most of the experimental data and plotted against $\tau V_o/L$, as shown in Figure IV-10 for PP106-4 and Figure V-11 for PP6823.

For comparison the third correlating scheme, which was based on a maximum force criterion, is shown as the dotted line on Figures V-10 and V-11. For convenience this line was calculated by the Ide-White analysis.

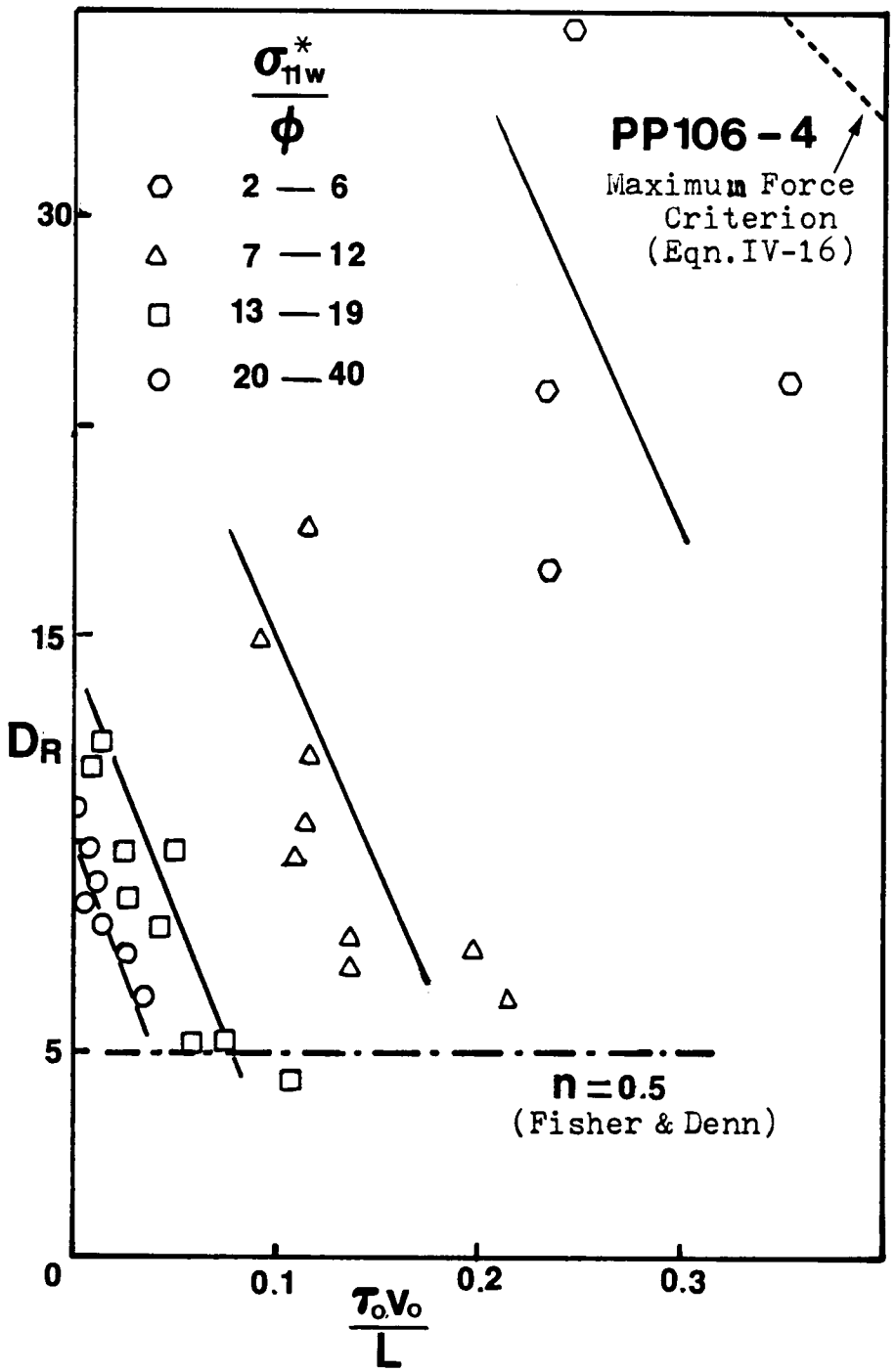


Figure V-10. Correlation of critical draw ratio as a function of elasticity number and force ratio (PP106-4).

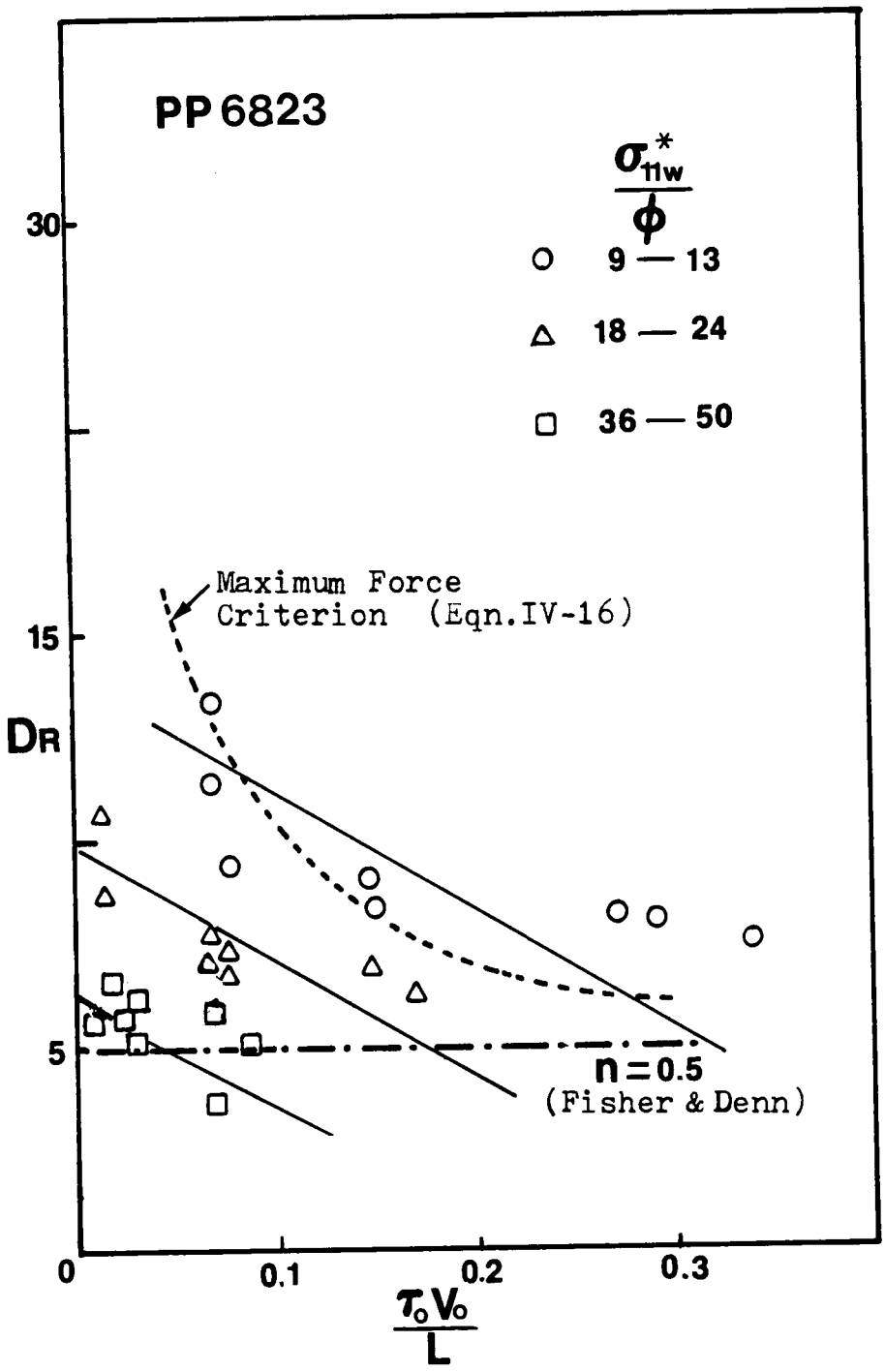


Figure V-11. Correlation of critical draw ratio as a function of elasticity number and force ratio (PP6823).

Equation IV-16, p. 45, although a similar result could have been drawn from the computer solutions of the present work. As discussed the die shear rate does not enter as a parameter in that analysis. But roughly speaking it seems to produce a low shear rate bound to the correlation based on the parameter.

Draw resonance theory suggested that the critical draw ratio showed dependence on an elasticity number and material parameters (power law index n). But in the range of the elasticity number from the present work predicted the critical draw ratios as constant 5 when the power law index n for the polypropylene was used 0.5. In fact, however, the critical draw ratios varied between 5 and 20 for PP106-4 and between 4 and 13 for PP6823. To explain this variation the ratio σ^*_{11w}/ϕ_{cr} was added empirically as another parameter. The range of values of the ratio σ^*_{11w}/ϕ_{cr} is more stable and straight lines for same ratio group were drawn in Figures V-10 and V-11. Approximately the same ratios X^*_{cr}/X^*_m from previous correlation were observed on the line of the same ratios σ^*_{11w}/ϕ_{cr} in these plots. And also the minimum points in the plot of the critical draw ratio versus initial velocity, as shown in Figure V-5, p. 76, disappeared in this plot ($D_{R_{cr}}$ vs. $1/x^*$ with $\sigma_{11w}{}^*/\phi_{cr}$). One could roughly superimpose two plots for two different polypropylenes although there was a little horizontal shift due to the choices of relaxation times τ.

In summary, among four correlating groups, two correlating groups having to do with the die swell and the dimensionless velocity gradient just downstream of the die swell region, were useful qualitatively but not quantitatively in an overall sense. Two other correlating groups

which proved to be more successful had to do with the maximum force criterion and the criterion which reflect the mismatch of the force in the die flow and the force in the spinline. The latter idea was quantified by introducing the ratio σ^*_{11w}/ϕ_{cr} which proved to be the most successful correlating group and was used as an additional parameter to explain the die shear rate effect.

CHAPTER VI

SUMMARY OF IMPORTANT RESULTS AND CONCLUSIONS

The present work involves an overall study of isothermal melt spinning including both steady state spinning and unsteady state spinning (draw resonance). A systematic study on two commercial polypropylenes (see Table III-1, p. 27) was carried out as a function of the variables one normally associates with draw resonance (namely, the die velocity, the take-up velocity, the spin length, the die diameter, the die length, the extrusion temperature and the environmental temperature) and also with particular attention to the variables that have to do with the die flow (that is, the die velocity, the die diameter, and the die length). Essentially all of the work was carried out under isothermal conditions (that is, such that the environmental temperature was kept at the same value as the melt temperature), although a few qualitative runs were made under cooling conditions.

An integral viscoelastic analysis for spinning, developed by Matsui and Bogue (52), which includes the shear rate in the die as a parameter, was solved numerically for comparison with data from steady spinning and also was used as a guide to correlating data in unsteady spinning (the onset of draw resonance). The major results from these experiments and analyses will now be summarized.

A. Steady Spinning

The diameter change along the spinline was measured using a Reticon Scan camera and the tension was measured using a Rothschild tensiometer. These data were compared with computer solutions of the integral analysis of Matsui and Bogue (Equation B-9 in Appendix) using both one element and three elements in the relaxation spectrum. In order to use this analysis it was necessary to evaluate certain rheological parameters (including the Bogue-White parameter b, the relaxation times τ_i and the moduli G_i). These were obtained by fitting shear and normal stresses data and dynamic data obtained by previous workers.

Generally computer solutions were in good agreement for fitting the experimental velocity distribution along the spinline, with the three element model fitting somewhat better than the one element model. However, the computer solution did not give the flat velocity distribution (plateau region) observed experimentally at large throughputs. The calculated and measured values of the spinline tension were also compared. Even though there were experimental difficulties in measuring the spinline tension, due to the friction between the guide rod and the fiber, the two values were in order of magnitude agreement. Experimentally it was found that the higher throughputs required higher tensions (at the same draw ratio) and the computer solutions showed the same results. Generally the three element simulations gave higher tensions than the one element computer simulations. These latter observations agreed with the results of Denn and Marrucci (17).

The computer analysis gave predictions for both the die swell and the velocity distribution along the spinline, the results for the latter having been discussed above. This die swell results will now be discussed. Because the shear rates in the die and the elongation rates in the spinline were quite different, some adjustment of the rheological parameters for these two parts was necessary. Die swell data without an applied force were used to adjust the rheological parameters and therefore the major result of the analysis was to predict the die swell in the presence of an applied force; such data were in reasonable agreement with the computer simulations and the analysis of White and Roman (83). The one element simulation gives only instantaneous die swell whereas the three element simulation gives both instantaneous and delayed die swell. While the quantitative fit of the delayed portion to the data is not very good, it is qualitatively of the correct shape.

The computer solutions for small values of b were compared with various steady state analyses based on the convected Maxwell model, including the analyses of Petrie (63), Zeichner (92), and White-Ide (84). These analyses showed that the velocity distribution along the spinline is exponential in length or linear in length depending on the applied force. The same results were obtained from the computer simulations provided that a particular value of the die shear rate was introduced. Therefore the prior analyses represent one case of a more general family of solutions provided by the present integral model.

An important result from the computer solution was that a maximum force (the so-called "blow-up point") occurs, under certain conditions,

as the take-up speed is increased. The appearance of the maximum force occurs only when the Bogue-White parameter b is larger than some critical value ($\frac{1}{\sqrt{3}}$). This maximum force was subsequently found also in the equation of White-Ide (84), but agreement between the velocity distribution from that equation and that from the computer simulation was sensitive to the shear rate in the die. Also an infinite velocity gradient was found at the take-up under conditions of maximum force; this was associated with incipient ductile failure. Thus the maximum force criterion was later used as a correlating for the onset of draw resonance.

B. Unsteady Spinning

Experimental measurements on unsteady spinning involved the monitoring the diameter as a function of the length and observation of the fluctuation of the tension at the take-up. Certain observations about the stability of the spinning could be made directly from the observed data. In general, variables that caused the die swell to increase, namely short die aspect ratios (small L/D) and large die shear rates, caused the spinning to be less stable. Concerning the environmental temperature, it was observed that nonisothermal spinning was more stable, although no quantitative study was done on this part of the problem. The other variables affecting the onset of draw resonance, including the spin length and the die flow variables, interacted in a complicated way and could not be correlated directly; generally, however, short spin lengths were more stable than long ones. An understanding of the interacting effects requires mathematical analysis which will be developed below.

Comparisons of the experimental critical draw ratios and periods of the fluctuation were made with existing theory. The critical draw ratio, characterizing the onset of draw resonance, was in the range of 5 to 20, in agreement with the analysis of Fisher and Denn (25) for a reasonable choice of the power law exponent n (see Figure III-2, p. 29). The period of the fluctuation, which is related to residence time in the spinning, was calculated by assuming several kinds of fluid behavior and compared with the measured values. The overall agreement between theory and experiment, as regards both the onset of draw resonance and the period of it, suggests that the basic instability being observed is in fact the one being described in the theory. Despite this general agreement, however, there are clearly deviations which are related to the shear flow in the die. In order to deal with these die flow effects, several correlating schemes were investigated.

Four correlating groups were considered. Two correlating groups had to do with the die swell region, namely the ratio of the die swell without an applied force to the die swell with an applied force, and the dimensionless velocity gradient just downstream of the die swell region. These two groups were useful qualitatively but not quantitatively in an overall sense.

Two other correlating groups which proved to be more successful had to do with the maximum force criterion and the criterion which reflected the mismatch of the force in the die flow and the force in the spinline. As noted earlier the point of maximum force was associated

with incipient ductile failure, which intuitively would seem to be related to the onset of draw resonance. This idea was quantified by introducing the ratio ϕ_{cr}/ϕ_m, where the force ϕ_{cr} was calculated from the computer at the onset of draw resonance and ϕ_m was obtained from the computer at the "blow-up point." These ratios were between 0.5 and 1.0. For the more thinning polymer (PP6823, b = 0.9) the ratios were about unity whereas for the less thinning polymer (PP106-4, b = 0.6) the ratios were of the order 0.5-0.9. Thus there is certainly some connection between the onset of draw resonance and the maximum force criterion even though this correlating group does not include a strong effect of the die shear rate.

The criterion having to do with the mismatch of force in the die flow and the force in the spinline obviously involves the die shear rate, which seemed to be the missing parameter in the previous correlation. This idea led to considering the dimensionless ratio σ^*_{11w}/ϕ_{cr}, where σ^*_{11w} is the dimensionless tensile stress in the die and ϕ_{cr} is the dimensionless spinline force at the onset of draw resonance. Draw resonance theory suggested that the critical draw ratio should depend on an elasticity number and material parameters (power law index n). When the ratio σ^*_{11w}/ϕ_{cr} was added empirically as another parameter, a correlation was achieved. In general the smaller the ratio σ^*_{11w}/ϕ_{cr} was, the more stable the spinning. Two different plots were prepared for the two different polymers although possibly a master plot could be constructed with somewhat different choices of the relaxation times.

LIST OF REFERENCES

LIST OF REFERENCES

1. D. Acierno, J. N. Dalton, J. M. Rodriguez and J. L. White, J. Appl. Poly. Sci., 15, 2395 (1971).

2. E. B. Bagley and J. J. Duffey, Trans. Soc. Rheol., 14:4, 545 (1970).

3. T. F. Ballenger and J. L. White, J. Appl. Poly. Sci., 25, 1949 (1971).

4. V. Bankar, J. E. Spruiell and J. L. White, The University of Tennessee, Knoxville, Poly. Sci. and Eng., 63 (1976).

5. A. Bergonzoni and A. Dicresce, Poly. Eng. Sci., 6, 45 (1966).

6. B. Bernstein, E. Kearsley and L. Zapas, J. Res. NBS, 68B, 103 (1964).

7. R. B. Bird, Ann. Rev. Fluid Mech., 8, 13 (1976).

8. L. Blyler and C. Gieniewski, presented at the 47th Annual Meeting of Soc. of Rheo., New York, Feb. 1977.

9. L. Blyler and G. Gieniewski, presented at U.S.-Japan Society of Rheol., Hawaii, March 1979.

10. D. C. Bogue and J. L. White, NATO Agardograph 144 (1970).

11. J. C. Chang and M. M. Denn, J. Non-Newtonian Fluid Mech., 5, 369-385 (1979).

12. J. C. Chang and M. M. Denn, Rheology, 3 (1980).

13. J. C. Chang, M. M. Denn and F. T. Geyling, I&EC Fundamentals, 20, 147 (1981).

14. I. J. Chen, G. E. Hagler, L. E. Abbott, D. C. Bogue and J. L. White, Trans. Soc. Rheol., 16, 473 (1972).

15. R. E. Christensen, J. S.P.E., 18, 751 (1962).

16. M. M. Denn, C.J.S. Petrie and P. Avenas, AICHE J., 21, 791 (1975).

17. M. M. Denn and G. Marrucci, J. Non-Newtonian Fluid Mech., 2, 159-167 (1977).

18. M. M. Denn, Denn's R and D Note (1979); AICHE J., 26, 292 (1980).

19. M. M. Denn, AICHE J., 26, 292 (1980).

20. G. Donnely and C. B. Weinberger, Ind. Eng. Chem. Fundamentals, 14, 334 (1975).

21. L. H. Drexler and C. D. Han, J. Appl. Poly. Sci., 17, 2355 (1973).

22. L. H. Drexler and C. D. Han, J. Appl. Poly. Sci., 17, 2369 (1973).

23. R. J. Fisher and M. M. Denn, AICHE J., 22, 236 (1976).

24. R. J. Fisher and M. M. Denn, AICHE J., 23, 23 (1977).

25. R. Fisher and M. M. Denn, Chem. Eng. Sci., 20, 1129 (1975).

26. D. K. Gagon and M. M. Denn, Poly. Eng. Sci. 21, 644 (1981).

27. D. Gelder, Ind. Eng. Chem. Fundamentals, 10, 534 (1971).

28. H. H. George, Poly. Eng. Sci., 22, No. 5, 292 (1982).

29. A. Ghijsels and J.J.S.M. Ente, presented at 8th International Congress on Rheology, Naples, Sept. 1980.

30. W. W. Graessley, S. D. Glasscock and R. L. Crawley, Trans. Soc. Rheo., 14, 519 (1970).

31. C. D. Han, R. Lamonte and Y. Shah, J. Appl. Poly. Sci., 16, 3307 (1972).

32. C. D. Han, Trans. Soc. Rheol., 18, 163 (1974).

33. C. D. Han, Rheology in Polymer Processing, Academic Press, New York (1976).

34. C. D. Han and Y. W. Kim, J. Appl. Poly. Sci., 20, 1555 (1976).

35. C. D. Han and S. Apte, J. Appl. Poly. Sci., 24, 62 (1979).

36. D. C. Huang and J. L. White, Poly. Eng. and Sci., 19, 609 (1979).

37. J. C. Hyun, AICHE J., 24, 418, 423 (1978).

38. J. C. Hyun, AICHE J., 26, 294 (1980).

39. Y. Ide and J. L. White, J. Appl. Poly. Sci., 19, 419 (1975).

40. Y. Ide and J. L. White, J. Non-Newtonian Fluid Mech., 2, 281 (1977).

41. Y. Ide and J. L. White, J. Appl. Poly. Sci., 22, 1061 (1978).

42. H. Ishihara and S. Kase, J. Appl. Poly. Sci., 14, 1597 (1970).

43. H. Ishihara and S. Kase, J. Appl. Poly. Sci., 19, 557 (1975).

44. H. Ishihara and S. Kase, J. Appl. Poly. Sci., 20, 169 (1976).

45. F. Kanel, Ph.D. Dissertation, University of Delaware, Newark, 1972.

46. S. Kase, T. Matsuo and Y. Yoshimoto, Seni Kikai Gakkaishi, 19, T63 (1966).

47. S. Kase, J. Appl. Poly. Sci., 18, 3279 (1974).

48. S. Kase and T. Matsuo, Appl. Poly. Sci., 20, 367 (1976).

49. A. S. Lodge, D. J. Evans and D. B. Scully, Rheo. Acta., 4, 140 (1965).

50. T. Matsmoto and D. C. Bogue, Trans. Soc. Rheo., 21:4, 453 (1977).

51. M. Matsui and D. C. Bogue, Poly. Eng. Sci., 16, 11 (1976).

52. M. Matsui and D. C. Bogue, Trans. Soc. Rheol., 21, 133 (1977).

53. R. A. Mendelson and F. L. Finger, J. Appl. Poly. Sci., 17, 797 (1973).

54. A. B. Metzner, W. T. Houghton, R. A. Sailer and J. L. White, Trans. Soc. Rheo., 5, 133 (1961).

55. W. Minoshima, J. L. White and J. E. Spruiell, The University of Tennessee, Knoxville, Poly. Sci. and Eng., Report No. 126 and 128 (1979).

56. L. W. Morland and E. H. Lee, Trans. Soc. Rheo., 4, 233 (1960).

57. N. Nakajima and M. Shida, Trans. Soc. Rheol., 10, 299 (1960).

58. R. E. Nickell, R. I. Tanner and B. Caswell, J. Fluid Mech., 65, 189 (1974).

59. J. R. Pearson and M. A. Matovich, Ind. Eng. Chem. Fundamentals, 8, 605 (1969).

60. J. R. Pearson and Y. T. Shah, Ind. Eng. Chem. Fundamentals, 13, 134 (1974).

61. C. J. Petrie and M. M. Denn, AICHE J., 22, 209 (1976).

62. C. J. Petrie, J. Non-Newtonian Fluid Mech., 4, 137 (1978).

63. N. Phan Thien, J. Rheol., 22, 259 (1978).

64. N. Phan Thien and R. I. Tanner, J. Non-Newtonian Fluid Mech., 2, 353 (1977).

65. R. Racin and D. C. Bogue, J. Rheol., 23, 263 (1979). M.S. Thesis, Poly. Eng., The University of Tennessee, Knoxville.

66. K. R. Reddy and R. I. Tanner, J. Rheol., 22, No. 6, 661-665 (1978).

67. Y. Sano and K. Orii, Sen. I. Gakkaishi, 24, 212 (1968).

68. Y. T. Shah and J.R.A. Pearson, I&EC Fundamentals, 11, No. 2 (1972).

69. Y. T. Shah and J. R. Pearson, Trans. Soc. Rheol., 16, 519 (1972).

70. J. A. Speart, Ph.D. Dissertation, University of Delaware, Newark (1972).

71. J. A. Spearot and A. B. Metzner, Trans. Soc. Rheol., 16, 495 (1972).

72. R. S. Spencer and R. E. Dillon, J. Colloid Sci., 4, 241 (1949).

73. R. I. Tanner, J. Poly. Sci., A-2, 8, 2017 (1970).

74. R. I. Tanner, Appl. Poly. Symposium No. 20, 201 (1973).

75. R. E. Tanner, R. E. Nickell and R. W. Bilger, Computer Methods Appl. Mech. Eng., 6, 155 (1975).

76. T. Takaki and D. C. Bogue, J. Appl. Poly. Sci., 19, 419 (1975).

77. G. Vassilatos, presented at the 68th Annual Meeting of AICHE, Los Angeles, Calif., Nov. 1975.

78. G. V. Vinogradov, A. Y. Malkin, G. Yanovskii, E. Borisenkova, B. Yarlykou and G. Berejhnaya, J. Poly. Sci., A-2, 10, 1061 (1972).

79. J. Vlachopoulous, M. Horie and S. Lidorikis, Trans. Soc. Rheol., 16:4, 669 (1972).

80. J. Vlachopoulos, J. Rheol. Acta, 13, 2 (1974).

81. J. L. White, Trans. Soc. Rheol., 19:2, 271 (1975).

82. J. L. White and J. F. Roman, J. Appl. Poly. Sci., 20, 1005 (1976).

83. J. L. White and J. F. Roman, J. Appl. Poly. Sci., 20, 1005 (1976) and 21, 869 (1977).

84. J. L. White and Y. Ide, J. Appl. Poly. Sci., 22, 3057 (1978).

85. J. L. White and A. Kondo, J. Non-Newtonian Fluid Mech., 3, 41-64 (1977/1978).

86. J. L. White and A. Kondo, J. Appl. Poly. Sci., 21 (1977).

87. J. L. White, J. Appl. Poly. Sci., 21, 2289 (1979).

88. J. L. White, Poly. Eng. Reviews, 1, No. 4, Dec. (1981).

89. M. Williams, R. Landel and J. Ferry, J. Am. Chem. Soc., 77, 3701 (1955).

90. C. Wust, M.S. Thesis, Poly. Eng., The University of Tennessee, Knoxville, 1978.

91. H. Yamane, M.S. Thesis, Poly. Eng., The University of Tennessee, Knoxville, 1982.

92. G. Zeichner, M.S. Thesis, Chem. Eng., University of Delaware, Newark, 1972.

93. G. R. Zeichner and P. D. Patel, presented at 2nd World Congress of Chemical Eng. and World Chemical Exposition, Montreal, Canada, Oct. 1981.

94. A. Ziabicki, Man-Made Fibers, 1, edited by H. Mark, S. Atlas and E. Caernia (New York: Wiley, 1967).

95. A. Ziabicki, Fundamentals of Fiber Formation (London: Wiley, 1976).

APPENDIX

APPENDIX

SUMMARY OF NEWTONIAN AND INTEGRAL VISCOELASTIC ANALYSES FOR THE METL SPINNING PROBLEM AND COMPUTER PROGRAM

A. Newtonian Analysis

Referring to Figure 1, we have the following equations

Mass balance: $PV_x \pi R^2 = W = \text{constant}$ (A-1)

Force balance: $Frheo = \sigma_{xx} \cdot \pi R^2 = \text{constant}$ (A-2)

From Equations A-1 and A-2

$$\int_{V_o}^{V_x} \frac{dV_x}{V_x} = \int_o^x \frac{Frheo}{3\eta W} dX \tag{A-3}$$

Therefore

$$V_x = V_o e^{KX} \tag{A-4}$$

where

$$K = \frac{Frheo}{3\eta W}$$

To convert to a dimensionless form let

$$R^* = \frac{R}{R_o} , \quad X^* = \frac{X}{\tau_1 V_o} , \quad \phi = \frac{Frheo}{\pi G R_o^2}$$

Solving from Equation A-3

$$\ln V^* = \frac{\phi}{3} \cdot X^* \tag{A-5}$$

Therefore

$$V^* = \exp\left(\frac{\phi}{3} \cdot X^*\right) \tag{A-6}$$

B. Integral Viscoelastic Analysis

Isothermal viscoelastic theory can be summarized by the following equations (6, 7, 10):

$$\sigma_{ij} = -P\delta_{ij} + \int_{-\infty}^{t} [m_1(t-t')C_{ij}^{-1} - m_2(t-t')C_{ij}]dt' \tag{B-1}$$

where $m_1(t-t')$ and $m_2(t-t')$ are deformation dependent memory functions, and C_{ij}^{-1} and C_{ij} are the relative Finger and Cauchy strain tensors. For a Maxwell memory function for m_1 and setting $m_2 = 0$, one obtains

$$\sigma_{ij} = -P\delta_{ij} + \int_{-\infty}^{t} \sum_n G_n \frac{e^{-(t-t')/\tau_n}}{\tau_n} C_{ij}^{-1}\, dt' \tag{B-2}$$

where σ_{ij} is the stress, P is the isotropic pressure, the G_n and τ_n are elastic moduli and relaxation times, C_{ij}^{-1} is the relative Finger strain tensor, t' is arbitrary past time, and t is the time under consideration. This is a simplified form in which the Cauchy strain tensor is omitted.

Matsui and Bogue (52) proposed the following nonisothermal form by generalizing concepts first suggested by Morland and Lee (57):

$$\sigma_{ij} = -P\delta_{ij} + \int_{-\infty}^{t} \sum_n G_n \frac{\exp\left(-\int_t^{t'} \frac{dt''}{\tau_n(t'')}\right)}{\tau_n(t')} C_{ij}^{-1}\, dt' \qquad \text{(B-3)}$$

where $\tau_n(\cdot) = A_T\{T(\cdot)\}\tau_n$ and A_T is the temperature shift factor, obtainable from the WLF equation or a similar correlation (89). Further they developed the following non-linear model:

$$\sigma_{ij} = -P\delta_{ij} + \int_{-\infty}^{t} \sum_n G_n \frac{\exp\left(-\int_t^{t'} \frac{dt''}{\tau_n^*(t'')}\right)}{\tau_n^*(t')} C_{ij}^{-1}\, dt' \qquad \text{(B-4)}$$

where $\tau_n^*(\cdot) = \tau_n^{\cdot} A_T\{T(\cdot)\}/[1 + b\Pi_d^{\frac{1}{2}} \tau_n^{\cdot} A_T\{T(\cdot)\}]$
and Π_d is the second invariant of the deformation rate. The b is an empirical dimensionless parameter.

For melt spinning (simple elongational deformation), using the spatial coordinates $X^i(t)$ at time t and the body coordinate $X^i(t')$ at an arbitrary past time t' and introducing a parabolic velocity distribution, that is $\dot{\gamma}(r) = |dV(r)/dr| = 4Vr/R^2$, they obtained finally for the r-averaged stress $\bar{\sigma}_{11}(t)$:

$$\bar{\sigma}_{11}(t) = \sum_n G_n \left\{ \int_{-\infty}^{0} \left[\int_0^1 \frac{\exp\left(-\int_{t'}^{t} \frac{dt''}{\tau_n^*(t'')}\right)}{\tau_n^*(t')} \cdot \left\{ \lambda_o^2 \left(1 + \frac{16\bar{V}^2 t'^2 \zeta^2}{R^2}\right) - \lambda_o^{-1} \right\} 2\zeta\, d\zeta \right] dt' + \int_0^t \frac{\exp\left(-\int_{t'}^{t} \frac{dt''}{\tau_n^*(t'')}\right)}{\tau_n^*(t')} \cdot (\lambda^2 - \lambda^{-1}) dt' \right\} \qquad \text{(B-5)}$$

where

$$\Pi_d^{\frac{1}{2}} = \begin{cases} \sqrt{3}\,\dfrac{dV}{dX} & (t' > 0) \\ \dot{\gamma}(r) = \dfrac{4\bar{V}r}{R^2} & (t' < 0) \end{cases}$$

ζ = (r/R)die or spinline, $\lambda = A(t')/A(t) = V(t)/V(t')$, $\lambda_o = A_o/A(t) = V(t)/V_o$. Later Wust (90) rearranged this equation using distance instead of time as the variable of integral

$$dt' = \frac{dX'}{V(X)} \tag{B-6}$$

and obtained

$$\sigma_{11} = \sum_n G_n \exp\left[\left(-\int_o^x \frac{dX''}{\tau_n(X'')V(X'')}\right)\left(\frac{V(x)}{Vx=0}\right)^{-\sqrt{3}b}\left\{(1+FKn)\left(\frac{V(x)}{Vdie}\right)^2 - \frac{Vdie}{V(X)}\right\} + \int_o^x \left(\frac{1}{\tau_n(x')V(x')} + \frac{\sqrt{3}b}{V(x')}\left|\frac{dV}{dx'}\right|\right) \cdot \left(\exp - \int_{x'}^x \frac{dx''}{\tau_n(x'')V(x'')}\right) \cdot \left(\left(\frac{V(x)}{V(x'')}\right)^{2-\sqrt{3}b} - \left(\frac{V(x)}{V(x')}\right)^{1+\sqrt{3}b}\right) dX'\right] \tag{B-7}$$

where $FK_n = \int_o^1 \frac{4\zeta^3\, d\zeta}{(K_n^{-1} + b\zeta)^2}$

$$K_n = \left(\frac{4\bar{V}\,\tau_n}{R}\right) \equiv \left(\dot{\gamma}_w \cdot \tau_n\right), \quad \zeta = \left(\frac{r}{R}\right) die$$

Also Wust (19) solved his from the spinline for the case of $\bar{\sigma}_{11} = 0$ (no take-up force) and obtained a result for the die swell.

The present author has put Wust's result into dimensionless form as follows:

Let $X^* = \frac{X}{\tau_1 V_o}$ $\qquad V^*(\ ) = V(X^*)$

$X^{*\prime} = \frac{X'}{\tau_1 V_o}$ and $\qquad V^*(') = V(X^{*\prime})$

$X^{*\prime\prime} = \frac{X''}{\tau_1 V_o}$ $\qquad V^*('') = V(X^{*\prime\prime})$

and

$$\alpha = \frac{V_o \text{ (in the die)}}{V_o^+ \text{ (after instant die swell)}}$$

$$\phi = \frac{F_{rheo}}{G_1 \pi R_o^2}$$

From the initial condition

$$V^* \cdot R^{*2} = 1 \tag{B-8}$$

one obtains finally

$$\phi = \frac{1}{V^*(\ )}\left[\exp\left(-\int_o^{X^*} \frac{dX^{*\prime\prime}}{V^*(\prime\prime)}\right) \cdot (V^*(\ )\alpha)^{-\sqrt{3}b} \cdot ((1 + FK_1)V^*(\ )^2 - \frac{1}{V^*(\ )}) + \int_o^{X^*}\left(\frac{1}{V^*(')} + \frac{\sqrt{3}b}{V^*(')} \cdot \frac{dV^*(')}{dX^{*\prime}}\right) \cdot \left(\exp - \int_{X^{*\prime}}^{X^*} \frac{dX^*}{V^*(\prime\prime)}\right) \left(\left(\frac{V^*(\ )}{V^*(')}\right)^{2-\sqrt{3}b} - \left(\frac{V^*(\ )}{V^*(')}\right)^{1+\sqrt{3}b}\right) dX^{*\prime}\right] \tag{B-9}$$

Instead of using α, Equation B-9 becomes as follows:

$$\phi = \frac{1}{V^*()}\left[\left(\exp -\int_0^{X^*}\frac{dX^{*\prime}}{V^*(\prime)}\right)\left(\frac{V^*(0^+)}{V^*(\ )}\right)^{\sqrt{3}b}\left((1+FK_1)V^{*2}(\ ) - \frac{1}{V^*(\ )}\right)\right.$$
$$+\int_0^{X^*}\left(\frac{1}{V^*(\prime)}+\frac{\sqrt{3}b}{V^*(\prime)}\cdot\frac{dV^*(\prime)}{dX^{*\prime}}\right)\left\{\exp\left(-\int_{X^{*\prime}}^{X^*}\frac{dX^{*\prime\prime}}{V^*(\prime\prime)}\right)\right\}$$
$$\left.\left\{\left(\frac{V^*(\ )}{V^*(\prime)}\right)^{2-\sqrt{3}b} - \left(\frac{V^*(\ )}{V^*(\prime)}\right)^{1+\sqrt{3}b}\right\} dX^{*\prime}\right] \qquad \text{(B-10)}$$

Wust also showed that if $\phi = 0$ and one time constant, then he obtained a die swell region at $X^* = 0$.

This form assumes one G and one : more general forms can be stated but will, of course, involve other material ratios $\left(\frac{G_2}{G_1}, \frac{G_3}{G_1}, \frac{G_4}{G_1}, \text{----} \frac{\tau_2}{\tau_1}, \frac{\tau_3}{\tau_1}, \frac{\tau_4}{\tau_1} \text{---}\right)$.

C. Computer Program for Isothermal Viscoelastic Integral Model

Three Element Model Program

Following is a listing of the main computer program and one subroutine used in the modeling of the melt spinning process. This program is modified from that of Wust's die swell analysis (M.S. Thesis, The University of Tennessee, Knoxville, 1976). The calculation of the second half of the stress equation is changed to get a direct double integration instead of using Wust's simplification. The programs are self-explanatory and the reader is asked to reference the Part B of Appendix and Chapter IV for further information about the equations or procedure.

```
C THIS PROGRAM IS SPECIFICALLY FOR MODELLING THE DIE SWELL
C WITH AND WITHOUT FORCE, THE VELOCITY DISTRIBUTION ALONG
C THE SPINLINE AND THE RESIDENCE TIME. THE PROGRAM IS EASILY
C MODIFIED FOR OTHER CASES(I.E.,ONE ELEMENT MODEL,THREE
C ELEMENTS MODEL AND MUTIPLE ELEMENTS MODEL).
C FIRST THERE WILL BE PRESENTED A LIST OF THE VARIABLES
C USED AND THE MEANING. THEN THE PROGRAM WITH COMMENTS
C WILL BE LISTED.
C
C
C LIST OF VARIABLES
C
C   AK      DIMENSIONLESS SHEAR RATE
C   B       NON-LINEAR FACTOR
C   BSQ     B TIMES THE SQUARE ROOT OF 3
C   C       USED IN CALCULATION OF F
C   C1      USED IN CALCULATION OF FIRST HALF OF STRESS EQ'N
C   C2      USED IN CALCULATION OF FIRST HALF OF STRESS EQ'N
C   C3      USED IN CALCULATION OF SECOND HALF OF STRESS EQ'N
C   C2G     CALCULATED FORCE EQUATION CONSTANT
C   CRT     N IF TELETYPE OUTPUT IS NOT DESIRED
C   DEL     INCREMENTAL DISTANCE
C   DI1     DISTANCE FROM THE DIE
C   DIFF    DIFFERENCE BETWEEN CALCULATED AND SET FORCE EQ'N
C           CONSTNAT
C   EQ1     VALUE OF EXPONENTIAL INTEGRAL FROM X'(I) TO X
C   F       EQUIVALENT FO SQUARE OF DIMENSIONLESS SHEAR RATE
C   FACG    DIMENSIONLESS ELASTIC MODULUS
C   FACTAU  DIMENSIONLESS RELAXATION TIME
C   FAI     PRESENT STEP VALUE OF INTEGRAL IN EXPONENTIAL INTEGRAL
C   FAK     AVERAGED VALUE OF FAI
C   FBK     VALUE OF INTEGRAL IN EXPONENTIAL INTEGRAL FROM X' TO X
C   FR      THE RECIPROCAL VALUE OF VELOCITY
C   FSG     VALUE OF INTEGRAL IN EXPONENTIAL INTEGRAL USED
C           TO CALCULATE THE EXPONENTIAL VALUE
C   FJ      SUMMED VALUE IN EXPONENTIAL INTEGRAL
C   G       ELASTIC MODULUS
C   GAMA    WALL SHEAR RATE
C   I       COUNTER FOR STEP NUMBER
C   IN      LOGICAL UNIT NUMBER OF INPUT DEVICE
C   IOUT1   LOGICAL UNIT NUMBER OF FIRST OUTPUT DEVICE(TELETYPE)
C   IOUT2   LOGICAL UNIT NUMBER OF SECOND OUTPUT DEVICE(FILE)
C   IP      COUNTER FOR GUESS NUMBER
C   NTG     NUMBER OF TAU'S AND G'S
C   PHI     SET FORCE EQUATION CONSTANT
C   Q       VALUE OF INTEGRAL IN EXPONENTIAL INTEGRAL
C           FROM X' TO X
C   R       RADIUS
C   RDIFF   RADIUS DIFFERENCE BETWEEN THIS AND PREVIOUS GUESS
C   RG      GUESSED RADIUS
C   RMULT   MAXIMUM ACCEPTABLE VALUE FOR DIFFERENCE BETWEEN
C           CALCULATED AND SET CONSTANTS. EQUAL TO PHI/1000
C   RTES    RESIDENCE TIME
C   S       PRESENT STEP VALUE OF INTEGRAL IN EXPONENTIAL
C           INTEGRAL(FINAL) FROM 0 TO X
C   S2      INTERMEDIATE VALUE OF STRESS USED IN SECOND HALF
C           OF STRESS EQ'N
C   S3      SUM OF S2
C   SG      PRESENT STEP VALUE OF INTEGRAL IN EXPONENTIAL
C           INTEGRAL(GUESSED) FROM 0 TO X
```

```
C  SIG     STRESS
C  SIGO    STRESS CALCULATED FROM FIRST HALF OF STRESS EQ'N
C  TAU     RELAXATION TIME
C  V       VELOCITY
C  ZS      ADJUSTMENT VALUE OF THE  TOTAL SHEAR RATE
C
C
C INITIALIZE
C
      DIMENSION RG(1100),V(1100),C2G(1100),SIG(1100)
      DIMENSION SG(9),R(1100),RTES(1100),FR(1100)
      DIMENSION FACTAU(9),FACG(9), TAU(9),G(9),S(9)
C
C SET ACTUAL VALUES EQUAL TO GUESSED VALUES.
C
      COMMON S,FACTAU,FACG,GAMA,TAU,SG,NTG
      COMMON V,DEL,I,SIG,BSQ,B,ZS
C
C SOME OUTPUT WILL BE WRITTEN ON THE TELETYPE (5);A FULL OUTPUT
C WILL BE WRITTEN IN FILE FOR22.DAT (22) FOR LATER OUTPUT
C TO THE LINEPRINTER.
C
      IOUT1=5
      IOUT2=22
C
C INPUT IS TELETYPE KEYBOARD (5).
C
      IN=5
C
C FIRST STEP
C
      I=1
      T=0.
C
C WRITE OUT LIST OF INPUT VARIABLES FOR PROGRAMMER REFERENCE.
C
      WRITE(IOUT1,10010)
C
C INPUT PROGRAM PARAMETERS.
C
      READ(IN,10030) B,NTG,PHI,GAMA,DEL,ZS,CRT
C
C WRITE THE PARAMETERS ON FILE NEEDED TO DUPLICATE THIS RUN
C FOR REFERENCE
C
      WRITE(IOUT1,10050) B,PHI, GAMA
      WRITE(IOUT2,10050) B,PHI,GAMA
C
C FOR EACH POLYMER, THE SPECIPIC TAU'S AND G'S WOULD BE
C INPUT OR SET HERE.
C
      TAU(1)=0.01
      TAU(2)=0.1
      TAU(3)=1.0
      G(1)=500000
      G(2)=100000
      G(3)=25000
C
C SET THE NUMBER OF TAU'S AND G'S TO BE USED. CAN ALSO BE AN
C INPUT VARIABLE FOR TESTING THE EFFECT OF HAVING MORE OR
```

```
C FEWER.
      DO 10 J=1,NTG
      S(J)=0.
C
C
C SET UP DIMENSIONLESS TAU'S AND G'S
C
      FACG(J)=G(J)/G(2)
      FACTAU(J)=TAU(J)/TAU(2)
C
C WRITE OUT DIMENSIONLESS TAU'S AND G'S ON THE FILE FOR
C FUTURE REFERENCE.
C
      WRITE(IOUT1,10070)J,FACTAU(J),J,FACG(J)
10    CONTINUE
C
C WRITE OUT PAGE HEADINGS.
C
      WRITE(IOUT2,10080)
      BSQ=8*SQRT(3.)
      RMULT=PHI/1000.
      IP=1
C
C FIRST GUESS AT RADIUS; MUST SET UP A 'DUMMY' GUESS TO BE
C ABLE TO USE LINEAR INTERPOLATION TO CONVERGE ON A RESULT.
C
      RG(IP)=1.0
C
C CONTINUITY TO CALCULATE VELOCITY
C
      V(I)=1./RG(IP)**2.
C
C CALL HEAT TRANSFER AND STRESS SUBROUTINES TO CALCULATE
C STRESS VALUE
C
20    CALL STRESS
C
C CALCULATE FORCE BALANCE CONSTANT.
C
      C2G(IP)=SIG(I)*RG(IP)**2.
C
C NEXT GUESS AT RADIUS.
C
      RG(IP+1)=RG(IP)*0.95
C
C SECOND & SUCCEEDING GUESSES ARE CALCULATED IN THIS PART;
C NEW RADIUS IS GUESSED FROM HERE UNTIL CONVERGENCE BY
C LINEAR INTERPOLATION.
C
30    IP=IP+1
      IF(IP.GE.101) GO TO 65
C
C IF GUESSED RADIUS IS LESS THAN ZERO, USE 10% OF PREVIOUS GUESS
C
      IF(RG(IP).LE.0.) RG(IP)=RG(IP-1)*0.1
C
C CONTINUITY TO CALCULATE NEW VELOCITY.
C
      V(I)=1./RG(IP)**2.
C
```

```
C CALL STRESS SUBROUTINE.
C
      CALL STRESS
C
C NEW FORCE BALANCE CONSTANT.
C
      C2G(IP)=SIG(I)*RG(IP)**2.
C
C COMPARISION OF CALCULATED AND SET FORCE BALANCE CONSTANT.
C
      DIFF=ABS(C2G(IP)-PHI)
C
C IF THE DIFFERENCE IS GRATER THAN ACCEPTABLE, GO TO LINEAR
C INTERPOLATION CALCULATION FOR NEW RADIUS.
C
      IF(DIFF.GE.RMULT) GO TO 50
C
C IF THE CALCULATED AND SET CONSTANTS ARE EQUAL, THE GUESSED
C RADIUS FOR THIS PASS IS THE ACTUAL RADIUS.
C
35    R(I)=RG(IP)
      DO 40 J=1,NTG
      S(J)=SG(J)
40    CONTINUE
      V(I)=1./R(I)**2.
      FR(I)=1./V(I)
      IF(I.EQ.1) GO TO 3
C
C CALCULATE THE RESIDENCE TIME FROM THE VELOCITY
C
      RTES(I)=T+TAU(2)*(FR(I-1)+FR(I))*DEL/2.
      T=RTES(I)
      GO TO 4
3     RTES(I)=0.
C
C DISTANCE
C
4     DI1=DEL*(I-1)
C
C IF TELETYPE OUTPUT IS NOT DESIRED (ONLY WRITE ON FILE),
C SKIP THIS.
C
      IF(CRT.EQ.1HN) GO TO 45
C
C TELETYPE OUTPUT
C
      WRITE(IOUT1,10090) DI1,R(I),V(I),SIG(I),RTES(I),IP
C
C FILE OUTPUT
C
45    WRITE(IOUT2,10090) DI1,R(I),V(I),SIG(I),RTES(I),IP
C
C TOTAL STEPS FOR THIS RUN IS 1000, MORE OR FEWER CAN BE
C SPECIFIED BY CHANGING THIS LINE.
C
      IF(I.EQ.1000) GO TO 70
C
C FIRST PASS THROUGH NEXT STEP.
C
      IP=1
```

```
C
C SET UP NEW GUESSED RADIUS AT 95% OF PREVIOUS VALUE.
C
      RG(IP)=R(I)*0.95
C
C NEXT STEP INDICATOR.
C
      I=I+1
C
C NEXT STEP VELOCITY.
C
      V(I)=1./RG(IP)**2.
C
C RETURN TO GUESSING AND STRESS CALCULATING LOOP. AGAIN,
C THIS HAS BEEN SET UP AS A 'DUMMY' (SEE PREVIOUS COMMENT).
C
      GO TO 20
50    CONTINUE
C
C LINEAR INTERPOLATION CALCULATIONS; WHEN DONE RETURN TO
C STRESS LOOP.
C
      RDIFF=ABS(RG(IP)-RG(IP-1))
C
C THIS LINE KEEPS THE COMPUTER FROM OVERFLOWING. THE FORCE AND
C RADIUS CAN BE OF THE FORM SO THAT A CHANGE IN RADIUS OF
C 10E-5 ONE WAY THEN THE OTHER WILL CAUSE THE CALCULATED
C CONSTANT TO FALL ON EITHER SIDE OF THE SET CONSTANT. THIS
C SOLUTION IS CORRECT TO THE DESIRED ACCURACY, BUT THE LIMITS
C ON COMPUTER ACCURACY WILL NOT SHOW THE RESULT. IF THE ABOVE
C IS TRUE, THE PRESENT RADIUS IS USED AS THE ACTUAL RADIUS.
C
      IF((RDIFF.LE.(RG(IP)*1.E-5))
     1.AND.((C2G(IP).GT.PHI.AND.C2G(IP-1).LT.PHI)
     2.OR.(C2G(IP).LT.PHI.AND.C2G(IP).GT.PHI))) GO TO 35
C
C TWO FORMS OF LINEAR INTERPOLATION DEPENDING UPON HOW THE
C CALCULATED AND SET NUMBERS ARE RELATED.
C
      IF(C2G(IP-1).GT.C2G(IP).AND.C2G(IP).GT.PHI) GO TO 60
      IF(C2G(IP-1).LT.C2G(IP).AND.C2G(IP).LT.PHI) GO TO 60
      RG(IP+1)=RG(IP)-(RG(IP)-RG(IP-1))*(C2G(IP)-PHI)/
     1(C2G(IP)-C2G(IP-1))
      GO TO 30
60    RG(IP+1)=RG(IP-1)-(RG(IP-1)-RG(IP))*(C2G(IP-1)
     1-PHI)/(C2G(IP-1)-C2G(IP))
      GO TO 30
C
C IF THE PROGRAM DOES NOT CONVERGE IN 100 STEPS, IT SAYS
C SO HERE.
C
55    WRITE(IOUT1,10095)
C
C AND WRITES OUT ALL GUESSED RADII AND CALCULATED CONSTANTS
C FOR TROUBLE SHOOTING.
C
      WRITE(IOUT1,10120) ((C2G(IK),RG(IK)),IK=1,100)
C
C AFTER COMPLETION, THE PROGRAM WILL LET THE USER RUS AGAIN
C IF DESIRED.
```

```
C
70      WRITE(IOUT1,10100)
        READ(IN,10110) AN
        IF(AN.NE.1HN) GO TO 5
5       STOP
10010   FORMAT(44H INPUT DATA: B,# OF T'S&G'S,PHI,GAMA,DEL,ZS,
        118H CRT OUTPUT?(Y/N) )
10030   FORMAT(F15.0,/,I1,/,F15.0,/,F15.0,/,F15.0,/,F15.0,/,A1)
10050   FORMAT(1H1,/,4H B =,F6.2,/,6H PHI =,G10.4,/,
        17H GAMA =,G10.4)
10070   FORMAT(8H FACTAU(,I2,3H) =,G8.2,5X,5HFACG(,I2,
        13H) =,G11.5)
10080   FORMAT(///,2X,24HDIMENSIONLESS PARAMETERS,/,2X,
        18HDISTANCE,6X,6HRADIUS,9X,8HVELOCITY,8X,6HSTRESS,
        28X,4HRTES)
10090   FORMAT(2X,F8.3,2X,1PE10.3,6X,1PE10.3,4X,1PE10.3,3X,
        11PE10.3,3X,I3)
10095   FORMAT(15H NO CONVERGENCE)
10100   FORMAT(////,9H ANOTHER?)
10110   FORMAT(A1)
10120   FORMAT(1X,4F15.6)
        END
C
C
C
        SUBROUTINE STRESS
C
C THIS SUBROUTINE TAKES THE VELOCITIES,RADII AND CALCULATES
C THE STRESS USING ISOTHERMAL VISCOELASTIC EQUATION.
C
C INITIALIZE
C
        DIMENSION V(1100),FU(9,1100),FAI(9,1100),SIG(1100)
        DIMENSION FAK(9,1100),FBK(9,1100) ,VA(1100)
        DIMENSION FACTAU(9),FACG(9),TAU(9),SG(9),S(9)
        COMMON S,FACTAU,FACG,GAMA,TAU,SG,NTG
        COMMON V,DEL,I,SIG,BSQ,B,ZS
C
C THIS LOOP CALCULATES THE INTEGRAL IN THE EXPONENTIAL FROM
C 0 TO X.
C TRAPEZOIDAL RULE IS USED.
C
        DO 20 J=1,NTG
        FU(J,I)=1./(V(I)*FACTAU(J))
        IF(I.EQ.1) GO TO 10
        SG(J)=S(J)+(FU(J,I-1)+FU(J,I))*DEL/2.
        GO TO 15
C
C IF THIS IS THE FIRST STEP, THE INTEGRAL IS ZERE.
C
10      CONTINUE
        SG(J)=0.
15      CONTINUE
C
C EACH INTEGRAL FOR EACH 0 TO X IS STORED (I.E. 0 TO X(1),
C 0 TO X(2), ETC.).
C THESE WILL BE USED LATER.
C
        FAI(J,I)=SG(J)
20      CONTINUE
```

```
C
C CALCULATE SOME OFTEN USED CONSTANTS FOR LATER USE.
C
      C1=V(I)**2.-1./V(I)
      C2=(V(1)/V(I))**BSQ
      SIGO=0.
C
C CALCULATE THE FIRST HALF OF THE STRESS EQUATION; SUM OVER ALL
C TAU'S AND G'S.
C
      DO 60 J=1,NTG
C
C CALCULATE THE DIMENSIONLESS CONSTANT TAU TIMES THE SHEAR RATE.
C
      AK=GAMA*TAU(J)
C
C IF B IS GREATER THAN 0, CALCULATE THE VARIABLE IN THE STRESS
C EQUATION CALCULATED CALLED FK.
C
      IF(B)40,40,50
30    C=1./B/AK
      F=4.*(1.5-3.*C-1./(1.+C)+3.*C**2.*ALOG(1.+1./C))/B/B
      GO TO 50
C
C IF B IS ZERO, F IS TAU SQUARED TIMES SHEAR RATE SQUARED.
C
40    F=AK*AK
50    CONTINUE
      FSG=SG(J)
C
C EXP(-NUMBER) WILL UNDERFLOW IF NUMBER IS GREATER THAN 100.
C SETTING NUMBER EQUAL TO 100 GETS THE JOB DONE WITHOUT
C AN UNDERFLOW.
C
      IF(FSG.GT.100.) FSG=100.
C
C ACTUAL CALCULATION OF FIRST HALF OF STRESS EQUATION.
C
      SIGO=SIGO+EXP(-FSG)*C2*(C1+ZS*V(I)**2.)*FACG(J)
60    CONTINUE
      S3=0.
C
C IF THIS IS THE FIRST STEP, THE SECOND HALF OF THE STRESS
C EQUATION IS JUST ZERO; SKIP CALCULATIONS.
C
      IF(I.EQ.1) GO TO 90
C
C CALCULATE THE SECOND HALF OF THE STRESS EQUATION.  SUM OVER
C ALL TAU'S AND G'S, AND ALL X'S(INTEGRATE FROM 0 TO X).
C
      DO 80 J=1,NTG
      S2=0.
C
C SUM OVER ALL X'S.
C
      DO 70 K=2,I
      VA(K)=1./2.*(V(K)+V(K-1))
      C3=V(I)/VA(K)
C
C CALCULATE THE EXPONENTIAL FROM X(I) TO X. THIS IS EQUAL TO
```

```
C THE EXPONENTIAL OF THE INTEGRAL FROM 0 TO X MINUS THE
C INTEGRAL FROM 0 TO X(I).
C
        FAK(J,K)=FAI(J,I)-(FAI(J,K-1)+FAI(J,K))/2.
        Q=FAK(J,K)
        IF(Q.GT.100.) Q=100.
C
C SEE COMMENT ABOVE.
C
        EQ1=EXP(-Q)
C
C ACTUAL CALCULATION OF THE SECOND HALF OF THE STRESS EQUATION.
C
        FBK(J,K)=((1./VA(K)+BSQ/VA(K)*(V(K)-V(K-1))/DEL)*EQ1
        1*(C3**(2.-BSQ)-(1./C3)**(1.+BSQ)))*DEL*FACG(J)
        S2=S2+FBK(J,K)
70      CONTINUE
C
C SUM OVER ALL TAU'S AND G'S.
C
        S3=S3+S2
80      CONTINUE
90      CONTINUE
C
C TOTAL CALCULATED STRESS.
C
        SIG(I)=S3+SIGO
100     RETURN
        END
```

One Element Model Program

This program is simplified version of previous program for one element model. All the symbols are the same except FK which is the relaxation times wall shear rate.

```
      DIMENSION RG(1100),V(1100),C2G(1100),SIG(1100)
      DIMENSION SG(1100),R(1100),FAI(1100)
      COMMON V,DEL,I,SIG,BSQ,FK,B,S,FAI,ZS
      IOUT1=5
      IOUT2=22
      IN=5
      I=1
      WRITE(IOUT1,10010)
      READ(IN,10030) B,PHI,FK,DEL,ZS,CRT
      WRITE(IOUT1,10050) B,PHI, FK
      WRITE(IOUT2,10050) B,PHI,FK
      S=0.
      WRITE(IOUT2,10080)
      BSQ=B*SQRT(3.)
      RMULT=PHI/1000.
      IP=1
      RG(IP)=1.0
      V(I)=1./RG(IP)**2.
20    CALL STRESS
      C2G(IP)=SIG(I)*RG(IP)**2.
      RG(IP+1)=RG(IP)*0.95
30    IP=IP+1
      IF(IP.GE.101) GO TO 65
      IF(RG(IP).LE.0.) RG(IP)=RG(IP-1)*0.1
      V(I)=1./RG(IP)**2.
      CALL STRESS
      C2G(IP)=SIG(I)*RG(IP)**2.
      DIFF=ABS(C2G(IP)-PHI)
      IF(DIFF.GE.RMULT) GO TO 50
35    R(I)=RG(IP)
      S=FAI(I)
      DI1=DEL*(I-1)
      IF(CRT.EQ.1HN) GO TO 45
      WRITE(IOUT1,10090) DI1,R(I),V(I),SIG(I),IP
45    WRITE(IOUT2,10090) DI1,R(I),V(I),SIG(I),IP
      IF(I.EQ.1000) GO TO 70
      IP=1
      RG(IP)=R(I)*0.95
      I=I+1
      V(I)=1./RG(IP)**2.
      GO TO 20
50    CONTINUE
      RDIFF=ABS(RG(IP)-RG(IP-1))
      IF((RDIFF.LE.(RG(IP)*1.E-5))
      1.AND.((C2G(IP).GT.PHI.AND.C2G(IP-1).LT.PHI)
      2.OR.(C2G(IP).LT.PHI.AND.C2G(IP).GT.PHI))) GO TO 35
      IF(C2G(IP-1).GT.C2G(IP).AND.C2G(IP).GT.PHI) GO TO 60
      IF(C2G(IP-1).LT.C2G(IP).AND.C2G(IP).LT.PHI) GO TO 60
      RG(IP+1)=RG(IP)-(RG(IP)-RG(IP-1))*(C2G(IP)-PHI)/
      1(C2G(IP)-C2G(IP-1))
      GO TO 30
60    RG(IP+1)=RG(IP-1)-(RG(IP-1)-RG(IP))*(C2G(IP-1)
      1-PHI)/(C2G(IP-1)-C2G(IP))
      GO TO 30
65    WRITE(IOUT1,10095)
      WRITE(IOUT1,10120) ((C2G(IK),RG(IK)),IK=1,100)
70    WRITE(IOUT1,10100)
      READ(IN,10110) AN
      IF(AN.NE.1HN) GO TO 5
5     STOP
```

```
10010   FORMAT(29H INPUT DATA: B,PHI,FK,DEL,ZS,
        118H CRT OUTPUT?(Y/N) )
10030   FORMAT(F15.0,/,F15.0,/,F15.0,/,F15.0,/,F15.0,/,A1)
10050   FORMAT(1H1,/,4H B =,F6.2,/,6H PHI =,G10.4,/,
        15H FK =,G10.4)
10080   FORMAT(///,2X,24HDIMENSIONLESS PARAMETERS,/,2X,
        18HDISTANCE,6X,6HRADIUS,9X,8HVELOCITY,8X,6HSTRESS)
10090   FORMAT(4X,F8.3,1PE15.3,6X,1PE13.3,4X1PE13.3,3X,I3)
10095   FORMAT(15H NO CONVERGENCE)
10100   FORMAT(////,9H ANOTHER?)
10110   FORMAT(A1)
10120   FORMAT(1X,4F15.6)
        END
        SUBROUTINE STRESS
        DIMENSION V(1100),FU(1100),FAI(1100),SIG(1100)
        DIMENSION FAK(1100),FBK(1100) ,VA(1100)
        COMMON V,DEL,I,SIG,BSQ,FK,B,S,FAI,ZS
        FU(I)=1./V(I)
        IF(I.EQ.1) GO TO 10
        FAI(I)=S+(FU(I-1)+FU(I))*DEL/2.
        GO TO 15
10      CONTINUE
        FAI(I)=0.
15      CONTINUE
        C1=V(I)**2.-1./V(I)
        C2=(V(1)/V(I))**BSQ
        SIGO=0.
        IF(B)40,40,50
30      C=1./B/FK
        F=4.*(1.5-3.*C-1./(1.+C)+3.*C**2.*ALOG(1.+1./C))/B/B
        GO TO 50
40      F=FK*FK
50      CONTINUE
        FSG=FAI(I)
        IF(FSG.GT.100.) FSG=100.
        SIGO=SIGO+EXP(-FSG)*C2*(C1+ZS*V(I)**2.)
        S2=0.
        S3=0.
        IF(I.EQ.1) GO TO 90
        DO 70 K=2,I
        VA(K)=1./2.*(V(K)+V(K-1))
        C3=V(I)/VA(K)
        FAK(K)=FAI(I)-(FAI(K-1)+FAI(K))/2.
        Q=FAK(K)
        IF(Q.GT.100.) Q=100.
        EQ1=EXP(-Q)
        FBK(K)=((1./VA(K)+BSQ/VA(K)*(V(K)-V(K-1))/DEL)*EQ1
        1*(C3**(2.-BSQ)-(1./C3)**(1.+BSQ)))*DEL
        S2=S2+FBK(K)
70      CONTINUE
        S3=S3+S2
90      CONTINUE
        SIG(I)=S3+SIGO
100     RETURN
        END
```

VITA

Sehyun Nam was born in Seoul, Korea, on February 11, 1949. After graduating from Seoul High School, he entered Seoul National University in February 1967 and received the Bachelor of Science and Engineering degree in Applied Chemistry in February 1971. He was in the military service for two years. He entered the Oregon State University in Corvallis in September 1973 and received the Master of Science degree in Chemical Engineering in June 1975. The following September he entered the University of Michigan in Ann Arbor and received the Master of Science and Engineering degree in Metallurgical and Materials Engineering in April 1979. He entered The University of Tennessee, Knoxville, in March 1979 and received the Doctor of Philosophy degree in Polymer Engineering in December 1982.

In August 1975 he married the former Kuisook Lee and has two sons.

He is a member of Sigma Xi, Phi Kappa Phi, Phi Lambda Upsilon, Alpha Sigma Mu and the Society of Plastic Engineers.